Transport in Lagrangian-Unsteady Flows: Dispersion in Diverging or Converging Ducts, and Transport Rate Enhancement Accompanying Laminar Chaos

by

Michelle D. Bryden

B.S., University of California, Davis (1992)
S.M., Massachusetts Institute of Technology (1994)

Submitted to the Department of Chemical Engineering
in partial fulfillment of the requirements for the degree of

Doctor of Philosophy in Chemical Engineering

at the

MASSACHUSETTS INSTITUTE OF TECHNOLOGY

February 1997

Author .....
Department of Chemical Engineering
Dec. 18, 1996

Certified by.....
Professor Howard Brenner
Willard H. Dow Professor of Chemical Engineering
Thesis Supervisor

Accepted by .....
Professor Robert Cohen
St. Laurent Professor of Chemical Engineering
Chairman, Departmental Committee on Graduate Students

Transport in Lagrangian-Unsteady Flows: Dispersion in Diverging or Converging Ducts, and Transport Rate Enhancement Accompanying Laminar Chaos

by

Michelle D. Bryden

Submitted to the Department of Chemical Engineering
on Dec. 18, 1996, in partial fulfillment of the
requirements for the degree of
Doctor of Philosophy in Chemical Engineering

Abstract

This thesis concerns transport phenomena in laminar, Lagrangian unsteady flow fields. First, a multiple-timescale technique is used to analyze convective dispersion in diverging or converging ducts. A long-time, asymptotic equation governing the cross-sectionally averaged solute probability density is derived and its coefficients computed from the exact, microscale transport problem. The form of this equation and its limits of applicability are shown to be dependent upon the number of spatial dimensions characterizing the duct. Additionally, the techniques developed for the case of rectilinear channel and duct boundaries are extended to incorporate curvilinear boundaries, and an illustrative calculation performed for the case of axisymmetric flow in a flared Venturi tube.

Secondly, generalized Taylor dispersion theory is used to study transport in chaotic laminar flows. Transport of a solute is considered for the case of laminar axial 'Poiseuille' flow in the annular region between two nonconcentric cylinders, accompanied by a laminar chaotic transverse flow induced via alternate rotation of the cylinders. A Brownian tracer introduced into the flow is allowed to undergo an instantaneous, irreversible reaction on the surface of the outer cylinder. The resulting effective, transversely- and time-averaged reaction rate, axial solute velocity, and axial convective dispersivity are computed and their values compared to those in the presence of comparable non-chaotic transverse flows. The presence of chaotic flow significantly increases the effective reaction rate, decreases the axial dispersivity, and causes the mean solute/solvent velocity ratio to approach the perfectly-mixed value of 1.0.

The Stokes flow occurring within a non-neutrally buoyant spherical droplet sus-

pended in an immiscible liquid which is undergoing simple shear is shown to be chaotic under many circumstances wherein the droplet translates by buoyancy through the entraining fluid. When solute initially dissolved within the droplet is extracted into the bulk fluid, the resulting extraction rate is significantly higher in the chaotic flow case.

Both chaotic flows studied reveal that commonly used qualitative measures of mixing effectiveness, such as Poincaré maps, do not always correctly indicate trends in the transport rate. Explicitly, the degree of enhancement does not strictly correlate with the qualitative degree of 'chaosity' shown in the map.

Thesis Supervisor: Professor Howard Brenner
Title: Willard H. Dow Professor of Chemical Engineering

Contents

List of Figures

Chapter 1

Introduction

This thesis concerns material (or equivalently heat) transport phenomena in complex flow fields, explicitly those that are Lagrangian unsteady due to either temporal variations or spatial variations in the direction of flow. In particular, the theory of generalized Taylor dispersion, or macrotransport processes, is further developed and utilized to analyze global reaction and dispersion processes occurring in two broad classes of flows: (i) those net unidirectional flows whose mean velocity varies along the direction of net flow; and (ii) laminar chaotic flows.

Macrotransport theory allows multi-dimensional microscale transport problems to be reduced to macroscopically equivalent one-dimensional problems in the direction of the mean flow, characterized by macroscale phenomenological coefficients (such as effective reaction-rate constant, solute velocity, and axial dispersivity) that can be calculated from the exact, microscale transport equations and boundary conditions. The prototypical example of a macrotransport analysis is G. I. Taylor's (1953) treatment of the dispersion of a passive solute dissolved in a fluid undergoing Poiseuille flow in a tube. Using clever intuitive approximations, Taylor demonstrated that the cross-sectionally-averaged solute concentration evolves according to a one-dimensional convective-dispersive type equation, in which the solute velocity is equal to the average velocity of the solvent, and the dispersion coefficient macroscopically quantifies

the axial spreading arising from the radial variations in the axial velocity profile. Aris (1956) later formalized these results through use of the method of moments, in addition to incorporating the effect of axial (vs. transverse, or radial) molecular diffusion, which Taylor had explicitly neglected.

Following these pioneering contributions, abundant research into so-called Taylor (or Taylor-Aris) dispersion phenomena has appeared in the scientific and engineering literature (see Brenner & Edwards 1993). The method of moments and related 'projection' techniques have been used to study dispersion in a variety of situations, including: (i) spatially-periodic flows, such as flow through model porous media; (ii) time-periodic flows, which are common in physiological flows; and (iii) dispersion of chemically reactive solutes. This thesis both: (i) expands upon the existing theory to analyze flows which were previously not amenable to classical dispersion theory – in particular flows in converging and diverging ducts; and (ii) applies existing macrotransport theory to novel chaotic laminar flows of potential practical and academic interest. Specifically, in the context of several examples, it is shown how existing macrotransport theory can be used to calculate the enhancement of *global* transport rates resulting from chaotic flows.

Chapter 2 of this thesis presents a multiple-timescale analysis of dispersion in diverging and converging flows. Classical Taylor dispersion theory based on moment methods is limited to those circumstances in which the mean velocity does not vary in the direction of net flow; yet many flows of interest do not fulfill this criterion. For example, flows in nature, such as occur in rivers and estuaries, rarely, if ever, maintain a constant width over the course of their entire length. Rather, their cross-sections expand (and occasionally contract) as they flow, leading to variations in the mean velocity along the flow path. Similarly, plumes (and jets) expand as they travel away from their origins. In industrial applications, the entrance and exit regions of reactors and other vessels typically involve gradual expansions and contractions, in which the mean velocity varies in the direction of flow.

Only a limited number of studies of dispersion phenomena in these types of flows exist. Those prior theoretical analyses are limited to small angles of divergence and/or (incorrectly) assume without theoretical justification that the macroscale equation has the same elementary form as in the constant cross-section case (Gill & Güceri 1971, Smith 1983, Mercer & Roberts 1990). Such converging-diverging problems are unamenable to existing techniques, such as the method of moments or gradient expansions. In the present work, a multiple-timescale expansion is used to determine the proper form of the governing macroscale equation, as well as to obtain values for the coefficients appearing therein. It is shown that the form of the macrotransport equation depends upon the dimensionality of the diverging or converging duct, differing significantly for two- vs. three-dimensional flows. Appropriate limits of applicability governing these asymptotic, long-time macrotransport descriptions of the mean solute transport process are established in terms of the physical parameters quantifying the microscale transport process.

The remaining chapters of this thesis apply macrotransport theory to laminar chaotic flows. A detailed review of the kinematics of chaotic flows is presented in Chapter 3, so only a brief description is provided at this point. A flow is said to be chaotic if its material particle trajectories display chaotic behavior; that is, if the coupled, possibly non-linear, set of equations for the particle position $\mathbf{x} \equiv \mathbf{x}(\mathbf{x}_0, t)$ (with $\mathbf{x}_0$ the position vector at time $t = 0$),

$$\frac{d\mathbf{x}}{dt} = \mathbf{v}(\mathbf{x}, t), \tag{1.0-1}$$

possesses chaotic solutions (i.e. two initially proximate particles follow exponentially diverging trajectories). Even a velocity field satisfying the linearized Navier-Stokes equations can display chaotic behavior, since $\mathbf{v}$ is often nonlinear in $\mathbf{x}$. Laminar flows may possess a recirculation region, which when periodically perturbed in time or space can create chaotic behavior. A much studied example is the journal-bearing flow, oc-

curring in the annular space between nonconcentrically positioned circular cylinders. Each cylinder is rotated independently and time-periodically. For sufficiently large eccentricities, the flow patterns resulting from the individual cylinder rotations contain a recirculation region adjacent to the stationary cylinder. It is the temporal perturbation of these two recirculation regions that results in chaotic motion.

It has been suggested that laminar chaotic flows would be useful in mixing applications, particularly for shear-sensitive solutes (for which turbulent mixing would prove undesirable), as well as for highly viscous fluids (for which production of a turbulent flow may be impractical). In fact, many existing mixer designs have been shown to produce chaotic flows; cf. Khakhar, Franjione & Ottino (1987), wherein the Kenics static mixer is shown to be equivalent to the chaotic partitioned-pipe mixer. Following the pioneering work of Aref (1984), much effort has been devoted to the study of chaotic flows (see Ottino 1990 for a review). However, the vast majority of research into chaotic flows has focused on demonstrating that particular flows display chaotic behavior, and on establishing which regions of the chaotic flow will be well mixed. That research, most of which consists of purely computational kinematics, has resulted mainly in visualizations of the regions exhibiting chaotic behavior and in establishing other primarily qualitative descriptions of the *extent* of mixing. Much less attention has been paid to quantifying the (presumably) enhanced *rate* of mixing, or to determining the extent by which rates of *transport* processes are enhanced by laminar chaotic flows.[1] In contrast, this thesis develops a universal method for globally quantifying the rate of chaotic transport, using ideas drawn from macrotransport theory for reactive solutes. This method is then used to study several chaotic flows and to illustrate the transport enhancement attained through the judicious selection of the parameters governing these flows. In addition, the important effect of molecular

[1] Throughout this thesis, the term 'mixing' will be used to denote the process by which an initially inhomogeneous fluid is rendered homogeneous, while the 'extent of mixing' is a measure of the degree of homogeneity of the final product. 'Transport' includes all heat- or mass-transfer processes, and is measured in terms of the amount of material or heat transferred per unit time.

diffusion, excluded from most prior work, is considered.

In Chapter 4, solute transport of within the chaotic flow existing in the annular space between alternately-rotating eccentric cylinders (also known as the 'journal-bearing flow') is considered. A first-order, instantaneous chemical reaction or solute deposition process is prescribed on the surface of the outer cylinder. Superposed on the two-dimensional chaotic transverse flow is an axial, pressure-driven 'Poiseuille' flow. Using macrotransport theory (Brenner & Edwards 1993), the effective reaction/deposition rate, mean axial solute velocity, and axial convective dispersivity are determined. Each of these three macroscale parameters provides an independent means for quantifying the degree of chaotic enhancement by comparing their respective relative values in the presence and absence of chaos.

The most direct and easily interpreted measure of the degree of chaotic enhancement is provided by the effective reaction rate. Since the reaction at the outer wall is assumed instantaneous, the overall reaction rate is determined exclusively by the transport of solute to the wall. Thus, the effective reaction rate furnishes a direct and simple measure of the transverse transport rate.

The effective axial solute velocity in the presence of the inhomogeneous reaction is increased above the mean solvent velocity via the depletion of solute from the slowest moving streamlines, existing near the reactive wall (cf. Shapiro & Brenner 1986). In a transversely well-mixed flow, this disparity in velocities is lessened; indeed, in a perfectly-mixed flow the solute and solvent velocities would be identical. Thus, the mean axial velocity of the reactive solute furnishes a simple global measure of the transport effectiveness of a given flow, although it is less easily interpreted than is the effective reaction rate.

Lastly, the axial convective Taylor dispersivity declines with improved transverse transport rates due to the increased rate at which the solute molecules sample the various axial velocities characterizing the Poiseuille streamlines. The dispersivity thereby provides an additional means of globally assessing the effectiveness of the

chaotic transverse transport.

By calculating these three macrotransport coefficients, it is shown that the transverse transport rate is significantly enhanced by the existence of chaotic flow within the annulus. Comparison of the effect of varying the flow parameters on each of the three macroscale coefficients reveals that the choice of optimal parameters for maximizing the transport rate is independent of which of the three quantitative measures is used to assess the effectiveness of the chaotic flow; that is, what is optimal for one is also optimal for the other two. In a more general context, it is shown that qualitative diagrams such as Poincaré maps, which are frequently used in visualizing chaotic flows, do not always provide accurate qualitative indications of the effectiveness of a given flow in enhancing the global transport rate. Explicitly, the quantitative degree of enhancement does not strictly correlate with the qualitative degree of 'chaosity' indicated by the map.

Chapter 5 addresses a novel *steady* chaotic flow, occurring within a spherical fluid droplet. The flow considered is that arising from translation of a non-neutrally buoyant droplet through an external fluid undergoing simple shear. This flow is of interest due to its ubiquity in applications, as well as to the ease with which it can be produced in the laboratory. It occurs (among other circumstances) when a droplet rises or falls through the annular space between two vertical concentric cylinders containing a Couette flow produced by their relative rotation. A comparable, yet nonchaotic, flow is produced by the translation of the non-neutrally buoyant droplet through a vertical Poiseuille flow occurring, say, in the same (non-rotating) annular apparatus — the only difference between the two flows being the relative orientation of the external shear and translational motions.

The parameter ranges for which the flow internal to the droplet is chaotic are first determined; following this, the rate of extraction of a passive solute initially dissolved within the droplet into the bulk fluid is considered for circumstances in which the bulk-phase mass-transfer coefficient is effectively infinite, and hence non-rate-limiting.

This extraction rate is conceptually equivalent to the effective chemical reaction rate considered in Chapter 4. It constitutes a simple and direct measure of the rate at which solute is transported through the droplet interior to the interface, from where it passes unrestricted into the bulk fluid. Results gleaned from this example once again demonstrate that: (i) laminar chaotic flows can significantly enhance transport rates; and (ii) the *extent of mixing*, as determined through Poincaré sections, does not always accurately correlate with the degree of enhancement observed in the *transport rate.*

References

[1] AREF, H. 1984 Stirring by chaotic advection. *Phys. Fluids* **143**, 1–21.

[2] ARIS, R. 1956 On the dispersion of a solute in a fluid flowing through a tube. *Proc. Roy. Soc.* A **235**, 66–77.

[3] BRENNER, H. & EDWARDS, D. A. 1993 *Macrotransport Processes.* Butterworth-Heinemann.

[4] GILL, W. N. & GÜCERI, U. 1971 Laminar dispersion in Jeffrey-Hamel flows: Part 1. Diverging channels. *AIChE J.* **17**, 207–214.

[5] KHAKHAR, D. V., FRANJIONE, J. G., & OTTINO, J. M. 1987 A case study of chaotic mixing in deterministic flows: the partitioned pipe mixer. *Chem. Eng. Sci.* **42**, 2909–2926.

[6] MERCER, G. N. & ROBERTS, A. J. 1990 Centre manifold description of contaminant dispersion in channels with varying flow properties. *SIAM J. Appl. Math.* **50**, 1547–1565.

[7] OTTINO, J. M. 1990 Mixing, chaotic advection, and turbulence. *Ann. Rev. Fluid Mech.* **22**, 207–253.

[8] SHAPIRO, M. & BRENNER, H. 1986 Taylor dispersion of chemically reactive species: Irreversible first-order reactions in bulk and on boundaries. *Chem. Eng. Sci* **41**, 1417–1433.

[9] SMITH, R. 1983 Longitudinal dispersion coefficients for varying channels. *J. Fluid Mech.* **130**, 299–314.

[10] TAYLOR, G. I. 1953 Dispersion of soluble matter in a solvent flowing slowly through a tube. *Proc. Roy. Soc.* A **219**, 186–203.

Chapter 2

Dispersion in diverging and converging ducts

Abstract

A multiple-timescale analysis is employed to analyze Taylor dispersion-like convective-diffusive processes in converging and diverging flows. A long time, asymptotic equation governing the cross-sectionally averaged solute probability density is derived. The form of this equation is shown to be dependent upon the number of spatial dimensions characterizing the duct or 'cone'. The two-dimensional case (nonparallel plates) is shown to be fundamentally different from that for three dimensions (circular cone) in that, in two dimensions, a Taylor dispersion description of the process is possible only for small Péclet numbers or angles of divergence. In contrast, in three dimensions, a Taylor dispersion description is always possible provided sufficient time has passed since the initial introduction of solute into the system. The convective Taylor dispersion coefficients $\overline{D_c}$ for the respective cases of low-Reynolds number flow between nonparallel plates and in a circular cone are computed and their limiting values, $\overline{D_c^0}$, for zero apex angle are shown to be consistent with the known results for Taylor dispersion between parallel plates and in a circular cylinder. When plotted in the nondimensional form of $\overline{D_c}/\overline{D_c^0}$ versus the half-vertex angle θ_0, the respective dispersivity results for the two cases hardly differ from one another, increasing monotonically from 1.0 for $\theta_0 = 0$ to approximately 2.6 for a fully flared duct, $\theta_0 = \pi/2$. Lastly, the techniques developed above for the case of rectilinear channel and duct boundaries are extended to the case of curvilinear boundaries, and an illustrative calculation performed for the case of axisymmetric flow in a flared Venturi tube.

2.1 Introduction

The problem of convective dispersion in ducts of constant cross-section, such as cylinders and parallel plates, has been well-studied. In those studies, the velocity profile and molecular dispersivity are taken to be independent of the axial (global) coordinate. In fact, application of the general theory of macrotransport processes in its current form (Brenner & Edwards 1993) explicitly requires that the phenomenological coefficients appearing in the microscale description of the process be independent of the global-space position.

A limited number of studies exist which address problems involving axially-varying velocity fields. Thus, Frankel & Brenner (1991) studied Taylor dispersion in unbounded shear flows, allowing the velocity to depend linearly on the global coordinate. Mercer & Roberts (1990) used centre manifold theory to treat the case of dispersion in channels with slowly varying cross-section and thus, varying velocity. Gill & Güceri (1971) conducted numerical studies of Taylor dispersion in flow between nonparallel flat plates, in addition to having derived a theoretical expression for the axial dispersion coefficient in channels possessing small angles of divergence. Lastly, Smith (1983) derived a expression for the dispersion coefficient in a varying channel whose small depth relative to its width allowed it to be treated as well-mixed in the vertical direction.

The method of multiple-timescales has been used to analyze Taylor dispersion in rectangular ducts (Pagitsas, Nadim & Brenner 1986). This method takes advantage of the separation of time-scales required for a macrotransport description of the process to exist. The present contribution presents a multiple-timescale analysis of dispersion between nonparallel flat plates and in a circular cone. The functional dependence of the macrotransport equation upon the dimensionality of the channel is established and circumstances quantified whereby such a dispersion description of the process is indeed possible. The Taylor dispersion coefficients for low-Reynolds number flow

between nonparallel flat plates and in a circular cone are calculated. Finally, an extension of the current multiple-timescale methods to cross-sectionally varying flows in curvilinear channels and ducts is presented, and illustrated by example. This material has previously appeared in the *Journal of Fluid Mechanics* (Bryden & Brenner 1996).

2.2 Kinematics of flow in an n-dimensional cone

The vector velocity field for axisymmetric radial flow in an n-dimensional cone of apex angle $2\theta_0$ (see figures 2-1a and 2-1b) is of the form

$$\boldsymbol{v} = \boldsymbol{i}_r v_r(r,\theta) \qquad \left(\begin{array}{ll} 0 < r < \infty, & -\theta_0 \leqslant \theta \leqslant \theta_0 \leqslant \pi \quad (n=2) \\ 0 < r < \infty, & 0 \leqslant \theta \leqslant \theta_0 \leqslant \pi \quad (n=3) \end{array} \right), \tag{2.2-1}$$

with

$$v_r = \frac{Q(\theta)}{r^{n-1}}. \tag{2.2-2}$$

Here, the inverse r^{n-1} dependence results from the requirement that the axisymmetric flow field satisfy the continuity equation

$$\frac{1}{r^{n-1}} \frac{\partial}{\partial r}(r^{n-1} v_r) = 0 \tag{2.2-3}$$

for incompressible radial flow. The algebraically-signed 'volumetric' flow rate through the duct, namely $Q = \int v_r \mathrm{d}S$ (with $\mathrm{d}S$ a scalar element of surface area on the surface $r =$ constant) is given explicitly by the expression

$$Q = 2\pi^{n-2} \int_0^{\theta_0} Q(\theta) \sin^{n-2}\theta \mathrm{d}\theta. \tag{2.2-4}$$

The exact solution of the Navier-Stokes equations for incompressible Jeffrey-Hamel

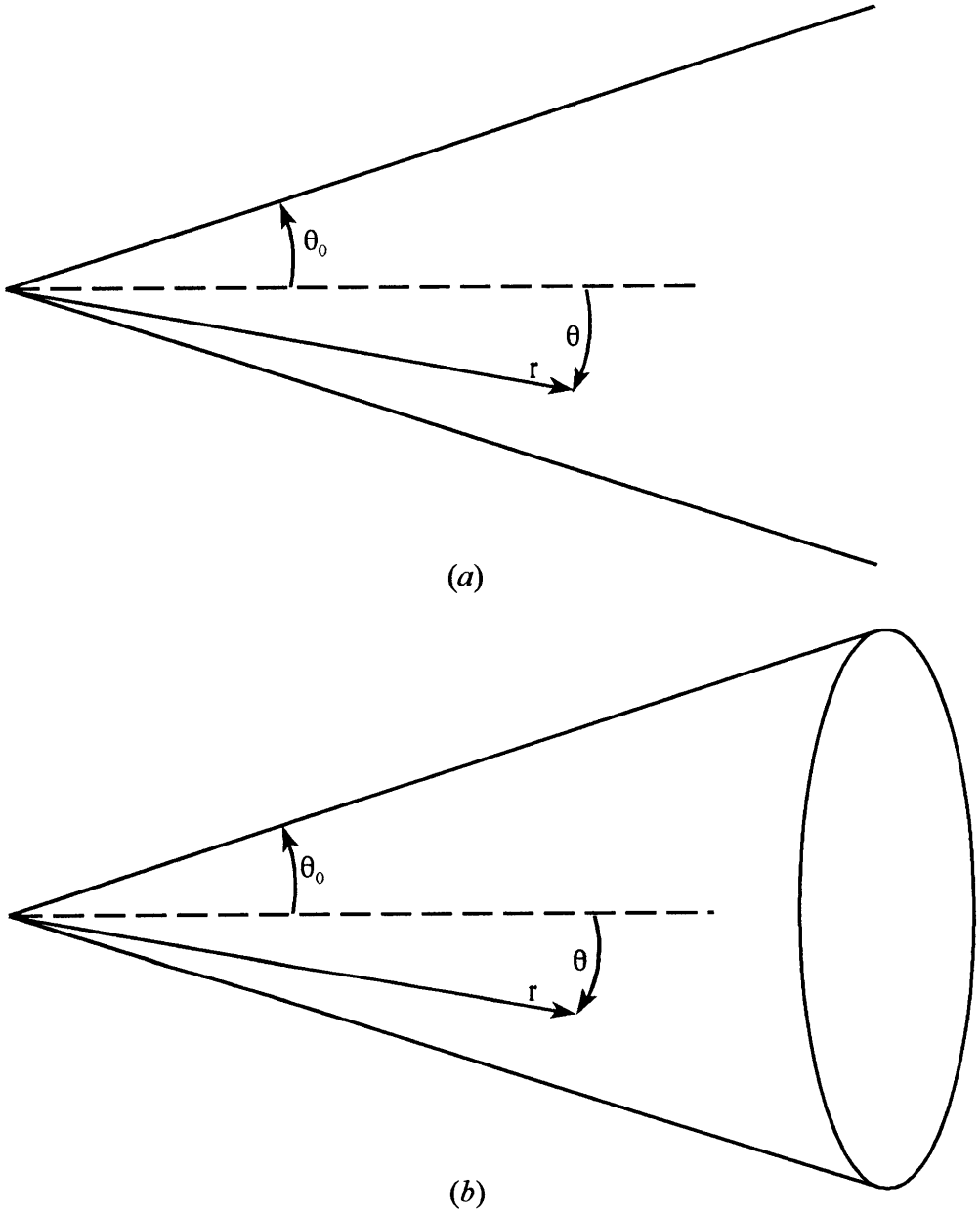

Figure 2-1: (a) Nonparallel plates (b) Circular cone

flow between nonparallel flat plates ($n = 2$) is well known (Rouse 1959; Goldstein 1965*a*) and can be expressed in terms of elliptic functions. For low Reynolds number flow this velocity field is

$$v_r = \frac{Q}{r} \frac{\cos 2\theta - \cos 2\theta_0}{\sin 2\theta_0 - 2\theta_0 \cos \theta_0} \qquad (n = 2). \tag{2.2-5}$$

While no comparable exact Navier-Stokes solution exists for flow in a circular cone (n=3) (Ackerberg 1965; Goldstein 1965*b*), the velocity field for low Reynolds number is (cf. Happel & Brenner 1983)

$$v_r = \frac{3Q}{2\pi r^2} \frac{\cos^2 \theta - \cos^2 \theta_0}{(1 + 2\cos \theta_0)(1 - \cos \theta_0)^2} \qquad (n = 3). \tag{2.2-6}$$

2.3 Microscale transport equation for convection and molecular diffusion in a diverging or converging duct

The governing equation for unsteady convection and diffusion of a dissolved or colloidal Brownian species between nonparallel plates or in a circular cone is

$$\frac{\partial C}{\partial t} + \frac{Q(\theta)}{r^{n-1}} \frac{\partial C}{\partial r} + \frac{D}{r^2} \left[\frac{1}{r^{n-3}} \frac{\partial}{\partial r} \left(r^{n-1} \frac{\partial C}{\partial r} \right) - \frac{1}{\sin^{n-2} \theta} \frac{\partial}{\partial \theta} \left(\sin^{n-2} \theta \frac{\partial C}{\partial \theta} \right) - \frac{\delta_{n3}}{\sin \theta} \frac{\partial^2 C}{\partial \phi^2} \right] = 0, \tag{2.3-7}$$

with D the molecular diffusivity, assumed constant, and δ_{n3} the Kronecker delta. This equation is to be solved for the solute concentration $C(r, \theta, (\phi), t)$ subject to the initial and boundary conditions:

$$C|_{t=0} = C_0, \tag{2.3-8}$$

$$\frac{\partial C}{\partial \theta} = 0 \quad \text{at} \quad \theta = 0 \quad \text{and} \quad \theta_0, \tag{2.3-9}$$

$$C \quad \text{is finite at} \quad r = 0, \tag{2.3-10}$$

$$C|_{\phi} = C|_{\phi+2\pi} \qquad (n = 3). \tag{2.3-11}$$

(In the two dimensional case, we have for simplicity by symmetry confined ourselves in the above to the half region $0 \leqslant \theta \leqslant \theta_0$). The first of these conditions represents a prescribed initial solute concentration, with $C_0(r, \theta, (\phi))$ a specified function. The second represents the condition of symmetry about the cone axis, together with the requirement of no flux through the duct walls. The remaining conditions (2.3-10) and (2.3-11) respectively represent the requirements of boundedness of the concentration field and single-valuedness of the latter in the azimuthal angle ϕ.

As the velocity field and molecular diffusion coefficient are both independent of the angle ϕ, this angle constitutes a 'dead' degree of freedom over which one can integrate in the $n = 3$ case. (Of course, in the $n = 2$ case no such integration is required.) To ultimately establish the macrotransport equation [see (2.5-50)], we therefore need solve only for the azimuthally averaged concentration field:

$$c(r, \theta, t) \stackrel{\text{def}}{=} \int_0^{2\pi} C(r, \theta, \phi, t) \mathrm{d}\phi \qquad (n = 3). \tag{2.3-12}$$

Upon introduction of the dimensionless quantities

$$\tau = \frac{tD}{\theta_0^2 r_0^2}, \qquad \Theta = \frac{\theta}{\theta_0}, \qquad R = \frac{r}{r_0}, \tag{2.3 - 13a, b, c}$$

where r_0 is a characteristic radial distance, (2.3-7) – (2.3-11) become

$$\frac{\partial c}{\partial \tau} + \varepsilon \frac{q(\Theta)}{R^{n-1}} \frac{\partial c}{\partial R} - \kappa \varepsilon^2 \frac{1}{R^{n-1}} \frac{\partial}{\partial R} \left(R^{n-1} \frac{\partial c}{\partial R} \right) - \frac{1}{R^2 \sin^{n-2}(\Theta \theta_0)} \times \frac{\partial}{\partial \Theta} \left(\sin^{n-2}(\Theta \theta_0) \frac{\partial c}{\partial \Theta} \right) = 0, \tag{2.3-14}$$

$$c|_{\tau=0} = c_0, \tag{2.3-15}$$

$$\frac{\partial c}{\partial \Theta} \quad \text{at} \quad \Theta = 0 \quad \text{and} \quad 1, \tag{2.3-16}$$

$$c \quad \text{is finite at} \quad R = 0, \tag{2.3-17}$$

in which c_0 is the prescribed value of c at τ =0,

$$q(\Theta) = \frac{Q(\Theta\theta_0)}{\overline{Q}}, \tag{2.3-18}$$

$$\varepsilon = \frac{\theta_0^2 \overline{Q}}{r_0^{n-2} D} \tag{2.3-19}$$

and

$$\kappa = \left(\frac{D r_0^{n-2}}{\overline{Q}\theta_0} \right)^2. \tag{2.3-20}$$

In the above, $\overline{Q} \equiv \int Q(\theta) \mathrm{d}S / \int \mathrm{d}dS$ is the algebraically-signed average 'volumetric' flow rate, explicitly defined as

$$\overline{Q} = \int_0^{\theta_0} Q(\theta) \sin^{n-2}\theta \mathrm{d}\theta \Big/ \int_0^{\theta_0} \sin^{n-2}\theta \mathrm{d}\theta. \tag{2.3-21}$$

The dimensionless parameter $|\varepsilon|$ is proportional to the ratio of the angular diffusion time τ_D to the convection time τ_Q from $r = 0$ to r_0, respectively defined as

$$\tau_D = \frac{\theta_0^2 r_0^2}{D}, \qquad \tau_Q = \frac{r_0^n}{n|\overline{Q}|}. \tag{2.3 - 22a, b}$$

2.4 Multiple time-scale analysis

Equation (2.3-14) may be recast in terms of the comparable Green's function (Brenner & Edwards 1993), the latter being formally equivalent to the conditional probability density $P(R, \Theta, \tau | R', \Theta')$ that a unit tracer introduced into the system at position

(R', Θ') at time $\tau = 0$ is present at the position (R, θ) at time τ:

$$\frac{\partial P}{\partial \tau} + \varepsilon \frac{q(\Theta)}{R^{n-1}} \frac{\partial P}{\partial R} - \kappa \varepsilon^2 \frac{1}{R^{n-1}} \frac{\partial}{\partial R} \left(R^{n-1} \frac{\partial P}{\partial R} \right) - \frac{1}{R^2 \sin^{n-2}(\Theta \theta_0)} \times \frac{\partial}{\partial \Theta} \left(\sin^{n-2}(\Theta \theta_0) \frac{\partial P}{\partial \Theta} \right) = \frac{\delta(R - R')}{R^{n-1}} \frac{\delta(\Theta - \Theta')}{\sin^{n-2}(\Theta \theta_0)} \delta(\tau). \tag{2.4-23}$$

This equation is to be solved subject to the boundary conditions

$$\frac{\partial P}{\partial \Theta} = 0 \quad \text{at} \quad \Theta = 0 \quad \text{and} \quad 1, \tag{2.4-24}$$

$$P \quad \text{is finite at} \quad R = 0, \tag{2.4-25}$$

$$R^{n-1} P \to 0 \quad \text{as} \quad R \to \infty. \tag{2.4-26}$$

In the long time limit and for $|\varepsilon| \ll 1$, the above system of microscale equations may be reduced to a comparable macroscale equation for the cross-sectionally averaged probability density, defined as

$$\overline{P} = \int_0^1 P \sin^{n-2}(\Theta \theta_0) \mathrm{d}\Theta \Big/ \int_0^1 \sin^{n-2}(\Theta \theta_0) \mathrm{d}\Theta, \tag{2.4-27}$$

through the use of a multiple-timescale analysis in which ε is a small parameter. (The physical implications of the requirement that ε be small are discussed in §2.6.) To accomplish this macrotransport analysis, introduce into (2.4-23) the sequence of time variables

$$\tau_m = \varepsilon^m \tau \qquad (m = 0, 1, 2, ..., \infty), \tag{2.4-28}$$

each of which is to be treated as an independent variable, and write

$$P(R, \Theta, \tau | R', \Theta') \equiv P(R, \Theta, \tau_0, \tau_1, \tau_2, ... | R', \Theta'). \tag{2.4-29}$$

Expand P in a perturbation series in ε:

$$P = \sum_{n=0}^{\infty} \varepsilon^n P_n(R, \Theta, \tau_0, \tau_1, \tau_2, ...|R', \Theta'). \tag{2.4-30}$$

The time derivative appearing on the left-hand side of (2.4-23) may then be written as

$$\frac{\partial P}{\partial \tau} = \sum_{n=0}^{\infty} \sum_{m=0}^{\infty} \varepsilon^{n+m} \frac{\partial P_n}{\partial \tau_m}. \tag{2.4-31}$$

Substitute (2.4-30) and (2.4-31) into (2.4-23) and equate terms of equal order in ε to obtain the following recursive sequence of equations governing the respective P_n:

$$\frac{\partial P_0}{\partial \tau_0} - \frac{1}{R^2 \sin^{n-2}(\Theta\theta_0)} \frac{\partial}{\partial \Theta} \left(\sin^{n-2}(\Theta\theta_0) \frac{\partial P_0}{\partial \Theta} \right) = \frac{\delta(R - R')}{R^{n-1}} \frac{\delta(\Theta - \Theta')}{\sin^{n-2}(\Theta\theta_0)} \delta(\tau), \tag{2.4-32}$$

$$\frac{\partial P_1}{\partial \tau_0} + \frac{\partial P_0}{\partial \tau_1} + \frac{q(\Theta)}{R^{n-1}} \frac{\partial P_0}{\partial R} - \frac{1}{R^2 \sin^{n-2}(\Theta\theta_0)} \frac{\partial}{\partial \Theta} \left(\sin^{n-2}(\Theta\theta_0) \frac{\partial P_1}{\partial \Theta} \right) = 0 \tag{2.4-33}$$

and

$$\frac{\partial P_2}{\partial \tau_0} + \frac{\partial P_1}{\partial \tau_1} + \frac{\partial P_0}{\partial \tau_2} + \frac{q(\Theta)}{R^{n-1}} \frac{\partial P_1}{\partial R} - \frac{1}{R^2 \sin^{n-2}(\Theta\theta_0)} \frac{\partial}{\partial \Theta} \left(\sin^{n-2}(\Theta\theta_0) \frac{\partial P_2}{\partial \Theta} \right)$$
$$- \frac{\kappa}{R^{n-1}} \frac{\partial}{\partial R} \left(R^{n-1} \frac{\partial P_0}{\partial R} \right) = 0, \tag{2.4-34}$$

up to and including terms of second order in ε. Each such equation is to be solved subject to the same boundary conditions set forth for P in (2.4-24)–(2.4-26).

Multiply (2.4-32) by $\sin^{n-2}(\Theta\theta_0)$, integrate from $\Theta = 0$ to $\Theta = 1$ and apply the boundary condition (2.4-24) to obtain

$$\frac{\partial \overline{P_0}}{\partial \tau_0} = 0 \qquad (\tau_0 > 0). \tag{2.4-35}$$

Thus, for long times ($\tau_0 \gg 1$),

$$P_0 \sim \overline{P_0}(R, \tau_1, \tau_2, ...|R') + \text{exp}, \tag{2.4-36}$$

in which 'exp' denotes terms which decay exponentially in τ_0.

Substitution of (2.4-36) into (2.4-33) furnishes an asymptotic equation governing P_1 for long times. Multiply (2.4-33) by $\sin^{n-2}(\Theta\theta_0)$, integrate from $\Theta = 0$ to 1, and apply the boundary condition (2.4-24) to derive the asymptotic relation

$$\frac{\partial \overline{P_1}}{\partial \tau_0} + \frac{\partial \overline{P_0}}{\partial \tau_1} + \frac{1}{R^{n-1}} \frac{\partial \overline{P_0}}{\partial R} \sim \text{exp}. \tag{2.4-37}$$

The second and third terms in the above equation are independent of τ_0. Thus, in order to prevent secular growth of $\overline{P_1}$ in τ_0, it is required that

$$\frac{\partial \overline{P_0}}{\partial \tau_1} = -\frac{1}{R^{n-1}} \frac{\partial \overline{P_0}}{\partial R}, \tag{2.4-38}$$

whence

$$\overline{P_1} \sim \text{exp}. \tag{2.4-39}$$

(This secular growth argument is equivalent to that used by Chatwin (1970)). Substitute (2.4-36), (2.4-35), and (2.4-39) into (2.4-33) to obtain

$$\frac{1}{\sin^{n-2}(\Theta\theta_0)} \frac{\partial}{\partial \Theta} \left(\sin^{n-2}(\Theta\theta_0) \frac{\partial P_1}{\partial \Theta} \right) \sim R^{3-n} \frac{\partial \overline{P_0}}{\partial R} (q(\Theta) - 1) + \text{exp}. \tag{2.4-40}$$

The above may be solved subject to the boundary and normalization conditions (2.4-24) and (2.4-39), yielding

$$P_1 \sim f(\Theta) R^{3-n} \frac{\partial \overline{P_0}}{\partial R} + \text{exp}, \tag{2.4-41}$$

where the function $f(\Theta)$ represents the solution of the boundary value problem

$$\frac{1}{\sin^{n-2}(\Theta\theta_0)}\frac{\partial}{\partial\Theta}\left(\sin^{n-2}(\Theta\theta_0)\frac{\partial f}{\partial\Theta}\right) = q(\Theta) - 1, \tag{2.4-42}$$

subject to the conditions

$$\frac{\partial f}{\partial\Theta} \quad \text{at} \quad \Theta = 0 \quad \text{and} \quad 1, \tag{2.4-43}$$

$$\int_0^1 f(\Theta)\sin^{n-2}(\Theta\theta_0)\mathrm{d}\Theta = 0. \tag{2.4-44}$$

It remains only to find the terms of $O(\varepsilon^2)$. By substituting the respective solutions (2.4-36) and (2.4-41) for P_0 and P_1 into (2.4-34) and integrating over the cross-sectional area, the dependence of $\overline{P_0}$ upon τ_2 may be obtained:

$$\frac{\partial\overline{P_2}}{\partial\tau_0} + \frac{\partial\overline{P_0}}{\partial\tau_2} - \frac{\kappa}{R^{n-1}}\frac{\partial}{\partial R}\left(R^{n-1}\frac{\partial\overline{P_0}}{\partial R}\right) - \frac{F(\theta_0)}{R^{n-1}}\frac{\partial}{\partial R}\left(R^{3-n}\frac{\partial\overline{P_0}}{\partial R}\right) \sim \exp. \tag{2.4-45}$$

Here,

$$-F(\theta_0) = \int_0^1 f(\Theta)q(\Theta)\sin^{n-2}(\Theta\theta_0)\mathrm{d}\Theta \Big/ \int_0^1 \sin^{n-2}(\Theta\theta_0)\mathrm{d}\Theta, \tag{2.4-46}$$

or in an alternative form which may be derived through use of (2.4-42)–(2.4-44) in the above,

$$F(\theta_0) = \int_0^1 \left(\frac{\mathrm{d}f}{\mathrm{d}\Theta}\right)^2 \sin^{n-2}(\Theta\theta_0)\mathrm{d}\Theta \Big/ \int_0^1 \sin^{n-2}(\Theta\theta_0)\mathrm{d}\Theta. \tag{2.4-47}$$

Prevention of the secular growth of $\overline{P_2}$ in τ_0 requires that

$$\frac{\partial\overline{P_0}}{\partial\tau_2} - \frac{\kappa}{R^{n-1}}\frac{\partial}{\partial R}\left(R^{n-1}\frac{\partial\overline{P_0}}{\partial R}\right) - \frac{F(\theta_0)}{R^{n-1}}\frac{\partial}{\partial R}\left(R^{3-n}\frac{\partial\overline{P_0}}{\partial R}\right) \sim 0 \tag{2.4-48}$$

and

$$\overline{P_2} \sim \exp. \tag{2.4-49}$$

2.5 The macrotransport equation

The macrotransport equation governing $\overline{P}$ (accurate to $O(\varepsilon^2)$) may be found by integrating (2.4-31) over the cross-sectional area and substituting (2.4-36), (2.4-38), (2.4-39), (2.4-48), and (2.4-49) into the resulting expression to obtain (in dimensional form)

$$\frac{\partial \overline{P}}{\partial t} + \frac{\overline{Q}}{r^{n-1}}\frac{\partial \overline{P}}{\partial r} - \frac{D}{r^{n-1}}\frac{\partial}{\partial r}\left(r^{n-1}\frac{\partial \overline{P}}{\partial r}\right) - \frac{\overline{D_c}}{r^{n-1}}\frac{\partial}{\partial r}\left(r^{3-n}\frac{\partial \overline{P}}{\partial r}\right) = \frac{\delta(r-r')}{r^{n-1}}\frac{\delta(t)}{\int_0^{\theta_0}\sin^{n-2}\theta \mathrm{d}\theta}, \tag{2.5-50}$$

wherein

$$\overline{D_c} = \frac{\overline{Q}^2}{D}\theta_0^2 F(\theta) \tag{2.5-51}$$

represents the convective contribution to the dispersivity. This equation is valid for both positive (diverging flow) and negative (converging flow) values of $\overline{Q}$. Note that inasmuch as $F(\theta_0)$ is always nonnegative [see (2.4-47)] it follows that $\overline{D_c}$ is always nonnegative irrespective of the direction of flow.

2.6 Range of validity of the global equation

The present analysis is valid provided that $|\varepsilon| \ll 1$ and $\tau_0 \gg 1$ (or equivalently $t \gg \theta_0^2 r_0^2/D$). It can be shown that the first requirement is automatically satisfied provided that the second constraint is met. A tracer particle initially introduced into the flow within a diverging or converging cone at the radial position r' will (on

average) be located at time t at the point

$$r_t = [n\overline{Q}t + (r')^n]^{(1/n)}. \tag{2.6-52}$$

(For converging flows, for which $\overline{Q} < 0$, the above is valid for $t < (r')^n/n|\overline{Q}|$, after which time the solute particle will, on average, have flowed out of the cone through the apex along with the solvent.) Substitution into (2.6-52) of the inequality

$$t \gg \frac{\theta_0^2 r_0^2}{D} \tag{2.6-53}$$

followed by subsequent rearrangement gives

$$\frac{n\theta_0^2 \overline{Q} r_0^2}{D[r_t^n - (r')^n]} \ll 1. \tag{2.6-54}$$

The characteristic length r_0 is to be chosen as the larger of the two lengths r_t and r'. Thus, for diverging flows ($Q > 0$) $r_0 = r_t$, while for converging flows ($Q < 0$) $r_0 = r'$. After replacement of r_0 in (2.3-19) and (2.6-54) with the appropriate length, comparison of the two constraints reveals that the requirement (2.6-53) is more restrictive than the requirement $|\varepsilon| \ll 1$. Thus, satisfaction of a single constraint suffices to guarantee that the macrotransport description (2.5-50) of the process is applicable.

Observe that ε, the ratio of the transverse diffusion time to the convection time, scales as r_0^{-n+2} (2.3-19). Hence, in three dimensions a macrotransport description of the process is always possible for some sufficiently large r_0 or, equivalently, for long enough times. For the two-dimensional case, the situation is different. In this case, ε is independent of r_0. Thus, circumstances exist for which no macrotransport description is possible, regardless of the length scale of the channel. Physically, this means that in some instances the transverse diffusion time τ_D is greater than or

equal to the convection time τ_Q. In such cases, corresponding to large flow rates or apex angles, a particle introduced into a diverging flow will be swept downstream so quickly that insufficient time exists for it to sample all angular positions. This is so because as the particle is convected downstream, the transverse distance through which it must travel in order to reach the most distant streamlines increases more rapidly than $(Dt)^{\frac{1}{2}}$, the lateral distance through which it has diffused. It may appear that this limitation would not be present for the case of converging flow, for which the particle encounters a decreasing cross-sectional area as it is convected toward the apex of the system. This impression is erroneous, however, for although the particle is confronted with a smaller area to sample, its velocity increases at precisely the same rate at which the cross-sectional area decreases, so that the particle still has insufficient time in which to sample all of the streamlines. In such circumstances, a purely asymptotic description of the process cannot be valid since the particle will 'remember' the angular position θ' at which it was originally introduced.

In contrast, in three dimensions, a macrotransport description is always possible for some sufficiently large r_0. Although the transverse distance that a particle in a diverging flow must sample increases as it is convected through the cone, the velocity with which it is convected decreases rapidly enough that the particle can sample all of the streamlines if given enough time. Likewise, in converging flow, the velocity increases more slowly than the cross-sectional area decreases, thus enabling the particle to sample all of the streamlines.

2.7 Examples: Low Reynolds number flow

2.7.1 Nonparallel Plates

Application of (2.4-42)–(2.4-44) together with (2.4-47) and (2.5-51) to the case of creeping flow between nonparallel plates, for which the velocity is given by (2.2-5),

gives

$$\overline{D_c} = \frac{\overline{Q}^2}{D}\frac{1}{12}\frac{6\theta_0^2 - 6\sin^2 2\theta_0 + 9\theta_0 \sin 2\theta_0 \cos 2\theta_0 + 4\theta_0^2 \sin^2 2\theta_0}{(\sin 2\theta_0 - 2\theta_0 \cos 2\theta_0)^2}. \tag{2.7-55}$$

It may be shown in the limit $\theta_0 \to 0$ that this reduces to the classical result for Taylor dispersion between flat plates. To do so, replace the flow rate with the average velocity, $\overline{V} \stackrel{\text{def}}{=} \overline{Q}/r$, introduce the half-distance, $h \stackrel{\text{def}}{=} \theta_0 r$, between the plates, and expand in a Taylor series about $\theta_0 = 0$ to obtain

$$\overline{D_c} \sim \overline{D_c^0}\left(1 + \frac{4}{15}\theta_0^2 + ...\right), \tag{2.7-56}$$

where

$$\overline{D_c^0} = \frac{2}{105}\frac{\overline{V}^2 h^2}{D} \qquad (n = 2) \tag{2.7-57}$$

is the classical result (Wooding 1960) for flow between parallel plates.

A plot of the convective contribution (2.7-55) to the dispersivity versus the half angle between the flat plates is given in figure 2-2. The dispersivity increases appreciably with increasing angles owing to the fact that the transverse velocity gradients $\partial v_r/\partial\theta$ increase with increasing angles of divergence.

For this two-dimensional situation, the macrotransport equation governing the angularly-averaged conditional probability density $\overline{P}(r, t|r')$ is

$$\frac{\partial \overline{P}}{\partial t} + \frac{\overline{Q}}{r}\frac{\partial \overline{P}}{\partial r} - \frac{\overline{D^*}}{r}\frac{\partial}{\partial r}\left(r\frac{\partial \overline{P}}{\partial r}\right) = \frac{\delta(r - r')}{r}\delta(t), \tag{2.7-58}$$

in which

$$\overline{D^*} = D + \overline{D_c} \tag{2.7-59}$$

is the total Taylor-Aris dispersivity. The solution of (2.7-58) may be found through

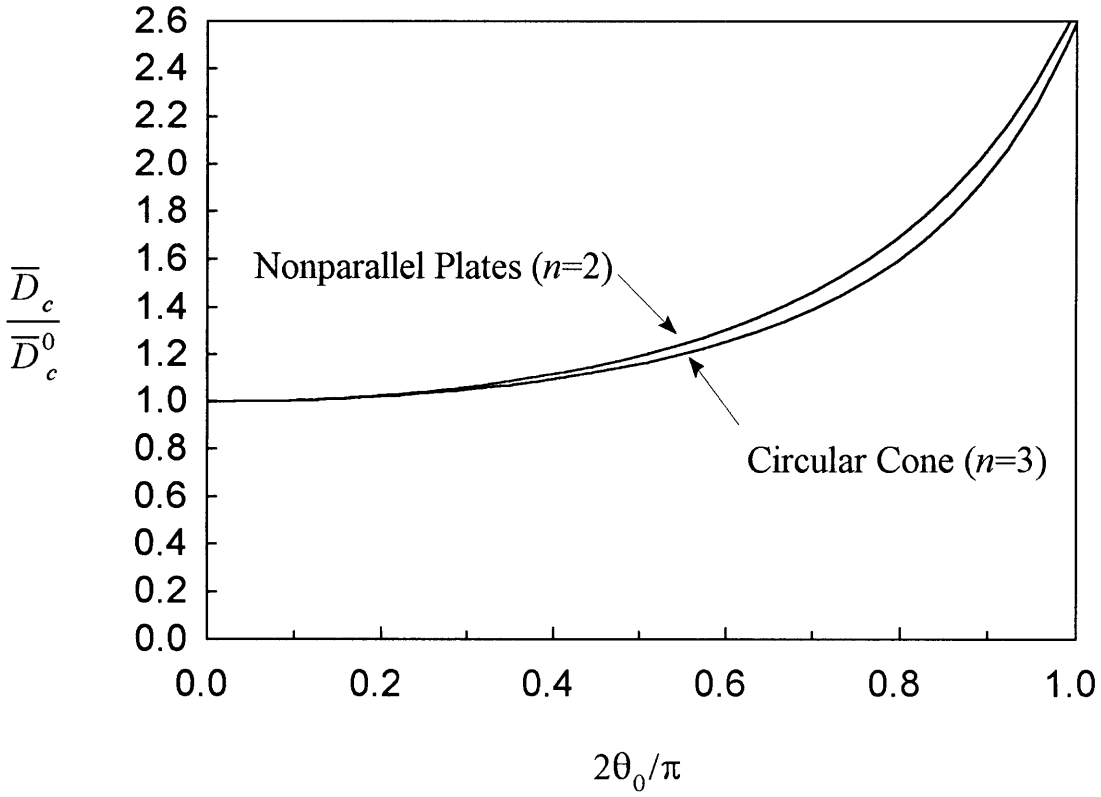

Figure 2-2: Convective contribution, $\overline{D_c}$, to the dispersion coefficient for axisymmetric low-Reynold's number flow between nonparallel plates or in a circular cone. Observe that for the limiting case where $\theta_0 = \pi/2$, the dispersivity ratio quantified by the ordinate attains the limiting values of $105/4\pi^2$ ($n = 2$) and $128/5\pi^2$ ($n = 3$).

use of Laplace transforms to be

$$\overline{P} = \frac{1}{2\overline{D}^* t}\left(\frac{r}{r'}\right)^{\frac{\mathrm{Pe}^*}{2}} \exp\left(-\frac{[r^2+(r')^2]}{4\overline{D}^* t}\right) \mathrm{I}_{\frac{|\mathrm{Pe}^*|}{2}}\left(\frac{rr'}{2\overline{D}^* t}\right), \tag{2.7-60}$$

in which

$$\mathrm{Pe}^* = \frac{\overline{Q}}{\overline{D}^*} \tag{2.7-61}$$

is the effective Péclet number and I_v is the modified Bessel function of order v .

Note that the two-dimensional case is unique in that the macrotransport equation (2.5-50) assumes the same functional form as the symmetric, purely radial form of the microscale equation (2.4-23). In contrast the three -dimensional macroscale equation possesses a different structure than the original microscale equation in regards to the final term appearing on the left-hand side of (2.5-50).

2.7.2 Circular cone

Solution of (2.4-42)–(2.4-44) for low-Reynolds number flow in a circular cone, for which the velocity is given by (2.2-6), followed by subsequent use of (2.4-47) and (2.5-51) yields (see figure 2-2):

$$\overline{D_c} = \frac{\overline{Q}^2}{15D}\frac{(1-\zeta_0)(2-3\zeta_0-23\zeta_0^2-38\zeta_0^3-8\zeta_0^4-2)+30\zeta_0^2(1+\zeta_0)^2\ln[2(\zeta_0+1)^{-1}]}{(1+2\zeta_0)^2(1-\zeta_0)^3}, \tag{2.7-62}$$

in which $\zeta_0 = \cos\theta_0$. As in the two-dimensional case, replacement of the flow rate with the average velocity $\overline{V} \overset{\mathrm{def}}{=} \overline{Q}/r^2$, introduction of the 'radius' $h \overset{\mathrm{def}}{=} \theta_0 r$ at any point in the cone, and expansion of the above in a Taylor series about $\theta_0 = 0$ demonstrates that in the limit $\theta_0 \to 0$, the dispersion coefficient reduces to the classical result for Taylor dispersion in a circular cylinder (Taylor 1953; Aris 1956):

$$\overline{D_c} \sim \overline{D_c^0}\left(1+\frac{13}{60}\theta_0^2+\ldots\right), \tag{2.7-63}$$

where

$$\overline{D_c^0} = \frac{1}{48}\frac{\overline{V}^2 h^2}{D} \qquad (n = 3). \tag{2.7-64}$$

The macroscale equation in three dimensions is

$$\frac{\partial \overline{P}}{\partial t} + \frac{\overline{Q}}{r^2}\frac{\partial \overline{P}}{\partial r} - \frac{\overline{D}}{r^2}\frac{\partial}{\partial r}\left(r^2\frac{\partial \overline{P}}{\partial r}\right) - \frac{\overline{D_c}}{r^2}\frac{\partial^2 \overline{P}}{\partial r^2} = \frac{\delta(r-r')}{r^2}\frac{\delta(t)}{1-\cos\theta_0}. \tag{2.7-65}$$

In this case, in contrast with the two-dimensional case (2.7-58), the convective dispersivity $\overline{D_c}$ contributes to the net transport differently than does the molecular diffusivity D, as can be seen by comparing the final two terms on the left-hand side of the above.

2.8 Discussion

2.8.1 Solute conservation

Although our analysis is valid for both converging and diverging flows, the semi-infinite configuration of the conical domain, coupled with the singularity of the velocity field at the apex $r = 0$, leads to fundamental differences in the temporal behavior of the probability densities for the respective cases of $Q > 0$ and $Q < 0$, all other things being equal. In particular, the total probability of a solute particle being located within the cone is conserved for diverging flow, but not for converging flow; rather, in the latter case there is a continuous loss of solute through the apex. Mathematically, this behavior may be seen by integrating the microscale equation (2.4-23) over the infinite domain V_∞ of the cone and applying the boundary conditions (2.4-24)–(2.4-26) to obtain (in dimensional form)

$$\frac{\mathrm{d}}{\mathrm{d}t}\int_{V_\infty} P \mathrm{d}V = Q\overline{P}|_{r=0}, \tag{2.8-66}$$

where $\mathrm{d}V \equiv \mathrm{d}S\mathrm{d}r \equiv r^{n-1}\sin^{n-2}\theta \mathrm{d}r\mathrm{d}\theta(\mathrm{d}\phi)$ is a 'volume' element. For $Q = 0$, the total amount of solute initially present in the cone is conserved for all time, as in the known results (Carslaw & Jaeger 1959) for pure diffusion in a wedge and in a circular cone. However, examination of the solution (2.7-60) of the macrotransport equation for $n = 2$ reveals that for $Q > 0$, $\overline{P}|_{r=0} = 0$ for all times $t > 0$. Hence, for diverging flow, the particle is always contained within the cone. The explanation for this phenomenon lies in the functional form of the velocity field, which varies inversely with radial position. A solute particle is never able to diffuse backwards to the apex of the cone because its diffusion is opposed by an infinite velocity in the positive direction. In contrast, for $Q < 0$, $\overline{P}$ assumes a finite positive value at the origin, namely

$$\overline{P}|_{r=0} = r'(2\overline{D}^* t)^{-\left(\frac{|\mathrm{Pe}^*|}{2}+1\right)} \exp\left(-\frac{(r')^2}{4\overline{D}^* t}\right). \tag{2.8-67}$$

Thus, solute exits the cone at its apex, eventually becoming entirely depleted.

2.8.2 Asymptotic behavior of the microscale field

Not only does our analysis result in an asymptotic equation for the macroscale probability density $\overline{P}$, but concomitantly it also furnishes an asymptotic approximation to the exact microscale probability density P. In particular, in combination, (2.4-30), (2.4-36) and (2.4-41) yield

$$P(r,\theta,t|r',\theta') \sim \overline{P}(r,t|r') + \frac{\overline{Q}\theta_0^2}{D} f(\theta/\theta_0) r^{3-n} \frac{\partial \overline{P}}{\partial r} + \ldots \quad . \tag{2.8-68}$$

This asymptotic expression is similar in appearance to the first two terms occurring in the expansion of Taylor (1954) (subsequently expanded upon by Gill 1967), with the exception of the presence of the coefficient r^{3-n} occurring in the second term on the right-hand side of the above, which arises from the varying cross-sectional area of the duct.

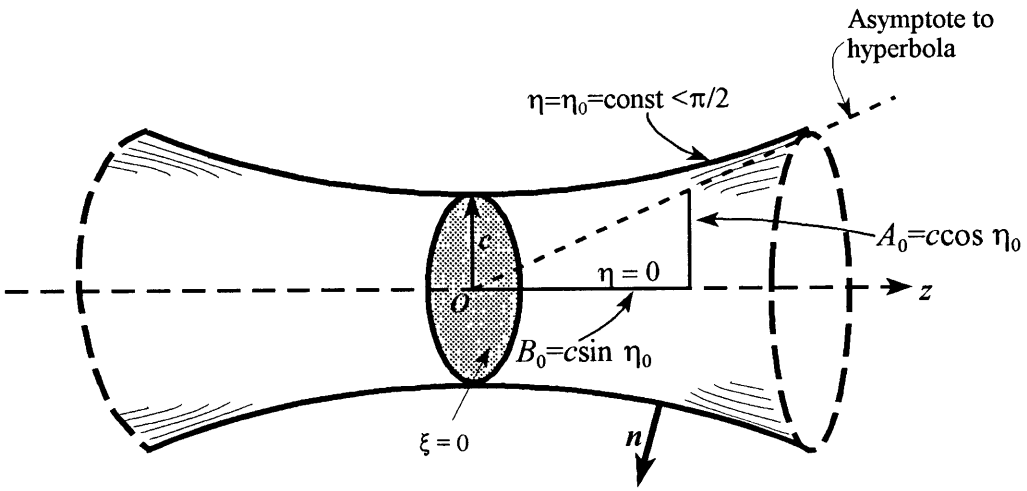

Figure 2-3: Hyperboloid of revolution ('Venturi' tube). The coordinate system is $q_1 = \xi$, $q_2 = \eta$, $q_3 = \phi$, with S_1 the domain $0 \leqslant \eta \leqslant \eta_0$, $0 \leqslant \phi < 2\pi$. The duct throat, corresponding to the value $\xi = 0$, is of radius c. The duct centerline corresponds to the value $\eta = 0$ and the unit normal vector $\boldsymbol{n}$ to the duct surface η_0 is the unit vector $\boldsymbol{i}_\eta = 0$ in oblate spherical coordinates. The major and minor axes A_0 and B_0 of the hyperboloid η_0 are respectively as shown in the sketch, with $B_0/A_0 = \tan\eta_0$; thus, the angle between the z-axis and the dashed asymptote corresponds physically to the angle η_0.

2.9 Dispersion in curvilinear, cross-sectionally varying channels and ducts

The methods described herein may be utilized to analyze dispersion in generally varying channels and ducts whose boundaries are curvilinear rather than rectilinear. We use general orthogonal curvilinear coordinates (Happel & Brenner 1983) (q_1, q_2, q_3) and consider 'unidirectional' flows whose streamlines lie along the q_1 coordinate curves. Flow through a hyperbolic cone or 'Venturi' tube (Happel & Brenner 1983, p.150) as in figure 2-3 constitutes an example of this class. We will confine ourselves to the three-dimensional, duct-flow case, although the analysis is easily extended to two-dimensional, channel flows. The surface of the duct will be taken to be defined by the functional relation $F(q_2, q_3) = \text{const}$. The continuity equation in such

a coordinate system is

$$\frac{\partial}{\partial q_1}\left(\frac{u_1}{h_2 h_3}\right) = 0, \tag{2.9-69}$$

in which the scalar $u_1(q_1, q_2, q_3)$ is the speed $h_i(q_1, q_2, q_3)$ and is the metrical coefficient in the q_i direction. The velocity field is thus of the form

$$u_1 = h_2 h_3 q(q_2, q_3). \tag{2.9-70}$$

In this notation, the convection-diffusion equation governing the conditional probability density $P(q_1, q_2, q_3, t|q_1', q_2', q_3')$ is

$$\frac{\partial P}{\partial t} + h_1 h_2 h_3 q(q_2, q_3)\frac{\partial P}{\partial q_1} - D h_1 h_2 h_3 \Big[\frac{\partial}{\partial q_1}\left(\frac{h_1}{h_2 h_3}\frac{\partial P}{\partial q_1}\right) + \frac{\partial}{\partial q_2}\left(\frac{h_2}{h_1 h_3}\frac{\partial P}{\partial q_2}\right) + \frac{\partial}{\partial q_3}\left(\frac{h_3}{h_1 h_2}\frac{\partial P}{\partial q_3}\right)\Big] = \delta(t)\delta(q_1 - q_1')\delta(q_2 - q_2')\delta(q_3 - q_3')h_1 h_2 h_3. \tag{2.9-71}$$

We now follow a procedure similar to that used in our previous analysis. It is again required that the convection time be much larger than the transverse diffusion time. The ratio of these times is given by $|\varepsilon|$, where

$$\varepsilon = \frac{\overline{Q}\|q_2\|^2\|h_1\|\|h_3\|}{D\|q_1\|\|h_2\|}. \tag{2.9-72}$$

Here, the brackets $\|...\|$ denote an appropriate norm of the quantity they bound; q_2 is the coordinate corresponding to the largest of the two transverse directions, and the constant $\overline{Q}$ is related to the volumetric flow rate Q through the duct (both $\overline{Q}$ and Q being independent of the 'axial' distance q_1) as follows:

$$\overline{Q} = Q \Big/ \int_{S_1} \mathrm{d}q_2 \mathrm{d}q_3, \tag{2.9-73}$$

where

$$Q = \int_{S_1} q(q_2, q_3) \mathrm{d}q_2 \mathrm{d}q_3. \tag{2.9-74}$$

Here, S_1 denotes the 'cross-sectional' domain corresponding to the surface defined by $q_1 = \text{const.}$ and bounded by the curvilinear duct wall, $F(q_2, q_3) = \text{const.}$

Upon performing a multiple-timescale analysis similar to that for the circular cone, the macrotransport equation governing the macroscale conditional probability density $\overline{P}(q_1, t|q_1')$ is ultimately found to be

$$\frac{\partial \overline{P}}{\partial t} + \frac{Q}{\overline{A}} \frac{\partial \overline{P}}{\partial q_1} - \frac{D}{\overline{A}} \frac{\partial}{\partial q_1} \left(\chi \frac{\partial \overline{P}}{\partial q_1} \right) - \frac{1}{\overline{A}} \frac{\partial}{\partial q_1} \left(\overline{D_c} \frac{\partial \overline{P}}{\partial q_1} \right) = \frac{1}{\overline{A}} \delta(t) \delta(q_1 - q_1'), \tag{2.9-75}$$

in which

$$\overline{A}(q_1) = \int_{S_1} \frac{\mathrm{d}A_1}{h_1} \tag{2.9-76}$$

and

$$\chi(q_1) = \int_{S_1} h_1 \mathrm{d}A_1, \tag{2.9-77}$$

where $\mathrm{d}A_1 = \mathrm{d}q_2 \mathrm{d}q_3 / h_2 h_3$ is a differential areal element on the surface $q_1 = \text{const.}$ The convective contribution $\overline{D_c}$ to the dispersion required in (2.9-75) is given by

$$\overline{D_c}(q_1) = -\frac{\overline{Q}^2}{D} \int_{S_1} v(q_2, q_3) g(q_1, q_2, q_3) \mathrm{d}q_2 \mathrm{d}q_3, \tag{2.9-78}$$

with

$$v = \frac{q(q_2, q_3)}{\overline{Q}}. \tag{2.9-79}$$

The function $g(q_1, q_2, q_3)$ appearing above represents the solution of the following boundary value problem:

$$\left[\frac{\partial}{\partial q_2} \left(\frac{h_2}{h_1 h_3} \frac{\partial g}{\partial q_2} \right) + \frac{\partial}{\partial q_3} \left(\frac{h_3}{h_1 h_2} \frac{\partial g}{\partial q_3} \right) \right] = v - \frac{\overline{A^{-1}}}{h_1 h_2 h_3} \int_{S_1} \mathrm{d}q_2 \mathrm{d}q_3, \tag{2.9-80}$$

$$\boldsymbol{n} \cdot \nabla g = 0 \quad \text{on} \quad F(q_2, q_3) = \quad \text{const.}, \tag{2.9-81}$$

$$\int_{S_1} g \frac{\mathrm{d}A_1}{h_1} = 0. \tag{2.9-82}$$

In the above, $\boldsymbol{n}$ represents the unit vector normal to the surface of the duct. Use of (2.9-80)–(2.9-82) in (2.9-78) allows $\overline{D_c}$ to be written in an alternative form which demonstrates that the dispersivity is nonnegative:

$$\overline{D_c} = \int_{S_1} \left[\left(h_2 \frac{\partial g}{\partial q_2} \right)^2 + \left(h_3 \frac{\partial g}{\partial q_3} \right)^2 \right] \frac{\mathrm{d}A_1}{h_1}. \tag{2.9-83}$$

The 'average' probability density function appearing in the macrotransport equation (2.9-75) is defined as

$$\overline{P} \stackrel{\text{def}}{=} \int_{S_1} P \frac{\mathrm{d}A_1}{h_1} \Big/ \int_{S_1} \frac{\mathrm{d}A_1}{h_1}. \tag{2.9-84}$$

In our prior discussion of dispersion in a cone and between non-parallel plates, the average utilized was an *area* average. The above average is equal to the *volume* average taken over an infinitesimal volume centered at a given 'axial' position q_1

$$\overline{P} = \lim_{\delta \to 0} \left(\int_{S_1} \int_{q_1 - \delta}^{q_1 + \delta} P \mathrm{d}V \Big/ \int_{S_1} \int_{q_1 - \delta}^{q_1 + \delta} \mathrm{d}V \right), \tag{2.9-85}$$

where $\mathrm{d}V = \mathrm{d}q_1 \mathrm{d}q_2 \mathrm{d}q_3 / h_1 h_2 h_3$ is a differential volume element. The quantity defined in (2.9-85) is identically equal to the area average in the conical geometry considered previously, since in that case h_1 is independent of q_2 and q_3.

The *physical* form of (2.9-75) becomes especially transparent in circumstances where the metrical coefficient h_1 is, at most, a function only of q_1, and hence independent of q_2 and q_3. Since the quantity $\mathrm{d}q_1/h_1 = \mathrm{d}l_1$, say, is the arc length, measured along the q_1-coordinate curve (Happel & Brenner 1983), it follows that when h_1 is of the form $h(q_1) \equiv h_1(l_1)$, the quantity $\mathrm{d}l_1$ is then an exact differential. Consequently,

the arc length l_1 possesses a global physical interpretation. In such circumstances, (2.9-76) and (2.9-77) become $\overline{A} = A_1/h_1$ and $\chi = h_1 A_1$, where $A_1(q_1) \equiv A_1(l_1)$ is the 'cross-sectional' area of the duct corresponding to the domain S_1. Moreover, the 'volume average' probability density $\overline{P}$ defined by (2.9-84) becomes identical with the (curvilinear) area-average probability density $\int_{S_1} P \mathrm{d}A_1/A_1$. In these circumstances, the macrotransport equation (2.9-75) governing $\overline{P} \equiv \overline{P}(l_1, t|l_1')$ adopts the form

$$\frac{\partial \overline{P}}{\partial t} + \frac{Q}{A_1}\frac{\partial \overline{P}}{\partial l_1} - \frac{D}{A_1}\frac{\partial}{\partial l_1}\left(A_1 \frac{\partial \overline{P}}{\partial l_1}\right) - \frac{1}{A_1}\frac{\partial}{\partial l_1}\left(\overline{D_c^*}\frac{\partial \overline{P}}{\partial l_1}\right) = \frac{1}{A_1}\delta(t)\delta(l_1 - l_1'), \quad (2.9\text{-}86)$$

in which

$$\overline{D_c^*} = \overline{D_c} h_1. \quad (2.9\text{-}87)$$

An example of a configuration for which h_1 is independent of q_2 and q_3 occurs for the circular cone case, where (Happel & Brenner 1983, p.504) with the choice $(q_1, q_2, q_3) = (r, \theta, \phi)$, we have that

$$h_1 = 1, \qquad h_2 = 1/r, \qquad h_3 = 1/r\sin\theta, \quad (2.9\text{-}88)$$

and hence $l_1 = r$, $A_1 = \chi = 2\pi(1 - \cos\theta_0)r^2$. In this case (2.9-86) reproduces (2.7-65).

2.9.1 Dispersion in a flared, 'Venturi' tube

As an application of the general curvilinear analysis embodied in (2.9-75), consider the problem of convection and diffusion in a 'Venturi' tube (i.e., a hyperboloid of revolution of one sheet, as in figure 2-3). Such a flow may be described in oblate spheroidal coordinates ($-\infty < \xi < \infty, \quad 0 \leqslant \eta \leqslant \pi/2, \quad 0 \leqslant \phi \leqslant 2\pi$), in which the hyperboloidal surface of the tube is $\eta = \eta_0$. (This coordinate system is identical to that appearing in Happel & Brenner (1983, p.512) with the exception of the ranges of η and ξ.) These coordinates are related to circular cylindrical coordinates (z, R, ϕ),

having their origin O at the center of the tube throat, by the relations

$$z = c\sinh\xi\cos\eta, \qquad R = c\cosh\xi\sin\eta. \tag{2.9-89a, b}$$

The coordinate surfaces ξ = const. and ϕ = const. are respectively oblate spheroids and meridian planes, the latter containing the z-axis.

The axisymmetric stream function for the low-Reynolds number flow through the tube is (Happel & Brenner 1983; Sampson 1891)

$$\Psi = \frac{Q}{2\pi}\frac{\zeta(\zeta^2 - 3\zeta_0^2) - (1 - 3\zeta_0^2)}{(1 + 2\zeta_0)(1 - \zeta_0)^2}, \tag{2.9-90}$$

in which $\zeta = \cos\eta$ and $\zeta_0 = \cos\eta_0$ denotes the surface of the duct, so that the streamlines are hyperbolas, lying on the coordinate surfaces η = const. in a meridian plane (ϕ = const). In contrast to the previous cases of flow in a circular cone or between nonparallel plates, in the present geometry the flow contains both 'diverging' and 'converging' regions and no singularity exists at the origin.

In this oblate spheroidal coordinate system, the quantities necessary for determination of the macroscale equation are

$$h_1 = h_2 = \frac{1}{c(\cosh^2\xi - \sin^2\eta)^{\frac{1}{2}}}, \tag{2.9-91}$$

$$h_3 = \frac{1}{c\cosh\xi\sin\eta} \tag{2.9-92}$$

and

$$q(\eta) = -\frac{\mathrm{d}\Psi}{\mathrm{d}\eta}. \tag{2.9-93}$$

The condition which must be met in order for the present multiple-timescale analysis

to apply is again $|\varepsilon| \ll 1$, with

$$\varepsilon = \frac{\overline{Q}\eta_0^2}{Dc\xi_0 \cosh \xi_0}, \tag{2.9-94}$$

in which ξ_0 is a characteristic value[1] of the 'axial' coordinate ξ, and

$$\overline{Q} = \frac{Q}{2\pi\eta_0}. \tag{2.9-95}$$

Solution of (2.9-80) subject to (2.9-81)–(2.9-82) yields

$$\frac{\partial g(\eta,\xi)}{\partial \eta} = \frac{3\eta_0}{c\cosh\xi \sin\eta} \frac{(1-\zeta)(\zeta-\zeta_0)(\zeta+\zeta_0+1)(\cosh^2\xi+\zeta_0^2-1)}{(1+2\zeta_0)(1-\zeta_0)^2(3\cosh^2\xi+\zeta_0^2+\zeta_0-2)}. \tag{2.9-96}$$

The resulting macroscale equation is then of the form (2.9-75) with

$$\overline{A}(\xi) = c^3 C_0 \lambda(3\lambda^2 + C_1), \tag{2.9-97}$$

$$\chi(\xi) = 3cC_0\lambda, \tag{2.9-98}$$

$$\overline{D_c}(\xi) = \frac{\overline{Q}^2}{cD} \frac{(\lambda^2+C_2)^2}{\lambda(3\lambda^2+C_1)^2} C_3, \tag{2.9-99}$$

in which $\lambda = \cosh\xi$, and the constants C_i are functions only of η_0 as follows:

$$C_0 = (2/3)\pi(1-\zeta_0), \tag{2.9-100}$$

$$C_1 = \zeta_0^2 + \zeta_0 - 2, \tag{2.9-101}$$

$$C_2 = \zeta_0^2 - 1, \tag{2.9-102}$$

[1]For long axial distances from the tube throat, the distance $r = (R^2+z^2)^{\frac{1}{2}}$ from the origin approximates $r \approx c\cosh\xi$, while the transverse distance approximates $h \approx c\eta_0 \cosh\xi$. The parameter ε is thus proportional to the ration of the transverse diffusion time τ_D to the axial convection time τ_Q, respectively defined as $\tau_D = h^2/D, \quad \tau_Q = r^3/\overline{Q}$.

$$C_3 = \frac{6\pi\eta_0^2}{5}\frac{(1-\zeta_0)(2-3\zeta_0-23\zeta_0^2-28\zeta_0^3-8\zeta_0^4)+30\zeta_0^2(\zeta_0+1)^2\ln[2(\zeta_0+1)^{-1}]}{(1+2\zeta_0)^2(1-\zeta_0)^4}. \tag{2.9-103}$$

The above Venturi tube results may be compared with the circular cone results, (2.7-62)–(2.7-65), as follows. Referring to figure 2-3, it is seen that at large distances $|\xi| \to \infty$ along the axis, the hyperboloidal duct surface is isomorphic with the surface of the circular cone of half-angle $\theta_0 \equiv \eta_0$ in figure 2-1(b). From (2.9-89 a,b), we find that the distance $r = (R^2 + z^2)^{\frac{1}{2}}$ from the origin O is $r = c(\cosh^2\xi - cos^2\eta)^{\frac{1}{2}}$, which for $|\xi| \to \infty$ asymptotes to $r \sim c\cosh\xi$. Additionally, from (2.9-91), we see that, asymptotically $h_1 \sim (c\cosh\xi)^{-1}$, which is independent of η and ϕ, and thus asymptotically fulfills the requirement set forth in the paragraph following (2.9-85). Use of the above asymptotic relation for h_1 and the dispersivity (2.9-99) in (2.9-87) reveals that in this limit, $\overline{D_c^*}$ is independent of the axial position $l_1 \sim r$ (l_1 being calculated from its definition, $\mathrm{d}l_1 = \mathrm{d}\xi/h_1$), and may therefore be brought to the outside of the derivative in which it appears in the macrotransport equation (2.9-86). The ratio $\overline{D_c^*}/A_1$ then reduces to the form

$$\frac{\overline{D_c^*}}{A_1} = \frac{\overline{Q}^2}{D}\frac{C_3}{18\pi(1-\zeta_0)r^2}, \tag{2.9-104}$$

which may be shown, through use of the respective (albeit slightly different) definitions (2.9-95) and (2.3-21) for $\overline{Q}$ in the hyperboloidal and conical cases, to be exactly equal to the dispersivity (2.7-62) in the case of a circular cone, bearing in mind that $\theta_0 \equiv \eta_0$. Straightforward calculation shows that the other terms appearing in the macrotransport equation (2.9-86) are also identical to their counterparts in the circular cone case, (2.7-65).

Finally, we note that the case of flow through a circular aperture in a wall occurs when $\eta_0 = \pi/2$ ($\zeta_0 = 0$).

References

[1] ACKERBERG, R. C. 1965 The viscous incompressible flow inside a cone. *J. Fluid Mech.* **21**, 47–81.

[2] ARIS, R. 1956 On the dispersion of a solute in a fluid flowing through a tube. *Proc. Roy. Soc.* A **235**, 66–77.

[3] BRENNER, H. & EDWARDS, D. A. 1993 *Macrotransport Processes.* Butterworth-Heinemann.

[4] BRYDEN, M. & BRENNER, H. 1996 Multiple-timescale analysis of Taylor dispersion in converging and diverging flows. *J. Fluid Mech.* **311**, 343–359.

[5] CARSLAW, H. S. & JAEGER, J. C. 1959 *Conduction of Heat in Solids.* Oxford University Press.

[6] CHATWIN, P. C. 1970 The approach to normality of the concentration distribution of a solute in a solvent flowing along a straight pipe. *J. Fluid Mech.* **20**, 321–352.

[7] FRANKEL, I. & BRENNER, H. 1991 Generalized Taylor dispersion phenomena in unbounded shear flows. *J. Fluid Mech.* **230**, 147–181.

[8] GILL, W. N. 1967. Analysis of axial dispersion with time variable flow. *Chem. Eng. Sci.* **22**, 1013–1017.

[9] GILL, W. N. & GÜCERI, U. 1971 Laminar dispersion in Jeffrey-Hamel flows: Part 1. Diverging channels. *AIChE J.* **17**, 207–214.

[10] GOLDSTEIN, S. 1965*a* *Modern Developments in Fluid Dynamics v1*. Dover (reprint).

[11] GOLDSTEIN, S. 1965*b* On backward boundary layers and flow in converging passages. *J. Fluid Mech.* **21**, 33–45.

[12] HAPPEL, J. & BRENNER, H. 1983 *Low Reynolds Number Hydrodynamics.* Kluwer.

[13] MERCER, G. N. & ROBERTS, A. J. 1990 Centre manifold description of contaminant dispersion in channels with varying flow properties. *SIAM J. Appl. Math.* **50**, 1547–1565.

[14] PAGITSAS, M., NADIM, A. & BRENNER, H. 1986 Multiple time scale analysis of macrotransport processes. *Physica* **135**A, 533–550.

[15] ROUSE, H. 1959 *Advanced Mechanics of Fluids*. Wiley.

[16] SAMPSON, R. A. 1891 On Stoke's current function. *Phil. Trans. Roy. Soc.* A **182**. 449–518.

[17] SMITH, R. 1983 Longitudinal dispersion coefficients for varying channels. *J. Fluid Mech.* **130**, 299–314.

[18] TAYLOR, G. I. 1953 Dispersion of soluble matter in a solvent flowing slowly through a tube. *Proc. Roy. Soc.* A **219**, 186–203.

[19] TAYLOR, G. I. 1954 Conditions under which dispersion of a solute in a stream of solvent can be used to measure molecular diffusion. *Proc. Roy. Soc.* A **225**, 473–477.

[20] WOODING, R.A. 1960 Instability of a viscous fluid of variable density in a vertical Hele-Shaw cell. *J. Fluid Mech.* **7**, 501–515.

Chapter 3

Laminar Chaos: Background

3.1 Introduction

The existence of chaotic laminar flows was first demonstrated by Aref (1984). The seemingly contradictory suggestion that chaos could exist within a laminar flow has since been confirmed both theoretically and experimentally in numerous studies (see Ottino 1990 for a review). In contrast to turbulent flows, in which the instantaneous flow field is chaotic and apparently random, in a laminar chaotic flow the flow field is completely known. The particle trajectories, however, may behave chaotically. Such flows may prove useful for improving transport in circumstances for which turbulent flows are impractical. For example, suspensions of living cells used in biotechnology cannot be subjected to the high shear rates produced by turbulent flows without causing damage to the cells. Similarly, many polymers suffer degradation due to locally high shear rates. In other instances, where the fluid is highly viscous, or even viscoelastic, it may not be practical to produce a turbulent flow. Laminar chaotic flows have the ability to provide thorough and rapid mixing without the high shear rates and potentially large power requirements accompanying turbulent flows.

Chaotic trajectories are possible because the Lagrangian equation

$$\frac{d\mathbf{x}}{dt} = \mathbf{v}(\mathbf{x}, t) \tag{3.1-1}$$

for the particle trajectories $\mathbf{x} \equiv \mathbf{x}(\mathbf{x}_0, t)$ (with $\mathbf{x}_0$ the initial position vector at time $t = 0$) comprises, in many instances, a set of coupled non-linear equations, with the instantaneous velocity $\mathbf{v}$ a non-linear function of the position vector $\mathbf{x}$. Chaos is often described as the exponential divergence (in time) of initial conditions. In the case of laminar flows, the presence of such exponential divergence assures that a solute locally dissolved within a fluid subjected to a chaotic laminar flow will soon disperse throughout the fluid even in the absence of molecular diffusion or turbulent eddies.

Moreover, small perturbations in the particle positions — caused for instance by molecular diffusion — are magnified by the chaotic flow, further increasing the extent of solute spreading. The unavoidability of such perturbations signifies that laminar chaotic flows are irreversible. [This observation provides the basis for a proposed separation technique based on differences in diffusivities (Aref & Jones 1989).] The common belief that laminar flows are necessarily reversible results from experiments and analyses with linear flows. Taylor's famous 'unmixing' experiment, for example, was conducted in a linear Couette flow, in which the trajectories constitute solutions of equations of the form

$$\begin{aligned} \frac{d\theta}{dt} &= f(r), \\ \frac{dr}{dt} &= 0, \end{aligned} \tag{3.1-2}$$

with r the radial coordinate and θ the angular coordinate. The position at time t of a particle initially located at (r_0, θ_0) is $(r_0, \theta_0 + f(r_0)t)$. Thus a perturbation in the particle position grows at most linearly in time, assuring that the flow is reversible. In general, however, pathlines in laminar flows need not be reversible and

this sensitivity to small perturbations enhances the mixing effectiveness of these flows (Dutta & Chevray 1995).

3.2 Examples of chaotic laminar flows

An incompressible flow must be either time-dependent and at least two dimensional (possessing two non-zero velocity components) or, if steady, three-dimensional in order to exhibit chaotic behavior. This conclusion derives from the observation that a two-dimensional flow is a Hamiltonian system, with the stream function ψ representing the Hamiltonian; that is,

$$v_1 = \frac{dx_1}{dt} = \frac{\partial \psi}{\partial x_2}, \qquad v_2 = \frac{dx_2}{dt} = -\frac{\partial \psi}{\partial x_1}. \tag{3.2-3}$$

A two-dimensional autonomous Hamiltonian system is always integrable. (See Doherty & Ottino 1988 for an explanation of Hamiltonian chaos directed towards chemical engineers.) Chaotic laminar flows may thus be divided into three categories: (i) two-dimensional, time-periodic flows; (ii) three-dimensional, spatially-periodic flows; and (iii) three-dimensional confined flows. These flows possess curved streamlines and are unsteady from a Lagrangian perspective, a result of temporal or spatial variations in the flow field. In each, the streamlines at successive times or positions cross one another. This crossing of streamlines provides the mechanism by which two particles, initially close to one another on the same streamline, may be transferred to different streamlines, thus allowing their relative positions to diverge in time. Examples of each of these three classes of flows are discussed in the following sections.

3.2.1 Three-dimensional spatially-periodic flows

The first example of a laminar chaotic flow was the so-called ABC flow,

$$\begin{aligned} v_1 &= A \sin x_3 + C \cos x_2, \\ v_2 &= B \sin x_1 + A \cos x_3, \\ v_3 &= C \sin x_2 + B \cos x_1, \end{aligned} \tag{3.2-4}$$

shown to be chaotic by Arnold (1965) and Hénon (1966) and investigated further by Dombre *et al.* (1986). Numerical integration of this flow to obtain the trajectories is straightforward, but the flow itself is not easily generated physically, as it requires the continuous application of a three-dimensional spatially-periodic force to the fluid.

A more realistic flow is represented by the partitioned-pipe mixer (Khakhar, Franjione & Ottino 1987, Kusch & Ottino 1992) (see figure 3-1). This spatially-periodic flow is generated by positioning flat plates along the centerline of a pipe. The plates are placed perpendicular to one another in a periodic fashion (i.e. first one plate of length l, say, followed by a second plate placed perpendicular to it, with this pattern repeated along the entire length of the tube). The pipe wall is rotated relative to the plates, while a pressure-driven laminar axial flow conveys the fluid through the apparatus. Transverse streamlines for this flow are illustrated in figure 3-1. In this flow, the requisite crossing of streamlines occurs when a given particle reaches the juncture between two plates, at which point it encounters a secondary flow oriented at right angles to the flow to which it had previously been subjected.

A similar spatially-periodic flow is the 'twisted-pipe' flow. The fluid motion here consists of an axial flow through a twisted pipe, the axis of curvature of which changes periodically along the axis of the pipe. The secondary flow induced by the pipe curvature thus varies periodically along the pipe, creating chaotic trajectories. This flow, proposed as an improved heat-exchanger design, has been demonstrated experimen-

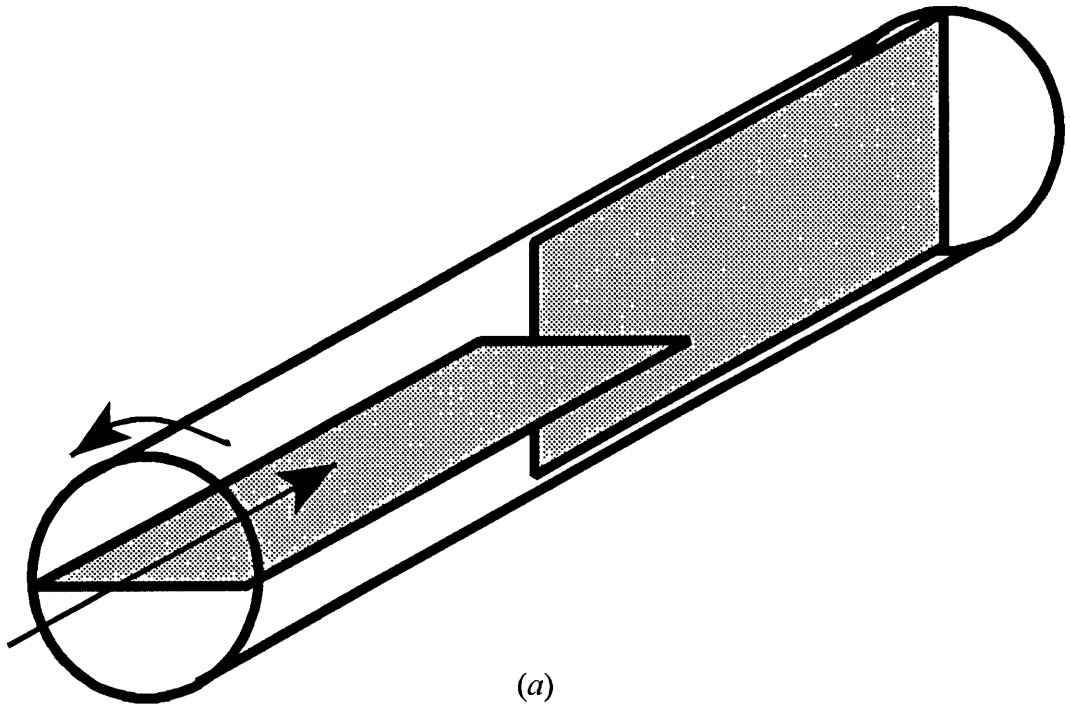

(*a*)

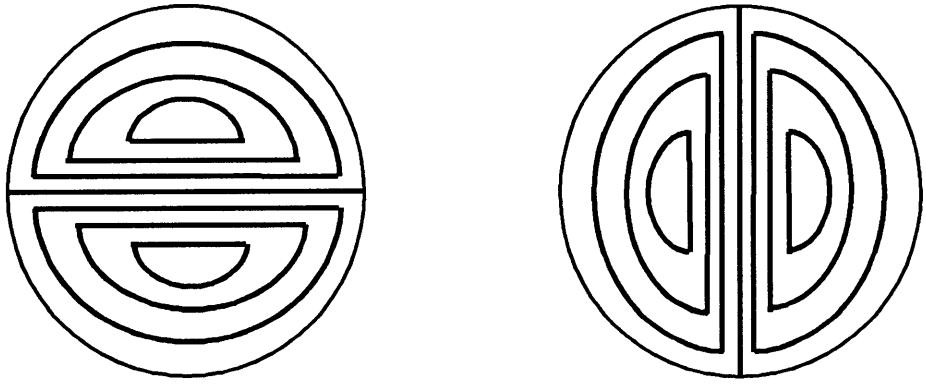

(*b*)

Figure 3-1: Partitioned-pipe mixer: (*a*) 'unit-cell' geometry; (*b*) transverse streamlines.

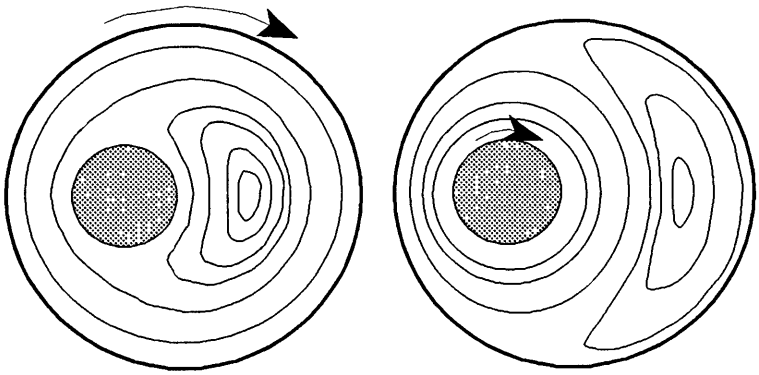

Figure 3-2: Streamlines in the annular region between rotating, nonconcentric cylinders: (*a*) Outer cylinder rotation; (*b*) Inner cylinder rotation.

tally to increase the heat-transfer rate (Acharya, Sen & Chang 1992).

3.2.2 Two-dimensional time-periodic flows

Two-dimensional flows which exhibit chaos include the blinking vortex flow (Aref 1984), time-periodic cavity flows (Jana & Ottino 1992), and eccentric annular flow (Aref & Balachandar 1986, Chaiken, Chu, Tabor & Tan 1987). Eccentric annular flow (figure 3-2) is considered in detail in this thesis. It is produced by the alternate (or other time-periodic) rotation of two cylinders, one located nonconcentrically within the other. For sufficiently large eccentricities, the transverse streamlines for single-cylinder rotation contain recirculating regions near the stationary cylinder (figure 3-2). Time-periodic rotation of the two cylinders provides the requisite crossing of streamlines at successive times and can produce chaos for the proper choices of geometry, rotation period, and relative angular velocities of the two cylinders.

3.2.3 Three-dimensional confined flows

All three-dimensional confined chaotic laminar flows studied to date in the literature are flows confined within a spherical domain. These include time-dependent spherical Couette flows (Cartwright, Feingold & Piro 1996) and flows within a droplet (Bajer

& Moffatt 1990, Stone, Nadim & Strogatz 1991). The flows considered by Stone *et al.* (1991) were those occurring within a neutrally-buoyant droplet suspended in a general three-dimensional linear external flow. The present work addresses a related but novel chaotic flow within a droplet, namely the flow generated within a non-neutrally buoyant droplet translating through an exterior fluid undergoing a simple shearing motion. This flow may be produced by allowing a bubble to translate by buoyancy through the annular space of a vertical concentric-cylinder Couette flow apparatus, possibly accompanied by a vertical Poiseuille flow (see figure 3-3). Figure 3-4 shows the droplet streamlines occurring in the interior of the droplet for the respective cases of translation of a non-neutrally buoyant bubble through a quiescent fluid and of a (non-translating) neutrally-buoyant droplet suspended within a simple shear flow. Superposition of these two flows can create chaotic trajectories, depending upon their relative orientation. For example, suppose that the direction of translational motion is perpendicular to the shear plane. The translational motion thus moves a particle contained within the droplet vertically through the plane of shear. As the particle moves in this vertical direction, it passes from one region of the shear-produced flow to another; these differing regions may possess crossing streamlines, a necessary precursor to chaos.

3.3 Assessment of laminar chaos

Several methods currently exist for assessing the effectiveness of a given laminar chaotic flow. Each, however, has limitations, being either difficult to compute, to interpret, or both.

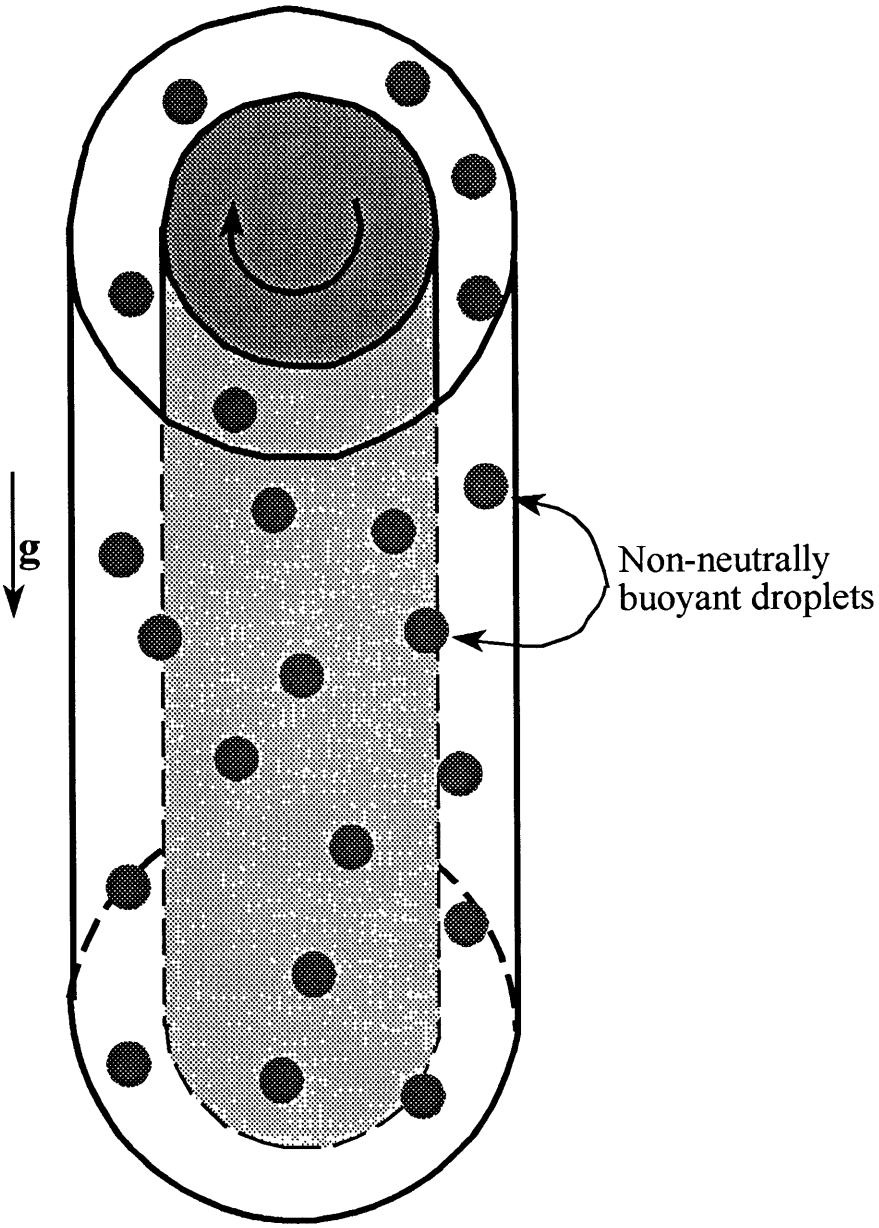

Figure 3-3: Annular flow apparatus for creating a chaotic laminar flow within a non-neutrally buoyant droplet. The droplet translates by buoyancy parallel to the axis of the cylinders, one of which is rotated to produce a Couette flow. A gravity- or pressure-driven axial laminar flow may also be present in the annular region between the cylinders.

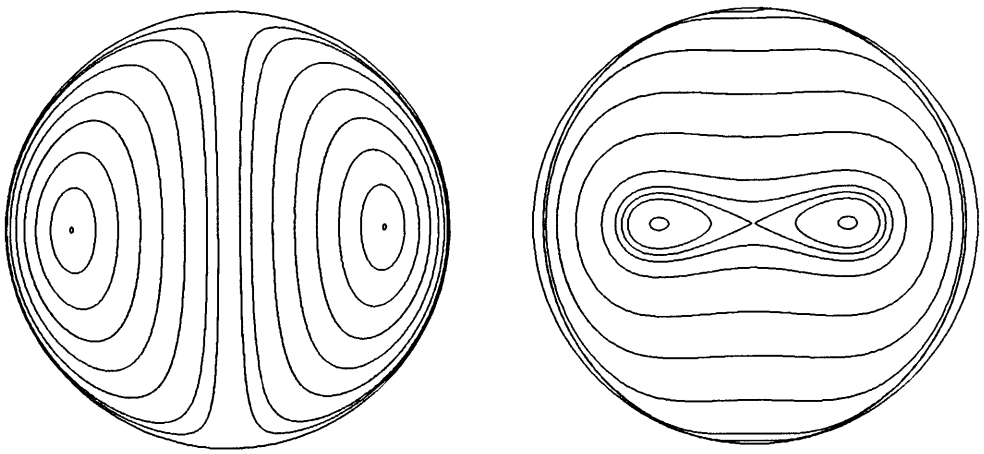

Figure 3-4: Streamlines within a spherical droplet: (a) translating through a quiescent fluid; (b) suspended within a simple shear flow.

3.3.1 Liapunov exponents

The rate of divergence of initial conditions, quantified by Liapunov exponents, is one measure commonly used for studying chaotic systems. In the case of laminar chaotic flows, Liapunov exponents are calculated by computing the trajectories of two initially proximate particles, initially joined by a vector $d\mathbf{X}_0$ and located at a point $\mathbf{X}_0$. The Liapunov exponents λ are then determined as follows:

$$\lambda(\mathbf{X}_0, d\mathbf{X}_0) \equiv \lim_{t\to\infty} \lim_{|d\mathbf{X}_0|\to 0} \left\{ \frac{1}{t} \ln\left(\frac{|d\mathbf{X}|}{|d\mathbf{X}_0|} \right) \right\}. \tag{3.3-5}$$

A positive Liapunov exponent indicates that initial conditions diverge exponentially in time, whereas a negative value corresponds to convergence; that is, two material particles, initially distant from one another, will eventually reach the same position, where they will remain for all subsequent times. Linear flows, such as Poiseuille or Couette flow, have two zero Liapunov exponents, a consequence of their linear (as opposed to exponential) divergence of initial conditions.

Liapunov exponents have the advantage of providing a quantitative measure of the degree of chaos. Unfortunately, they are difficult to calculate. Each N-dimensional

flow has up to N independent exponents, one for each linearly independent initial orientation of the vector $d\mathbf{X}_0$ joining the two particles. Special precautions are necessary to assure that the Liapunov exponent for each orientation is calculated correctly. Without these precautions, calculations for almost all orientations will yield the value of the maximum exponent (Lichtenberg & Lieberman 1983).

Even when one is assured of correctly calculating all of the Liapunov exponents, questions as to their usefulness and interpretation remain. As these exponents are functions of position, characterization of an entire flow field necessitates calculating many exponents at various positions. At best, this furnishes a large set of *local* measures of the effectiveness of the flow in promoting chaotic mixing, with no clear protocol for comparing the relative *global* effectiveness of different flow fields. Indeed, even the local interpretation of Liapunov exponents in quantifying the degree of chaos is not clear. For instance, is a flow possessing two exponents with large magnitudes – one positive and one negative – more or less effective than a flow with two smaller exponents, both of which are positive?

3.3.2 Poincaré sections

A tool which overcomes many of the difficulties with the computation and interpretation of Liapunov exponents is the Poincaré section. These plots provide a visual image of the trajectories within a given flow field. The information gleaned from these diagrams unambiguously indicates which regions of a given flow display chaotic behavior and, conversely, which are non-chaotic, or regular. These plots, widely used in the laminar chaos literature, are qualitatively useful in assessing the mixing ability of flows, as they provide a clear visualization of the location and extent of unmixed (regular) islands. The extent of these unmixed regions must be minimized if one wishes to produce a homogeneous mixture.

A Poincaré section is produced by integration of (3.1-1) to produce the Lagrangian

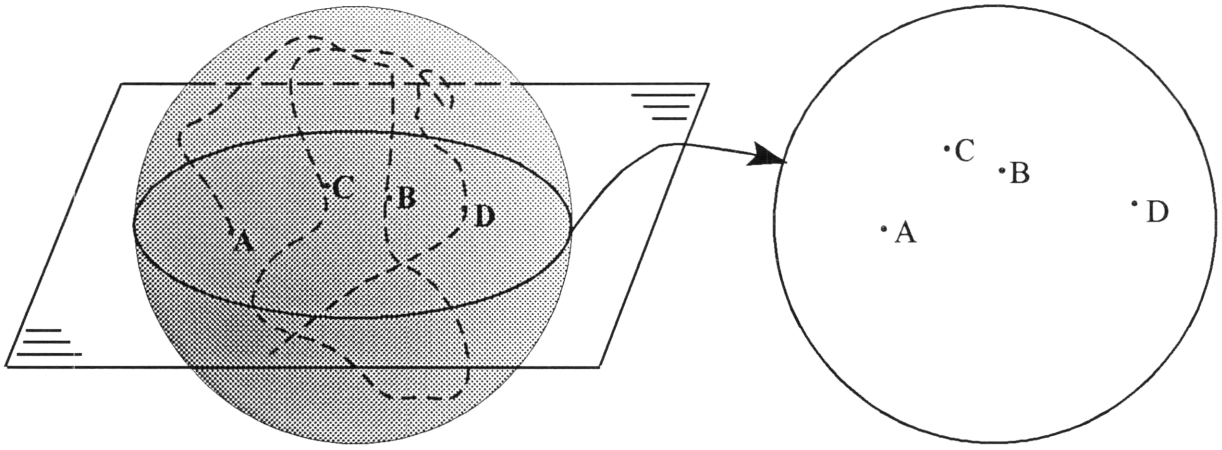

Figure 3-5: Construction of the Poincaré section for a flow within a spherical droplet.

trajectories $\mathbf{x} \equiv \mathbf{x}(\mathbf{x}_0, t)$ for several initial positions $\mathbf{x}_0$, typically spaced equidistant from one another throughout the flow. A plot of the complete particle trajectories would be contain so much information as to be confusing. Rather, the N-dimensional plot of the particle trajectories is reduced to a set of points plotted in an $N-1$ dimensional space. For instance, a Poincaré section corresponding to a three-dimensional confined flow, such as the flow existing within a spherical droplet (figure 3-5) consists of the intersection of the particle trajectories, which are curves in three-dimensional space, with an appropriately chosen plane. Time- and spatially-periodic flows are portrayed as in figure 3-6 by representing the trajectories as occurring within a torus, the periodic variable being represented by the coordinate around the torus. The intersection of a plane normal to the torus axis with the torus provides the Poincaré sections. Thus, a two-dimensional time-periodic flow with time period T is represented by plotting the positions of the particles at time t and at successive times $t + nT$, with n an integer. The Poincaré section for a three-dimensional spatially-periodic flow is constructed by plotting the two-dimensional positions of particles as they pass through the planes $z = z_0 + nl$, with z the coordinate along which the flow is periodic and l the spatial period.

Poincaré sections provide an easily-interpreted visualization of the behavior of a given flow field. A region of the flow which is chaotic will contain many apparently

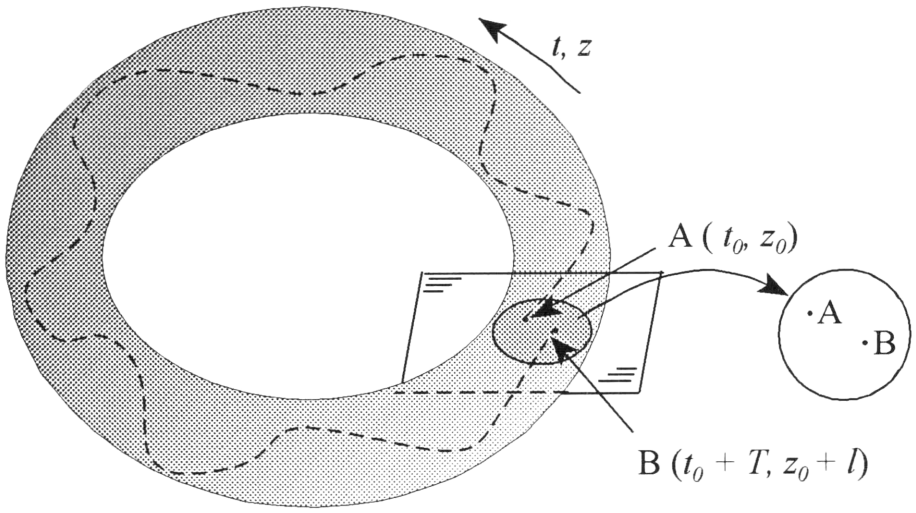

Figure 3-6: Construction of the Poincaré section for a time- or spatially-periodic flow.

randomly distributed points; non-chaotic regions will consist of easily identifiable closed curves. A completely regular flow will often produce a Poincaré section that simply reproduces the streamlines of the flow. In other circumstances, particularly in the case of confined three-dimensional flows, a non-chaotic flow will contain only closed pathlines; for such flows it is not possible to produce a meaningful Poincaré section, as the pathlines of each particle will intersect a given plane at only a finite (usually small) number of positions.

Poincaré sections are invaluable in determining which regions of a given flow are chaotic. As pointed out by Swanson & Ottino (1990), however, these diagrams may be subject to misinterpretation. One major failing is that many sets of initial conditions are plotted on the same diagram. Thus, no means exists to distinguish between the various trajectories corresponding to different initial conditions. Some chaotic trajectories may preferentially sample one portion of the chaotic region, but it is not possible to discern this from the Poincaré sections. To overcome this limitation, Swanson & Ottino (1990) suggest using a different color for each initial condition portrayed.

Unfortunately, Poincaré sections do not provide any *rate* information. They pro-

vide only a picture of the extent of chaos within a flow and suggest the degree of mixing which is possible, but furnish no indication as to the length of time required to achieve mixing.[1] Thus, while these plots may be useful in mixing applications for predicting whether or not a given flow provides effective mixing, they are less useful in predicting the utility of a given flow in enhancing the rate of heat- or mass-transfer processes. Also, they fail to include molecular diffusion, the effect of which may be significant, as diffusion allows solute molecules to escape from the regular regions in which they would otherwise be trapped. Furthermore, no *quantitative* measure of chaotic effectiveness can be gleaned from Poincaré sections.

3.3.3 Experimental studies

Purely kinematical experimental investigations of chaotic flows yield information similar to that contained within Poincaré sections. Such experiments (e.g. Swanson & Ottino 1990, Kusch & Ottino 1992, Dutta & Chevray 1995, Saatdjian *et al.* 1996) consist primarily of (non-diffusive) tracer studies, in which the position and shape of a finite domain into which a tracer is initially introduced is tracked over a period of time. Such experiments possess the advantage of allowing the introduction of a small, finite 'blob' of tracer. In a chaotic flow, this blob will distort and stretch, providing a direct illustration of the divergence of initial conditions. The analogous computations are less straightforward, since the set of initial conditions is necessarily discrete rather than continuous.

Related experiments consist of *continuous* injection of a tracer into the flow at a given point in order to visualize the streaklines. These experiments are especially useful in three-dimensional flows, allowing visualization of the unmixed regions of the flow, or KAM tori (Kusch & Ottino 1992). Furthermore, these experiments permit

[1]Moreover, as the particle trajectories are purely deterministic, it is impossible to incorporate molecular diffusion (Brownian motion) effects into the analysis, and hence to assess the role of diffusion in the convective mixing process.

investigation of those three-dimensional flows which are not amenable to analysis via Poincaré sections (owing to the loss of information inherent in the reduction of dimensionality occurring in the construction of these plots). For example, the eccentric helical annular mixer (Kusch & Ottino 1992) consists of eccentrically positioned cylinders, undergoing time-periodic rotation about their longitudinal axes, accompanied by an axial laminar flow in the annular region between the cylinders. A Poincaré plot of this flow lacks any information regarding the axial transport, while streakline experiments reveal complex three-dimensional structures (Kusch & Ottino 1992). Ultimately, however, such experimental tracer studies of mixing effectiveness possess the same major disadvantage as do Poincaré sections, namely that their purely qualitative visual nature fails to furnish global rate information.

3.4 Heat- and mass-transfer rate enhancement via laminar chaos

Much of the current literature concerning laminar chaotic flows focuses on exploiting their sensitivity to initial conditions and to small perturbations in the particle positions (due, for example, to molecular diffusivity or inertia) to improve mixing in initially homogeneous fluids (Ottino 1990, Ottino *et al.* 1992, Aref & Balachandar 1986, Swanson & Ottino 1990, among others). These investigations focus on qualitative visualizations of the regions of flow exhibiting chaotic behavior obtained through numerical computation of the Poincaré sections, in combination with experimental tracer studies.

The above-cited studies do not address the interaction between molecular diffusion and chaotic flows, nor do they consider the enhancement of transport rates by laminar chaos. A small number of theoretical papers do, however, address the issue of chaos-enhanced transport. Thus, Jana & Ottino (1992) studied heat transfer in

a chaotic cavity flow. They considered the approach to equilibrium of an initially isothermal fluid which is perturbed by a step change in the wall temperature, and found significant enhancement of the heat-transfer rate in circumstances for which chaotic transport was present. The extent of heat-transfer enhancement exhibited a strong dependence on the Péclet number Pe, exhibiting a maximum at intermediate values of Pe. Ghosh, Chang & Sen (1992) investigated heat transfer between rotating eccentric cylinders maintained at different temperatures. Although their work was limited to small eccentricities and small oscillations superposed on otherwise steady rotary flows, conditions under which chaotic transport would be expected to be small, they nevertheless observed a significant increase in heat transfer occurring in circumstances where chaotic transport was present. Adopting a different approach, Toussaint, Carrière & Raynal (1995) studied the rate of decay of an initially inhomogeneous scalar field in the presence of both chaotic and non-chaotic flows, demonstrating that the rate of decay to homogeneity was greater in the chaotic flow case.

Jones & Young (1994) studied shear dispersion in a twisted pipe for circumstances wherein chaotic particle trajectories were present. Previous studies of Taylor dispersion in curved tubes, involving regular, non-chaotic particle trajectories (Nunge, Lin, & Gill 1972, Janssen 1976, Johnson & Kamm 1986), found that the secondary flow induced by tube curvature acted to decrease the convective dispersion by a factor of up to five below that occurring in a straight tube under comparable conditions. Jones & Young (1994) concluded that the presence of chaotic advection decreases the axial dispersion to an even larger extent than does regular secondary flow, changing the dependence of the dispersivity upon the Péclet number from the classical Pe^2 behavior (Taylor 1953) to $Pe \ln Pe$.

While the studies cited above suggest that chaotic flows may be useful in enhancing transport rates, they do not generally provide a unique quantitative measure of chaotic transport effectiveness. In contrast, the present work develops quantitative

measures, such as the effective rate of transport-limited reactions and the rate of extraction of solute from a droplet in circumstances for which the transport processes internal to the droplet are limiting. Explicitly, two flows are examined, namely eccentric annular flow and flow within a non-neutrally buoyant droplet undergoing simple shear. Chemical engineering applications of these flows, including enhancement of the rate of transport-limited reactions, reduction of axial dispersion, and enhancement in the rate of solute extraction from a droplet into a surrounding bulk phase are studied. Particular attention is paid to the correspondence (or lack thereof) between predictions of transport effectiveness based upon Poincaré sections and the present quantitative measures. More generally, this thesis develops a general philosophy based on the theme of macrotransport processes (Brenner & Edwards 1993) enabling the simple, global quantification of the effect of laminar chaos on whole classes of transport processes.

References

[1] AREF, H. 1984 Stirring by chaotic advection. *Phys. Fluids* **143**, 1–21.

[2] AREF, H. & BALACHANDAR, S. 1986 Chaotic advection in a Stokes flow. *Phys. Fluids* **29**, 3515–3521.

[3] AREF, H. & JONES, S.W. 1989 Enhanced separation of diffusing particles by chaotic advection. *Phys. Fluids* **1**, 470–474.

[4] ACHARYA, N., SEN, M. & CHANG, H.-C. 1992 Heat transfer enhancement in coiled tubes by chaotic mixing. *Int J. Heat Mass Transfer* **35**, 2475–2489.

[5] ARNOLD, V. I. 1965 Sur la topologie des écoulements stationnaires des fluids parfaits. *C. R. Acad. Sci. Paris Ser.*A **261**, 17–20.

[6] BAJER, K. & MOFFATT, H.K. 1990 On a class of steady confined Stokes flows with chaotic streamlines. *J. Fluid Mech.* **212**, 337–363.

[7] BRENNER, H. & EDWARDS, D. A. 1993 *Macrotransport Processes.* Butterworth-Heinemann.

[8] CARTWRIGHT, J.H.E., FEINGOLD, M. & PIRO, O. 1996 Chaotic advection in three-dimensional unsteady incompressible laminar flow. *J. Fluid Mech.* **316**, 259 –284.

[9] CHAIKEN, J., CHU, C. K., TABOR, M., & TAN, Q. M. 1987 Lagrangian turbulence and spatial complexity in a Stokes flow. *Phys. Fluids* **30**, 687–694.

[10] DOHERTY, M. F. & OTTINO, J. M. 1988 Chaos in deterministic systems: strange attractors, turbulence, and applications in chemical engineering. *Chem. Eng. Sci.* **43**, 139–183.

[11] DOMBRE, T., FRISCH, U., GREENE, J.M., HÉNON, M., MEHR, A. & SOWARD, A. M. 1986 Chaotic streamlines in the ABC flows. *J. Fluid Mech.* **167**, 353–391.

[12] DUTTA, P. & CHEVRAY, R. 1995 Enhancement of mixing by chaotic advection with diffusion. *Exp. Thermal Fluid Sci.* **11**, 1–12.

[13] GHOSH, S., CHANG, H. -C., & SEN, M. 1992 Heat-transfer enhancement due to slender recirculation and chaotic transport between counter-rotating eccentric cylinders. *J. Fluid Mech.* **238**, 119–154.

[14] HÉNON, M. 1966 Sur la topologie des linges de courant dans un cas particulier. *C. R. Acad. Sci. Paris Ser.* A **262**, 312–14.

[15] JANA, S. C. & OTTINO, J. M. 1992 Chaos-enhanced transport in cellular flows. *Phil. Trans. R. Soc. Lond.* A. **338**, 519–532.

[16] JANSSEN, L. A. M. 1976. Axial dispersion in laminar flow through coiled tubes. *Chem. Eng. Sci.* **31**, 215–218.

[17] JOHNSON, M. & KAMM, R. D. 1986 Numerical studies of steady flow dispersion at low Dean number in a gently curving tube. *J. Fluid Mech.* **172**, 329–345.

[18] JONES, S. W. & YOUNG, W. R. 1994 Shear dispersion and anomalous diffusion by chaotic advection. *J. Fluid Mech.* **280**, 149–172.

[19] KHAKHAR, D. V., FRANJIONE, J. G., & OTTINO, J. M. 1987 A case study of chaotic mixing in deterministic flows: the partitioned pipe mixer. *Chem. Eng. Sci.* **42**, 2909–2926.

[20] KUSCH, H. A. & OTTINO, J. M. 1992 Experiments on mixing in continuous chaotic flows. *J. Fluid Mech.* **236**, 319–348.

[21] LICHTENBERG, A. J. & LIEBERMAN, M. A. 1983 *Regular and Chaotic Motion* Springer.

[22] NUNGE, R. J., LIN, T. -S., & GILL, W. N. 1972 Laminar dispersion in curved tubes and channels. *J. Fluid Mech.* **51**, 363–383.

[23] OTTINO, J. M. 1990 Mixing, chaotic advection, and turbulence. *Ann. Rev. Fluid Mech.* **22**, 207–253.

[24] OTTINO, J. M., MUZZIO, F. J., TJAHJADI, M., FRANJIONE, J. G., JANA, S. C., & KUSCH, H. A. 1992 Chaos, symmetry, and self-similarity: Exploiting order and disorder in mixing processes. *Science*. **257**, 754–760.

[25] SAATDJIAN, E., MIDOUX, N., GASTOU CHASSAING, M.I., LEPREVOST, J.C. & ANDRÉ, J.C. 1996 Chaotic mixing and heat transfer between confocal ellipses: experimental and numerical results. *Phys. Fluids* **8**, 677–691.

[26] STONE, H.A., NADIM, A. & STROGATZ, S. 1991 Chaotic streamlines inside drops immersed in steady Stokes flows. *J. Fluid Mech.* **232**, 629–646.

[27] SWANSON, P.D. & OTTINO, J.M. 1990 A comparative computational and experimental study of chaotic mixing of viscous fluids. *J. Fluid Mech.* **213**, 227–249.

[28] TOUSSAINT, V., CARRIÈRE, P. & RAYNAL, F. 1995 A numerical Eulerian approach to mixing by chaotic advection. *Phys. Fluids* **7**, 2587–2600.

Chapter 4

Reaction and dispersion in eccentric annular flow

Abstract

Generalized Taylor dispersion theory is used to study the chaotic laminar transport of a reactive solute between eccentric rotating cylinders in the presence of an inhomogeneous chemical reaction. The circumstance considered is that of laminar axial 'Poiseuille' flow in the annular region between the two nonconcentric cylinders, accompanied by a secondary, generally chaotic, flow induced via alternate rotation of the cylinders. A Brownian tracer introduced into the flow is assumed to undergo an instantaneous, irreversible reaction on the surface of the outer cylinder. The resulting effective, transversely- and time-averaged reaction rate, axial solute velocity, and axial convective dispersivity are computed. When chaos is present, the effective reaction rate is increased to a value several times larger than occurs in the absence of chaotic transport. It is found that an optimum alternation frequency exists, and that this frequency decreases with increasing transverse Péclet number (Pe_q). It is also observed that the maximum achievable reaction rate increases with Pe_q. The effect of laminar chaotic transport on the mean axial solute/solvent velocity ratio is to drive its value towards the perfectly-mixed value of 1.0, despite the removal of solute from the slower-moving axial streamlines near the outer (reactive) cylinder wall. Lastly, in the presence of transverse chaotic transport, the convective, Taylor contribution to the axial solute dispersivity acquires a value up to several orders of magnitude smaller than that achievable by means of non-chaotic convection.

4.1 Introduction

The present chapter utilizes Taylor dispersion theory for time-periodic, chemically reactive systems (Shapiro & Brenner 1990) to assess the effect of laminar chaos on both transverse and axial solute transport rates. The situation considered is that of net axial annular flow taking place between eccentric cylinders which are alternately rotated. This flow has been studied both experimentally and computationally by Kusch & Ottino (1992). In addition, flow between rotating eccentric cylinders (in the absence of axial flow) has been studied extensively as a simple example of a system in which the phenomenon of laminar chaos occurs under well-defined conditions (Aref & Balachandar 1986, Chaiken *et al.* 1987, Swanson & Ottino 1990, Kaper & Wiggins 1993). A Brownian tracer particle, likened to a diffusing solute molecule, is assumed to undergo instantaneous irreversible reaction on the outer cylinder surface[1] following its initial introduction into the annular space between the cylinders. A global, purely axial, transversely- and time-averaged description of the resulting reactive transport process is sought and ultimately found. In particular, the effective reaction or wall deposition rate, mean axial solute velocity, and axial dispersivity are computed. Since the deposition is assumed instantaneous, its rate is limited by the transport of solute to the wall rather than by the true kinetics of the reaction or deposition process. Hence, the effective reaction rate furnishes a quantitative global measure of the transport effectiveness in a given secondary (i.e., transverse) flow field. The convective or Taylor contribution to the axial dispersivity also depends on the lateral transport, varying inversely with molecular diffusivity in a purely axial flow. Thus, the effect of any enhancement in the net transverse transport is to decrease the axial dispersion, whence the latter also furnishes an additional, independent measure of the transport

[1]We will on occasion refer to this instantaneous irreversible process as 'deposition', having in mind the model of a Brownian aerosol or hydrosol particle being deposited on the outer wall and held there permanently (Shapiro & Brenner 1986, Shapiro, Kettner & Brenner 1991).

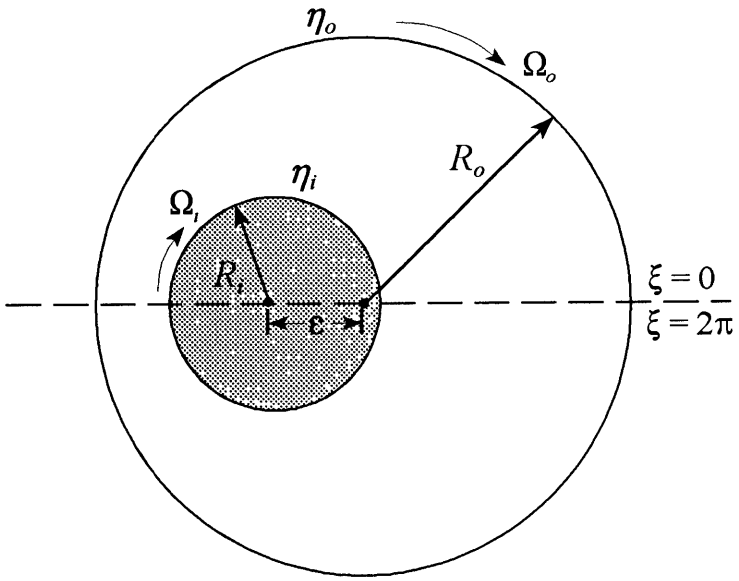

Figure 4-1: Eccentric cylinders. Bipolar coordinates.

effectiveness of a given chaotic flow field. This material has previously appeared in the *Journal of Fluid Mechanics* (Bryden & Brenner 1996).

4.2 Geometry and flow

Consider an infinitely long circular cylinder of radius R_i positioned nonconcentrically within another, larger cylinder of radius R_o, their centers being separated by a distance ε (Figure 4-1). (Throughout, subscripts i and o, when they appear, represent the values of the functions to which they are affixed on the inner and outer cylinders, respectively.) A point within the eccentric annular space bounded by the two cylinders will be denoted $(z, \boldsymbol{q})$, with z the axial position parallel to the cylinder axes, and $\boldsymbol{q} \equiv \boldsymbol{q}(\eta, \xi)$ the 'local', transverse position vector in the plane perpendicular to the z axis. Here, η and ξ are cylindrical curvilinear coordinates, explicitly bipolar coordinates in the present context (Happel & Brenner 1983).

A transverse flow is produced by rotating the inner and outer cylinders alternately,

each for the same period T at the respective angular velocities Ω_i and Ω_o. The secondary, local-space velocity field is then given by

$$\boldsymbol{u}(\boldsymbol{q},t) = \begin{cases} \boldsymbol{u}_i(\boldsymbol{q}), & 2nT < t < (2n+1)T, \\ \boldsymbol{u}_o(\boldsymbol{q}), & (2n+1)T < t < 2(n+1)T, \end{cases} \tag{4.2-1}$$

$(n = 0, 1, 2, ...)$, where $\boldsymbol{u}_i$ and $\boldsymbol{u}_o$ are the quasi-steady, Stokes flow, bipolar-coordinate velocity fields (Ballal & Rivlin 1976) respectively resulting from rotation of the inner and outer cylinders. The quasi-steady assumption is valid provided that the period of modulation T is large compared with the viscous time scale L^2/ν, where L is a characteristic length, say $R_o - R_i$, and ν the kinematic viscosity. The assumption of Stokes flow is justified provided the Reynolds number $\mathrm{Re} = R^2\Omega/\nu$ is less than unity (San Andres & Szeri 1984).

In addition to the unsteady two-dimensional transverse flow produced by the rotation of the cylinders, a steady laminar axial flow $\boldsymbol{U} = \boldsymbol{i}_z U(\boldsymbol{q})$ is superposed. This Poiseuille-like bipolar-coordinate flow field is given by Snyder & Goldstein (1965), among others (Piercy, Hooper & Winney 1933).

4.3 Probability density transport

Consider an effectively point-size Brownian solute particle introduced at time t' into the flow $\boldsymbol{U} + \boldsymbol{u}$ occurring between the two eccentric cylinders. The particle will be assumed to undergo transport by convection and diffusion in the annular space while undergoing instantaneous, irreversible deposition on the outer cylinder. Let $P \equiv P(z, \boldsymbol{q}, t|\boldsymbol{q}', t')$ denote the conditional probability density that the tracer is located at the point $(z, \boldsymbol{q})$ at time t, given that it was initially introduced into the fluid at the point $(0, \boldsymbol{q}')$ at time t'. This probability density is governed by the following

boundary-value problem:

$$\frac{\partial P}{\partial t} + U(\boldsymbol{q})\frac{\partial P}{\partial z} + \boldsymbol{u}(\boldsymbol{q},t)\cdot\nabla_q P - D\Big(\frac{\partial^2 P}{\partial z^2} + \nabla_q^2 P\Big) = \delta(z)\delta(\boldsymbol{q}-\boldsymbol{q}')\delta(t-t'), \quad (4.3\text{-}2)$$

$$P = 0 \quad \text{on} \quad \partial\boldsymbol{q}_o, \quad (4.3\text{-}3)$$

$$\boldsymbol{n}\cdot\nabla_q P = 0 \quad \text{on} \quad \partial\boldsymbol{q}_i, \quad (4.3\text{-}4)$$

$$|z|^m P \to 0 \quad \text{as} \quad z \to \pm\infty \quad (m = 0,1,2,...). \quad (4.3\text{-}5)$$

Here, D is the molecular diffusivity, ∇_q the local-space (two-dimensional) gradient operator, $\boldsymbol{n}$ the unit normal vector, and $\partial\boldsymbol{q}_\alpha$ a point lying on the surface of a circular cylinder, η_α = constant ($\alpha = i, o$). Boundary condition (4.3-3) is a consequence of the instantaneous irreversible solute deposition on the outer cylinder, while (4.3-4) represents the condition of no flux through the inner cylinder wall. Equation (4.3-5) is necessitated by the requirement that the probability density be bounded as $|z| \to \infty$ in such a way that the axial moment integrals

$$\int_{-\infty}^{\infty} z^m P \mathrm{d}z \quad (4.3\text{-}6)$$

implicit in the subsequent theory converge for all non-negative integers m and for all local points $\boldsymbol{q} \in \boldsymbol{q}_0$, in which $\boldsymbol{q}_0$ represents the two-dimensional annular domain ($0 \leqslant \xi < 2\pi, \quad \eta_o \leqslant \eta \leqslant \eta_i$) lying perpendicular to the axes of the cylinders, η_i and η_o.

4.4 Global, axial transport description

A macroscale description of the transport processes outlined above may be obtained through application of the time-periodic moment-matching scheme described by Shapiro & Brenner (1990). This method allows the calculation of mean trans-

port coefficients which are independent of the exact initial conditions, thus providing global information about the transport processes and eliminating the necessity of performing a separate calculation for each new set of initial conditions.

Define the time- and transverse position-averaged conditional probability density

$$< \overline{P} > (z,t|\boldsymbol{q}',t') = \frac{1}{2T}\int_t^{t+2T}\int_{q_0} P(z,\boldsymbol{q},t|\boldsymbol{q}',t')\mathrm{d}\boldsymbol{q}\mathrm{d}t. \tag{4.4-7}$$

Here, the transverse average of a function $f(z,\boldsymbol{q},t)$ is defined as

$$\overline{f}(z,t) = \int_{q_0} f(z,\boldsymbol{q},t)\mathrm{d}\boldsymbol{q}, \tag{4.4-8}$$

whereas

$$< f > (z,\boldsymbol{q},t) = \frac{1}{2T}\int_t^{t+2T} f(z,\boldsymbol{q},t)\mathrm{d}t \tag{4.4-9}$$

denotes the time-average of the function over one period, $2T$. For asymptotically long times $< \overline{P} >$ obeys the following one-dimensional system of macroscale, axial convection–dispersion–(first-order, irreversible) reaction equations (Shapiro & Brenner 1990):

$$\frac{\partial < \overline{P} >}{\partial t} + \overline{U^*}\frac{\partial < \overline{P} >}{\partial z} - \overline{D^*}\frac{\partial^2 < \overline{P} >}{\partial z^2} + \overline{K^*} < \overline{P} >= A(\boldsymbol{q}',t')\delta(z)\delta(t-t'), \tag{4.4-10}$$

$$|z|^m < \overline{P} > \to 0 \quad \text{as} \quad z \to \pm\infty. \tag{4.4-11}$$

The macroscale phenomenological coefficients $\overline{K^*}, \overline{U^*}$, and $\overline{D^*}$ respectively represent the effective solute reaction-rate constant, axial velocity, and axial dispersivity. These axial position- and time-independent constants are given in terms of quadratures of the microscale phenomenological and geometric data by the expressions

$$\overline{K^*} = K, \tag{4.4-12}$$

$$\overline{U^*} = \frac{1}{2T}\int_0^{2T}\int_{q_0} U(\boldsymbol{q})P_0^{\infty}(\boldsymbol{q},t)A(\boldsymbol{q},t)\mathrm{d}\boldsymbol{q}\mathrm{d}t \tag{4.4-13}$$

and

$$\overline{D^*} = D + \overline{D_c^*}, \tag{4.4-14}$$

where

$$\overline{D_c^*} = \frac{1}{2T}\int_0^{2T}\int_{q_0} B(\boldsymbol{q},t)P_0^{\infty}(\boldsymbol{q},t)A(\boldsymbol{q},t)[U(\boldsymbol{q}) - \overline{U^*}]\mathrm{d}\boldsymbol{q}\mathrm{d}t \tag{4.4-15}$$

is the Taylor (i.e., 'convective') contribution to the axial dispersivity. Here, the local-space P_0^{∞} and A fields together with the reactivity coefficient K are found from the following adjoint pair of transverse-space eigenvalue problems:

$$\frac{\partial P_0^{\infty}}{\partial t} + \boldsymbol{u}\cdot\nabla_q P_0^{\infty} - D\nabla_q^2 P_0^{\infty} - KP_0^{\infty} = 0, \tag{4.4-16}$$

$$P_0^{\infty} = 0 \quad \text{on} \quad \partial\boldsymbol{q}_o, \tag{4.4-17}$$

$$\boldsymbol{n}\cdot\nabla_q P_0^{\infty} = 0 \quad \text{on} \quad \partial\boldsymbol{q}_i, \tag{4.4-18}$$

$$P_0^{\infty}(\boldsymbol{q},t+2T) = P_0^{\infty}(\boldsymbol{q},t), \tag{4.4-19}$$

$$\frac{1}{2T}\int_t^{t+2T}\int_{q_0} P_0^{\infty}\mathrm{d}\boldsymbol{q}\mathrm{d}t = 1; \tag{4.4-20}$$

and

$$\frac{\partial A}{\partial t} + \boldsymbol{u}\cdot\nabla_q A + D\nabla_q^2 A + KA = 0, \tag{4.4-21}$$

$$A = 0 \quad \text{on} \quad \partial\boldsymbol{q}_o, \tag{4.4-22}$$

$$\boldsymbol{n}\cdot\nabla_q A = 0 \quad \text{on} \quad \partial\boldsymbol{q}_i, \tag{4.4-23}$$

$$A(\boldsymbol{q},t+2T) = A(\boldsymbol{q},t), \tag{4.4-24}$$

$$\int_{q_0} P_0^{\infty} A\mathrm{d}\boldsymbol{q} = 1. \tag{4.4-25}$$

The B field required in the determination of $\overline{D^*}$ represents the solution of the following

boundary-value problem:

$$\frac{\partial(BP_0^\infty)}{\partial t} + \boldsymbol{u}\cdot\nabla_q(BP_0^\infty) - D\nabla_q^2(BP_0^\infty) - KBP_0^\infty = P_0^\infty[U(\boldsymbol{q}) - \overline{U^*}], \qquad (4.4\text{-}26)$$

$$BP_0^\infty = 0 \quad \text{on} \quad \partial\boldsymbol{q}_o, \qquad (4.4\text{-}27)$$

$$\boldsymbol{n}\cdot\nabla_q(BP_0^\infty) = 0 \quad \text{on} \quad \partial\boldsymbol{q}_i. \qquad (4.4\text{-}28)$$

The term appearing on the right-hand side of (4.4-10) represents a 'fictitious' initial condition, which differs from the true, delta function initial condition by the factor $A(\boldsymbol{q}', t')$. The need for such a fictitious initial condition arises from the fact (Shapiro & Brenner 1990) that the macroscale equation (4.4-10) is valid only for asymptotically long times, and hence does not accurately describe the transport occurring at short times. Use of a fictitious initial condition corrects for this 'anomalous' behavior by properly accounting for the solute transport and reaction occurring *prior* to the time at which the macroscale equation (4.4-10) becomes applicable. As a result of this initial condition, $<\overline{P}>$ depends upon both the initial transverse position $\boldsymbol{q}'$ and the initial time t' (the latter through the combination $t-t'$), although the macroscale phenomenological coefficients $\overline{K^*}$, $\overline{U^*}$, and $\overline{D^*}$ appearing in (4.4-10) are independent of the initial conditions. The value of $A(\boldsymbol{q}', t')$ may be used to determine the utility of the present asymptotic analysis. In instances in which most of the solute has already been consumed by chemical reaction prior to this asymptotic analysis becoming valid, $A(\boldsymbol{q}', t')$ will be extremely small and the distinction between a small amount of solute remaining and zero residual solute will be mout from a practical point of view. In other instances, such as when the solute is initially introduced in a region relatively distant from the reactive wall, $A(\boldsymbol{q}', t')$ will be close to unity. Thus, our macroscale analysis will possess greater utility in practical applications. However, practical considerations aside, our analysis nevertheless provides a simple quantitative measure of

the effectiveness of laminar chaos in enhancing the transverse transport rate.

Introduce the dimensionless variables

$$\tau = \frac{tD}{R_o^2}, \quad \mathrm{Pe}_q = \frac{\overline{u}R_o}{D}, \quad \mathrm{Pe}_Q = \frac{\overline{V}R_o}{D}, \quad \kappa = \frac{KR_o^2}{D}, \quad \hat{\boldsymbol{u}} = \frac{\boldsymbol{u}}{\overline{u}},$$
$$\hat{U} = \frac{U}{\overline{V}}, \quad \hat{B} = \frac{B}{R_o \mathrm{Pe}_Q}, \quad \hat{P}_0^\infty = P_0^\infty R_o^2, \quad \hat{\nabla}_q = R_o \nabla_q, \tag{4.4-29}$$

in which

$$\overline{u} = \Omega_o R_o \tag{4.4-30}$$

is the circumferential velocity of the outer cylinder, and

$$\overline{V} = \int_{q_0} U(\boldsymbol{q}) d\boldsymbol{q} \Big/ \int_{q_0} d\boldsymbol{q} \tag{4.4-31}$$

is the average axial solvent velocity. (The denominator of (4.4-31) is simply the cross-sectional area $\pi(R_o^2 - R_i^2)$ of the annular domain.) This yields the following nondimensional system of differential equations governing the fields $\hat{P}_0^\infty$, A, and $\hat{B}$:

$$\frac{\partial \hat{P}_0^\infty}{\partial \tau} + \mathrm{Pe}_q \hat{\boldsymbol{u}} \cdot \hat{\nabla}_q \hat{P}_0^\infty - \hat{\nabla}_q^2 \hat{P}_0^\infty - \kappa \hat{P}_0^\infty = 0, \tag{4.4-32}$$

$$\frac{\partial A}{\partial \tau} + \mathrm{Pe}_q \hat{\boldsymbol{u}} \cdot \hat{\nabla}_q A + \hat{\nabla}_q^2 A + \kappa A = 0, \tag{4.4-33}$$

$$\frac{\partial (\hat{B}\hat{P}_0^\infty)}{\partial \tau} + \mathrm{Pe}_q \hat{\boldsymbol{u}} \cdot \hat{\nabla}_q (\hat{B}\hat{P}_0^\infty) - \hat{\nabla}_q^2 (\hat{B}\hat{P}_0^\infty) - \kappa \hat{B}\hat{P}_0^\infty = \hat{P}_0^\infty \left(\hat{U}(\boldsymbol{q}) - \frac{\overline{U^*}}{\overline{V}} \right), \tag{4.4-34}$$

which are to be solved subject to the boundary conditions given by (4.4-17)–(4.4-20), (4.4-22)-(4.4-25), and (4.4-27)–(4.4-28), respectively, with B replaced by $\hat{B}$ and P_0^∞ by- $\hat{P}_0^\infty$. In addition, for the macroscale coefficients, one obtains

$$\frac{\overline{U^*}R_0}{D} = \frac{\mathrm{Pe}_Q}{2\Upsilon} \int_0^{2\Upsilon} \int_{q_0} \hat{U}(\boldsymbol{q}) \hat{P}_0^\infty(\boldsymbol{q}, \tau) A(\boldsymbol{q}, \tau) \mathrm{d}\boldsymbol{q} \mathrm{d}\tau \tag{4.4-35}$$

and

$$\frac{\overline{D_c^*}}{D} = \frac{\mathrm{Pe}_Q^2}{2\Upsilon}\int_0^{2\Upsilon}\int_{q_0}\hat{B}(\boldsymbol{q},\tau)\hat{P}_0^{\infty}(\boldsymbol{q},\tau)A(\boldsymbol{q},\tau)\Big(\hat{U}(\boldsymbol{q}) - \frac{\overline{U^*}}{\overline{V}}\Big)\mathrm{d}\boldsymbol{q}\mathrm{d}\tau, \tag{4.4-36}$$

in which $\Upsilon = TD/R_0^2$. The relevant parameters to be investigated in quantifying $\overline{K^*}$, $\overline{U^*}$, and $\overline{D_c^*}$ are thus Pe_q, Υ, and Ω_i/Ω_o, in addition to the geometric factors R_i/R_o and (dimensionless) eccentricity $\epsilon = \varepsilon/(R_o - R_i)$.

4.5 Solution scheme

In order to facilitate determining the eigenvalue κ – representing the effective Damköhler number for the reaction – define the field $p_0^{\infty}(\boldsymbol{q},t)$ as follows:

$$\hat{P}_0^{\infty}(\boldsymbol{q},\tau) = p_0^{\infty}(\boldsymbol{q},\tau)\exp(\kappa\tau). \tag{4.5-37}$$

From (4.4-32), the p_0^{∞} field is thus governed by the relation

$$\frac{\partial p_0^{\infty}}{\partial\tau} + \mathrm{Pe}_q\hat{\boldsymbol{u}}\cdot\hat{\nabla}_q p_0^{\infty} - \hat{\nabla}_q^2 p_0^{\infty} = 0, \tag{4.5-38}$$

whereas the equation for the $\hat{B}$ field becomes

$$\frac{\partial(\hat{B}p_0^{\infty})}{\partial\tau} + \mathrm{Pe}_q\hat{\boldsymbol{u}}\cdot\hat{\nabla}_q(\hat{B}p_0^{\infty}) - \hat{\nabla}_q^2(\hat{B}p_0^{\infty}) = p_0^{\infty}\Big(\hat{U}(\boldsymbol{q}) - \frac{\overline{U^*}}{\overline{V}}\Big). \tag{4.5-39}$$

In terms of the new variables, κ is now given by

$$\kappa = -\lim_{\tau\to\infty}\frac{1}{2\Upsilon}\ln\left(\frac{\int_{q_0}p_0^{\infty}(\boldsymbol{q},\tau+2\Upsilon)\mathrm{d}\boldsymbol{q}}{\int_{q_0}p_0^{\infty}(\boldsymbol{q},\tau)\mathrm{d}\boldsymbol{q}}\right). \tag{4.5-40}$$

Similarly, upon replacing A by

$$A(\boldsymbol{q},\tau) = a(\boldsymbol{q},\tau)\exp(-\kappa\tau), \tag{4.5-41}$$

the new field a obeys the equation

$$\frac{\partial a}{\partial \tau} + \mathrm{Pe}_q \hat{\boldsymbol{u}} \cdot \hat{\nabla}_q a + \hat{\nabla}_q^2 a = 0. \tag{4.5-42}$$

The trio of boundary-value problems posed in the preceding paragraph were solved sequentially. Spatially uniform initial conditions were imposed upon each of the above three functions and calculations carried out until each attained its asymptotic, time-periodic behavior, which was independent of the arbitrarily chosen initial conditions. In order to avoid instabilities associated with (4.5-42), a new time variable $\theta = -\tau$ was introduced, yielding the following stable equation for $a(\boldsymbol{q},\theta)$:

$$\frac{\partial a}{\partial \theta} - \mathrm{Pe}_q \hat{\boldsymbol{u}} \cdot \hat{\nabla}_q a - \hat{\nabla}_q^2 a = 0. \tag{4.5-43}$$

This equation is identical to that governing the p_0^∞ field, with the exception of the algebraic sign of the convective term. Owing to the symmetry of the problem, it was not necessary to solve for the a and p_0^∞ fields separately. Rather, the a field was obtained by inverting the p_0^∞ field about the axis joining the centers of the two cylinders while reversing its time dependence.

The equations were explicitly written in bipolar coordinates (η,ξ) and subsequently solved by an implicit finite-difference method. All the calculations utilized a radius ratio value of $R_i/R_o = 0.3$, while the other parameters were varied over appropriate ranges. First, the eccentricity was varied over its entire range $(0 < \epsilon < 1)$, from the concentric- to the tangent-cylinder case. Pe_q was varied over the range zero to 10^6; large transverse Péclet numbers are of particular interest because species pos-

sessing small molecular diffusivities experience extremely small effective reaction rates in the absence of transverse convection, thus making lateral transport enhancement essential in attempting to achieve more rapid reaction rates. In addition to varying Pe_q, which is equivalent to varying the angular velocities of both cylinders, we also studied the effect of the angular velocity ratio Ω_i/Ω_o, including distinguishing between co-rotating cylinders ($\Omega_i/\Omega_o > 0$) and counter-rotating cylinders ($\Omega_i/\Omega_o < 0$). Varying this ratio over a range similar to that employed for Pe_q allowed us to assess the effect of varying the velocity of the inner cylinder, while holding the velocity of the outer cylinder fixed. Finally, the alternation period Υ was varied over the range 10^{-5} to 1, respectively corresponding to very rapid oscillation and to a period equal to the diffusion time.

4.6 Results

4.6.1 Reactivity Coefficient

Figure 4-2 illustrates the dependence of the effective reaction-rate coefficient on the eccentricity, while figure 4-3 shows representative streamlines for these flow conditions.

Figure 4-2 reveals that in the absence of any flow (curve 1), the net deposition rate decreases slightly with increasing eccentricity. This simply reflects the increasing average distance that a particle must travel in order to reach the reactive outer wall. Rotation of the outer cylinder singly (curve 2) leads to only a modest increase in the reaction rate over that in the absence of transverse flow. This increase is due to the separation occurring on the inner cylinder (see figure 4-3*a*), which serves to transport the reactive species from the area adjacent to the inner cylinder to the central region, thereby increasing the gradient driving the diffusion towards the outer wall. In comparison with the preceding case of rotation of the outer cylinder, a much more dramatic increase in the deposition rate is observed when the inner cylinder is

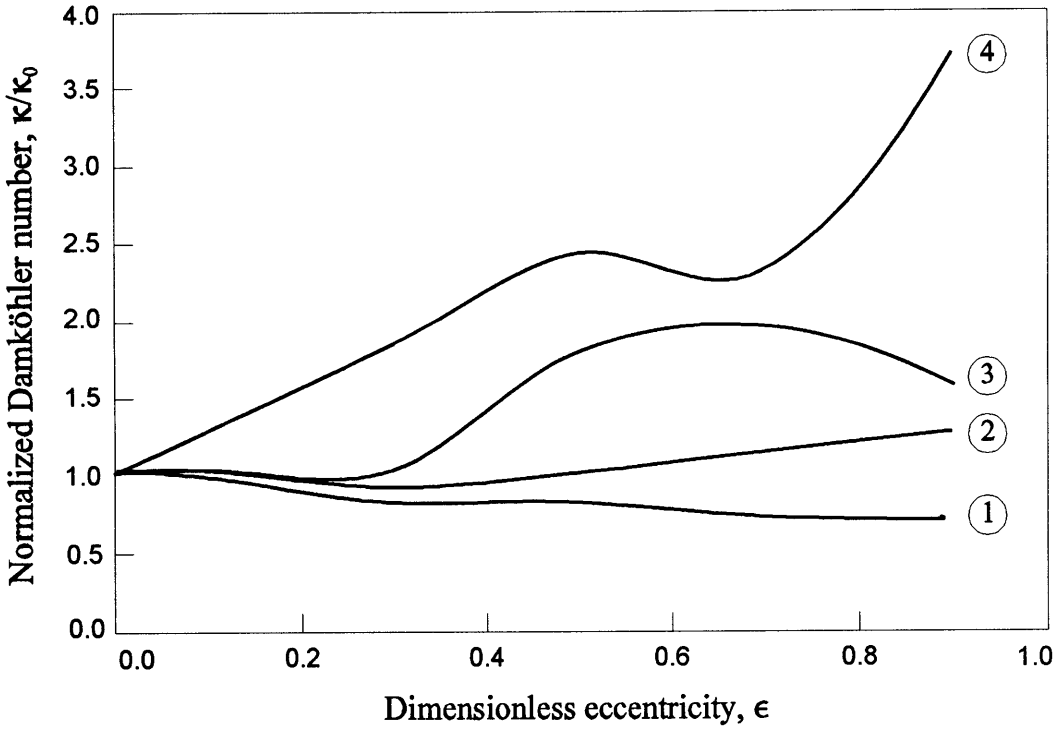

Figure 4-2: Dependence of the ratio of the effective Damköhler number κ to its value κ_0 at zero eccentricity and in the absence of transverse flow on the dimensionless eccentricity ϵ for $R_i/R_o = 0.3$: (1) no transverse flow; (2-4): $\mathrm{Pe}_q = 5000$, $\Omega_i/\Omega_o = 6$, with (2) outer cylinder rotation; (3) inner cylinder rotation; (4) alternate rotation, $\Upsilon = 0.001$.

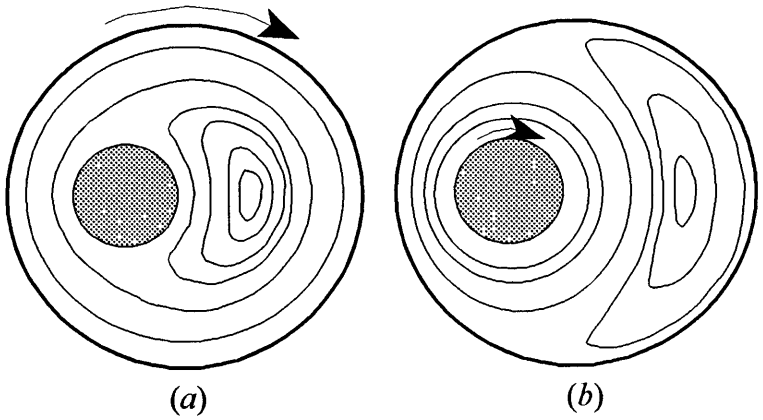

Figure 4-3: Streamlines for $R_i/R_o = 0.3$, $\epsilon = 0.5$: (a) Outer cylinder rotation (b) Inner cylinder rotation.

rotated singly (curve 3). This is a consequence of the location of the separation point. When the inner cylinder is rotated, separation occurs at the outer, reactive wall (see figure 4-3*b*). Thus, the effect of the separation is to transport species from the central portion of the annulus to the region very close to the reaction site, greatly enhancing the effective reaction rate.

The remaining curve displayed in figure 4-2 (curve 4) represents a situation in which the cylinders rotate alternately – circumstances for which chaotic advection has been shown to occur (Aref & Balachandar 1986, Chaiken *et al.* 1987, Swanson & Ottino 1990). When each cylinder is successively rotated for a period $\Upsilon = 0.001$, the deposition rate attains a value above that which could be achieved solely from rotation of the inner cylinder alone (curve 3). This clearly demonstrates the transport enhancement occasioned by laminar chaos for this set of parameters. Comparison of the Poincaré sections (figure 4-4) for these parameters with the resulting deposition rate shows that while there is some relationship between the Poincaré sections and the deposition rate, the conclusions drawn from these diagrams may be different than the calculated results. For instance, a large island is present in the Poincaré section for $\epsilon = 0.7$, suggesting that the mixing achieved in this geometry is less effective than that for either $\epsilon = 0.3$ or $\epsilon = 0.5$, where the only regular regions occur in thin bands close to the outer cylinder. In contrast, the calculated results show that the effective reaction rate for $\epsilon = 0.7$ is only slightly smaller than that for $\epsilon = 0.5$ and is, in fact, larger than that for $\epsilon = 0.3$.

The effect of the alternation period Υ on the deposition rate is illustrated in figure 4-5. It is seen that an enhanced deposition rate, over that attained by simply rotating the inner cylinder continuously, occurs only over a limited range of frequencies, a result similar to that observed by Ghosh *et al.* (1992) in their study of heat transfer. The increase observed in the deposition rate with switching period for small periods may be explained by examining the Poincaré sections for these flow conditions (figure 4-6).

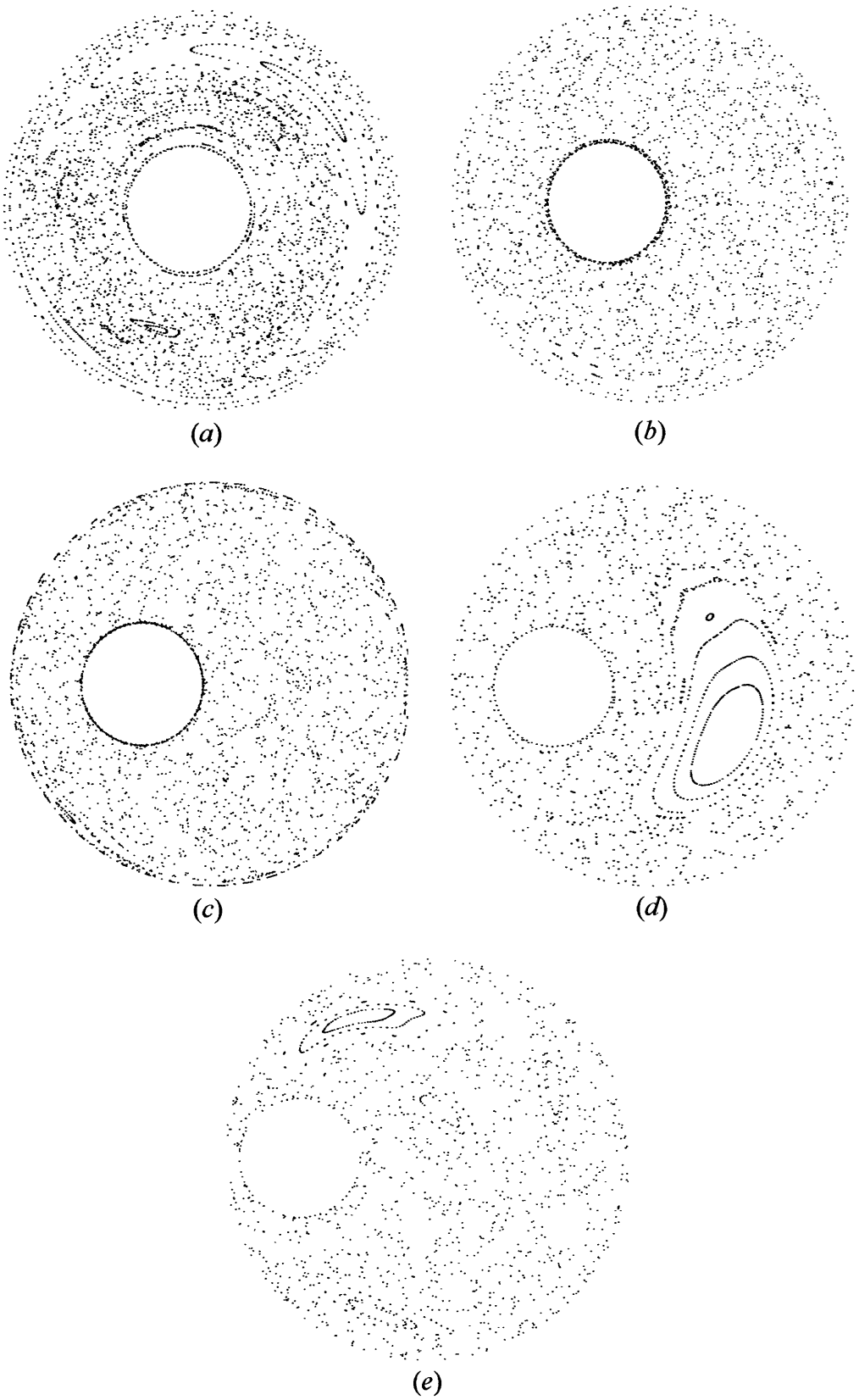

Figure 4-4: Poincaré sections for alternate rotation, with $R_i/R_o = 0.3$, $\mathrm{Pe}_q = 5000$, and $\Upsilon = 0.001$: (*a*) $\epsilon = 0.1$, (*b*) $\epsilon = 0.3$, (*c*) $\epsilon = 0.5$, (*d*) $\epsilon = 0.7$, (*e*) $\epsilon = 0.9$.

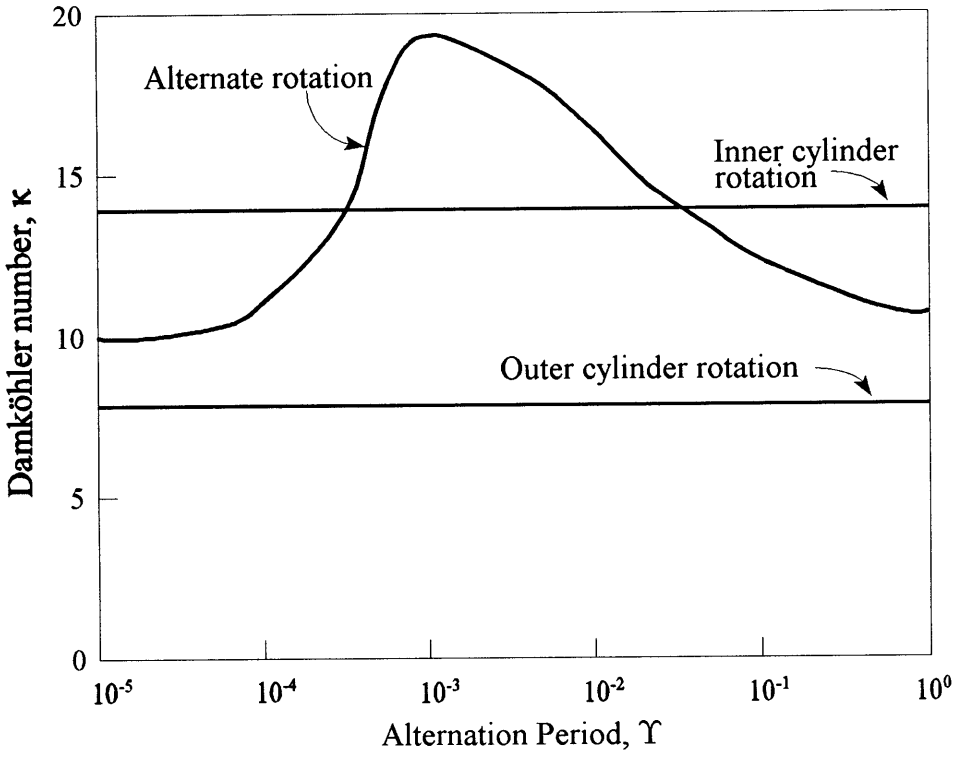

Figure 4-5: Dependence of the effective Damköhler number κ on the alternation period Υ for $R_i/R_o = 0.3$, $\epsilon = 0.5$, $\Omega_i/\Omega_o = 6$, $\mathrm{Pe}_q = 5000$.

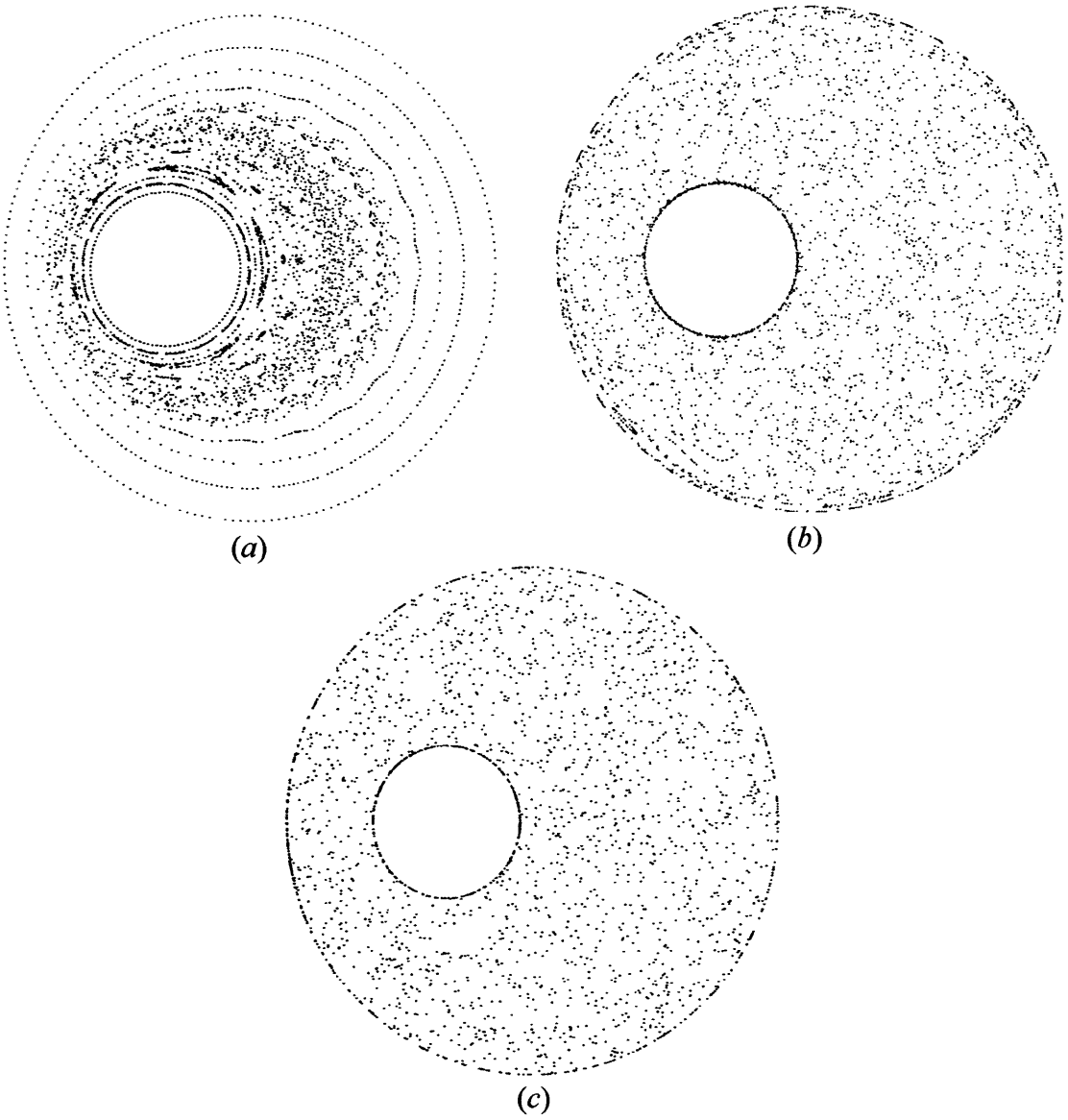

Figure 4-6: Poincaré sections for alternate rotation, with $R_i/R_o = 0.3$, $\mathrm{Pe}_q = 5000$, and $\epsilon = 0.5$: (a) $\Upsilon = 0.0001$ (b) $\Upsilon = 0.001$ (c) $\Upsilon = 0.01$

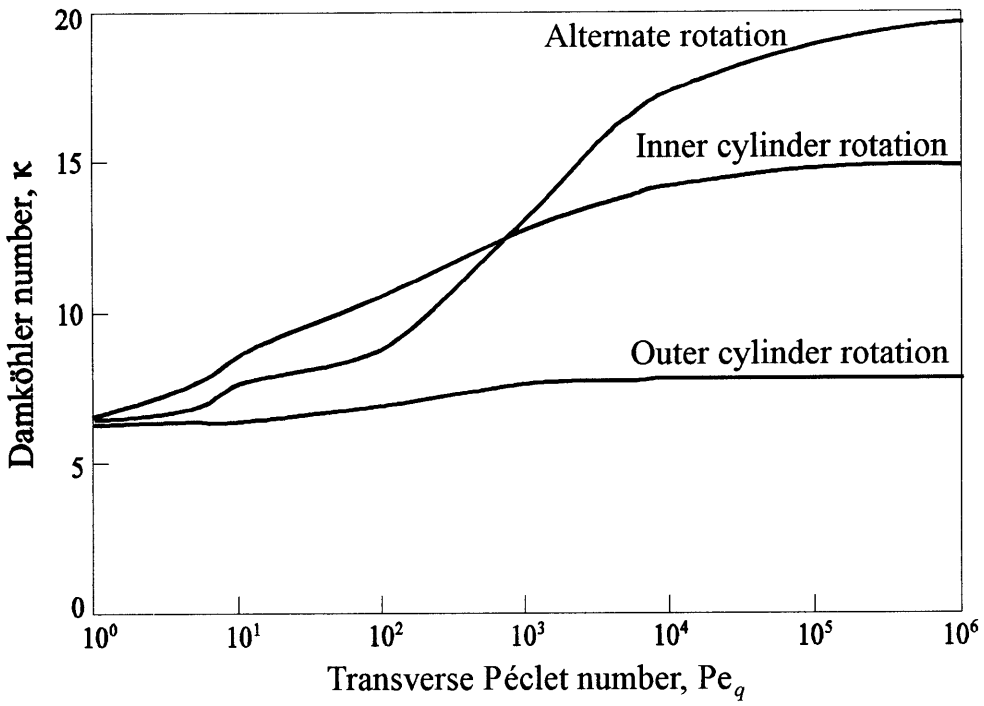

Figure 4-7: Dependence of the effective Damköhler number κ on Pe_q for $R_i/R_o = 0.3$, $\epsilon = 0.5$, $\Omega_i/\Omega_o = 6$, $\Upsilon = 0.01$.

There is a dramatic increase in the extent of the chaotic regions at the smallest periods (compare figures 4-6*a* and *b*). For longer periods, no such explanation is possible, since here the extent of chaotic regions is comparable to that present at the optimum alternation period. One possible explanation is that for these longer switching periods it takes longer for a comparable amount of mixing to occur, thus decreasing the effective reaction rate. Another possibility is that when molecular diffusion is present, very long switching periods allow sufficient time for diffusive transport to establish a pseudo-steady state during each half of the cycle, corresponding to that which occurs when one cylinder rotates continuously. The net rate of transport to the outer cylinder is thus (approximately) simply the average of the respective rates attained when each cylinder is rotated individually.

Figure 4-7 displays the dependence of deposition rate on transverse Péclet number. In the absence of diffusion, Aref & Balachandar (1986) and Chaiken *et al.* (1987)

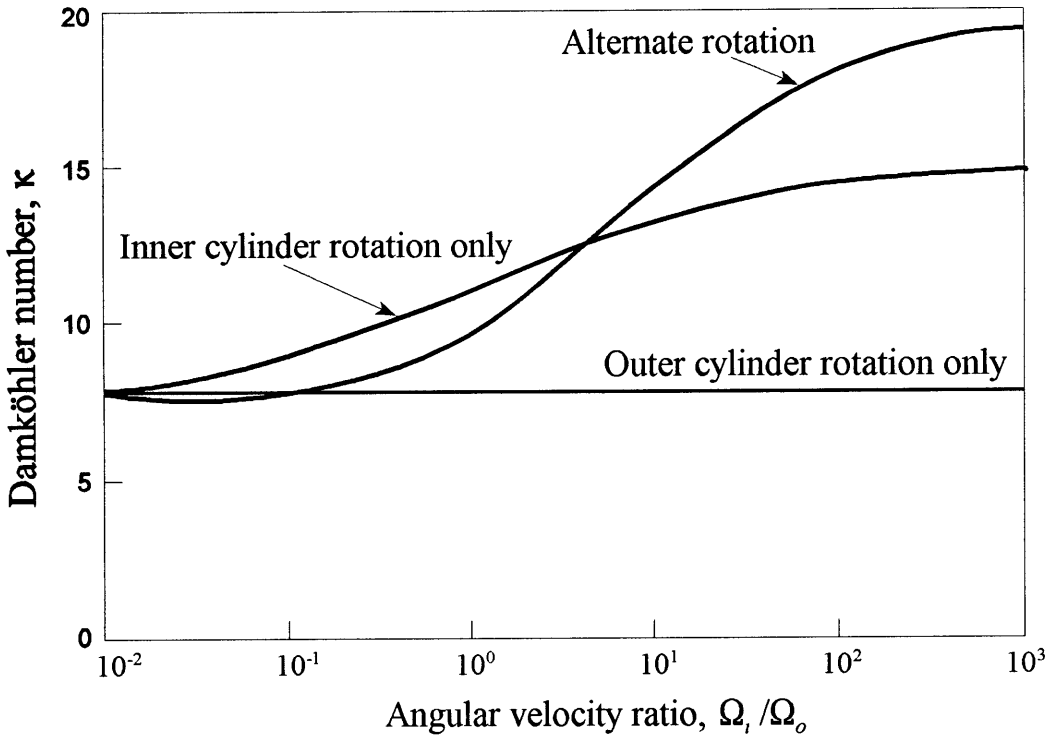

Figure 4-8: Dependence of the effective Damköhler number κ on the angular velocity ratio Ω_i/Ω_o for $R_i/R_o = 0.3$, $\epsilon = 0.5$, $\mathrm{Pe}_q = 1000$, $\Upsilon = 0.01$

observed that the extent of mixing depends only on the on the products $\Omega_i T$ and $\Omega_o T$ (i.e., the angular distances traveled by each cylinder during one period) rather than on the angular velocity and switching period individually. Here, the rate depends on each of these parameters separately, as can be seen by comparing figures 4-5 and 4-7, which would be the same if the rate depended only on the total distance traveled during each period. It is seen that for $\mathrm{Pe}_q \lesssim 500$, the deposition rate for alternate rotation falls into the envelope between the respective rates attained for continuous, single-cylinder rotation. For large Péclet numbers the deposition rate reaches an asymptotic value 1.3 times that attained by rotating only the inner cylinder, and 2.5 times that achieved in the complete absence of convection ($\mathrm{Pe}_q = 0$).

Figure 4-8 depicts the effect of varying the angular velocity Ω_i of the inner cylinder, while keeping constant both the switching period Υ and the angular velocity Ω_o of the outer cylinder. Comparison of these results with those observed when the

velocities of both cylinders are varied (figure 4-7) shows that the asymptotic limit for the deposition rate is independent of the angular velocity of the outer cylinder. Moreover, the value of the parameter $\mathrm{Pe}_q\Omega_i/\Omega_o$ at which the deposition rate in the presence of chaotic flow first exceeds that achieved through rotation of the inner cylinder alone is independent of whether the angular velocity of only the inner cylinder or the angular velocities of both cylinders are varied. It thus appears that for large Péclet numbers the rotation rate of the inner cylinder alone controls the deposition rate. This is physically reasonable, since it is the rotation of the inner cylinder that creates a separation region near the outer (reactive) wall. Rotation of the outer cylinder contributes little to the enhancement of the deposition rate on its own, but in combination with alternate rotation of the inner cylinder it serves to transport solute particles from areas lying outside of the separation region to the area of separation, where the local deposition rate is higher. Also investigated was the effect of rotating the cylinders in opposite directions rather than in the same direction (i.e., negative values of Ω_i/Ω_o). In the absence of diffusion, Poincaré plots indicate that better mixing is achieved with co-rotating cylinders than with counter-rotation (Chaiken *et al.* 1987). This trend is not observed here. For example, an effective Damköhler number of 19.05 occurs for $\mathrm{Pe}_q = 5000$, $\Upsilon = 0.001$, $\epsilon = 0.5$, and $\Omega_i/\Omega_o = 6$ (co-rotation) versus a value of 19.13 for the equivalent counter-rotation case.

The period Υ_{max} for which the maximum deposition rate occurs is shown in figure 4-9. This optimum period is given by $\Upsilon_{max} = C\mathrm{Pe}_q^{-1}$ (where C is a constant) – at least for large Pe_q, equivalent to small diffusivities. This trend is consistent with the observation in the absence of diffusion that the extent of mixing depends only on the angular distance traveled during each period. However, the maximum deposition rate κ_{max} attainable depends upon Pe_q, increasing with increasing Pe_q, as seen in figure 4-10. While the extent of chaotic mixing is the same in each of these instances, the rate at which transverse transport occurs varies with Pe_q. In the purely deterministic case

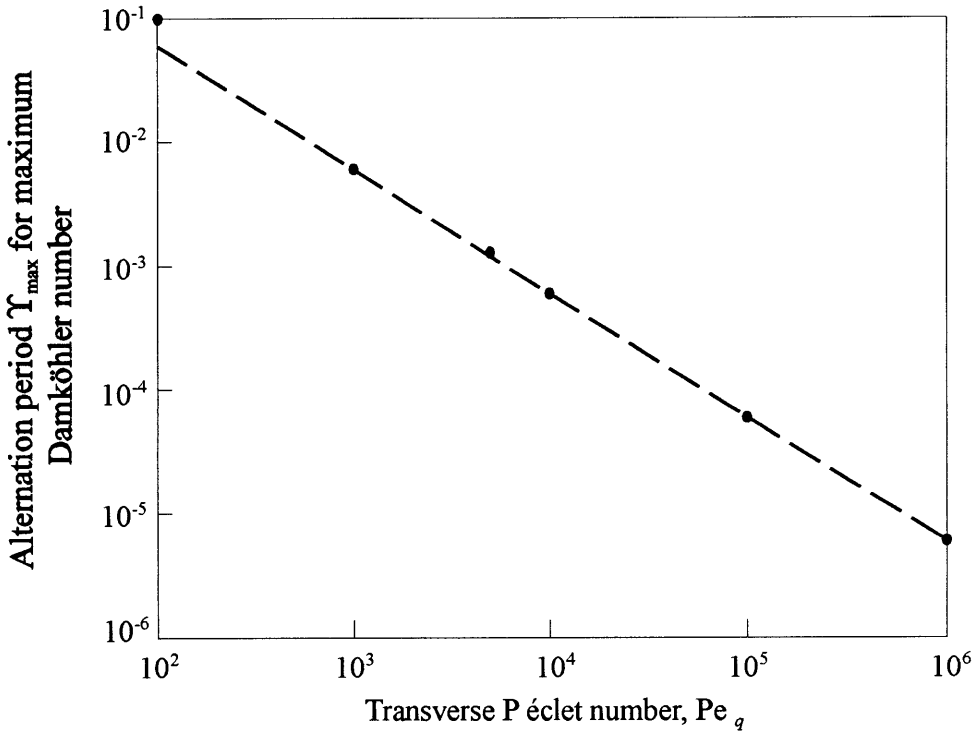

Figure 4-9: Dependence upon Pe_q of the alternation period at which the maximum effective Damköhler number is achieved, with $R_i/R_o = 0.3$, $\epsilon = 0.5$, $\Omega_i/\Omega_o = 6$. The slope of the line is -1.0

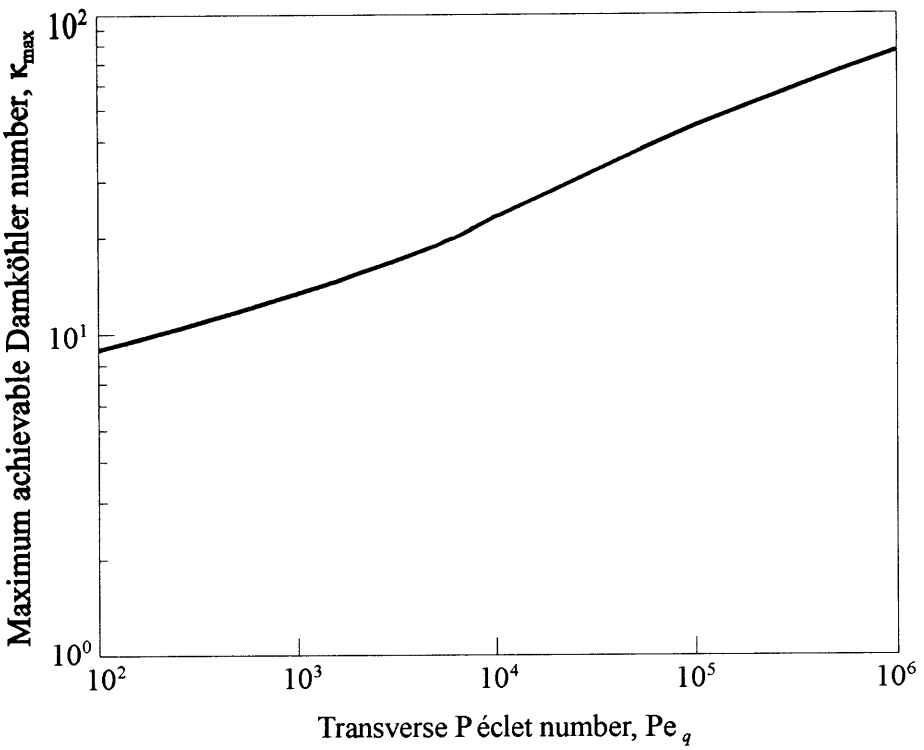

Figure 4-10: Dependence of the maximum achievable Damköhler number upon Pe_q, with $R_i/R_o = 0.3$, $\epsilon = 0.5$, $\Omega_i/\Omega_o = 6$.

the rate would vary linearly with angular velocity, but here, with diffusion present, the rate of increase is lessened, with the deposition rate varying approximately as $Pe_q^{0.25}$.

4.6.2 Effective axial velocity

Figure 4-11 illustrates the dependence of the mean axial solute velocity upon Pe_q for $\epsilon = 0.5$. For small Pe_q the average solute velocity $\overline{U^*}$ exceeds the mean annular 'Poiseuille' velocity $\overline{V}$ of the solvent for both continuous rotation of a single cylinder and successive alternate rotation of both. This is a consequence of the fact that the reaction at the outer cylinder removes solute from the slowest-moving axial streamlines, so that the only solute molecules to survive the trip downstream – and hence reach the exit of the system, where they are monitored – are those that have prefer-

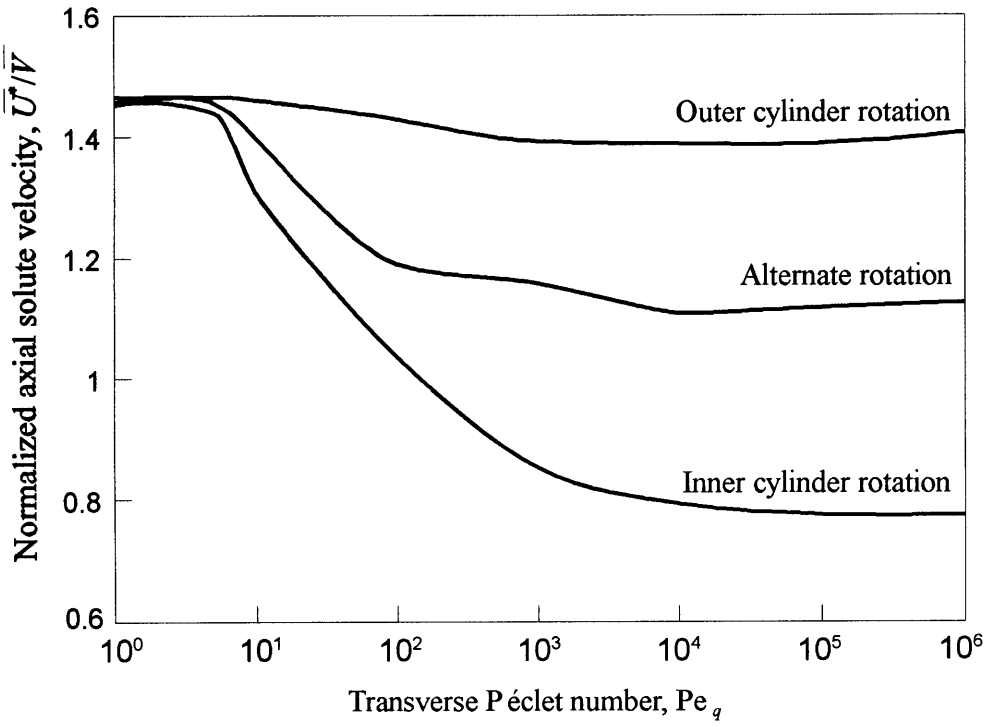

Figure 4-11: Dependence of the mean axial solute velocity upon Pe_q, with $R_i/R_o = 0.3$, $\epsilon = 0.5$, $\Omega_i/\Omega_o = 6$ and $\Upsilon = 0.01$.

entially sampled the (faster-moving) axial streamlines existing near the center of the annular space. As Pe_q is increased, the mean solute velocity decreases significantly for situations in which only the inner cylinder is rotated. In this circumstance, the recirculating flow near the reactive outer cylinder transports solute from some of the faster-moving axial streamlines to the reaction site, thereby decreasing the solute concentration along the faster streamlines, and hence reducing the average solute velocity below that of the passive solvent carrier. In the case of rotation of the outer cylinder alone, $\overline{U^*}$exceeds $\overline{V}$ for all Pe_q because, as is true for small Pe_q, the solute is preferentially removed from the slower-moving streamlines. When the cylinders are rotated alternately with a period of $\Upsilon = 0.01$, the velocity ratio $\overline{U^*}/\overline{V}$ falls between the values for each of the cylinders rotating individually, ultimately attaining an asymptotic value of 1.1 for very large Pe_q. From these data it cannot be unequivocally established whether laminar chaos is the cause of the effective solute velocity approaching the perfectly-mixed value of 1.0, or if rotating the cylinders alternately is simply causing this velocity to adopt a value intermediate between those attained by rotating each of the cylinders individually.

The transverse Péclet number dependence of the axial solute velocity at the optimum alternation period is illustrated in figure 4-12. For large Pe_q, the alternation period that maximizes the effective reaction rate is also the period at which the normalized solute velocity is closest to unity. For smaller Pe_q, the optimums differ only slightly from one another. In this figure, as in figure 4-11, the effective velocity when laminar chaos is present again lies between those for the individual single cylinder rotations, but here it is clearer that the effect of chaotic transport is to cause $\overline{U^*}/\overline{V}$ to approach the perfectly-mixed value of 1.0

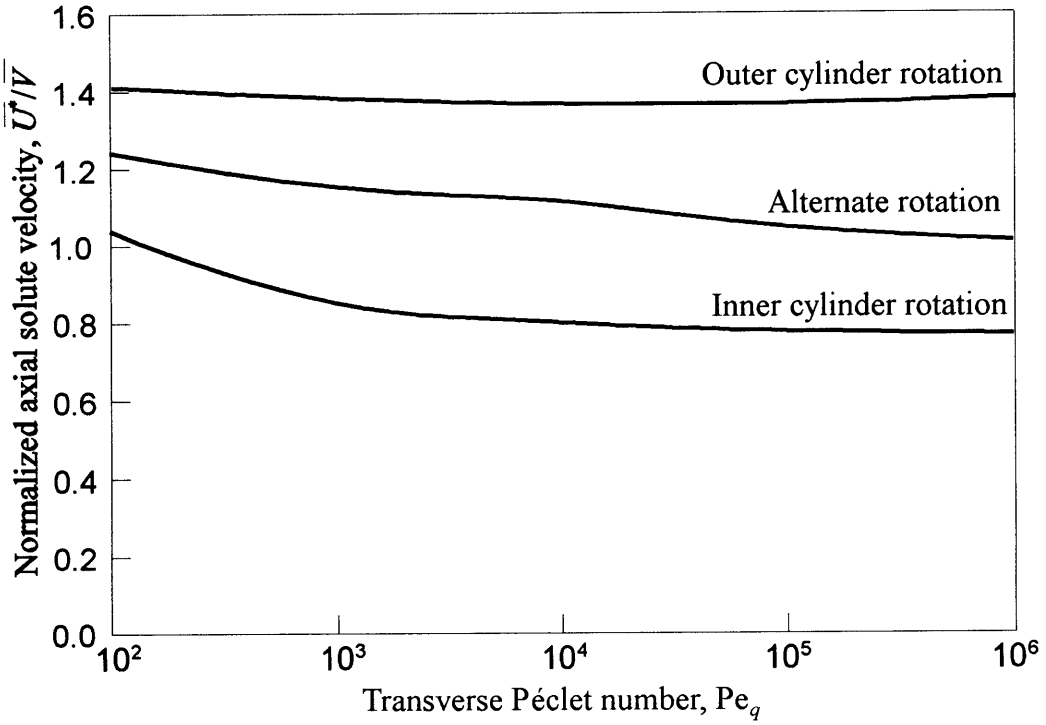

Figure 4-12: Effective solute velocity at the optimum rotation period, with $R_i/R_o = 0.3$, $\epsilon = 0.5$, and $\Omega_i/\Omega_o = 6$.

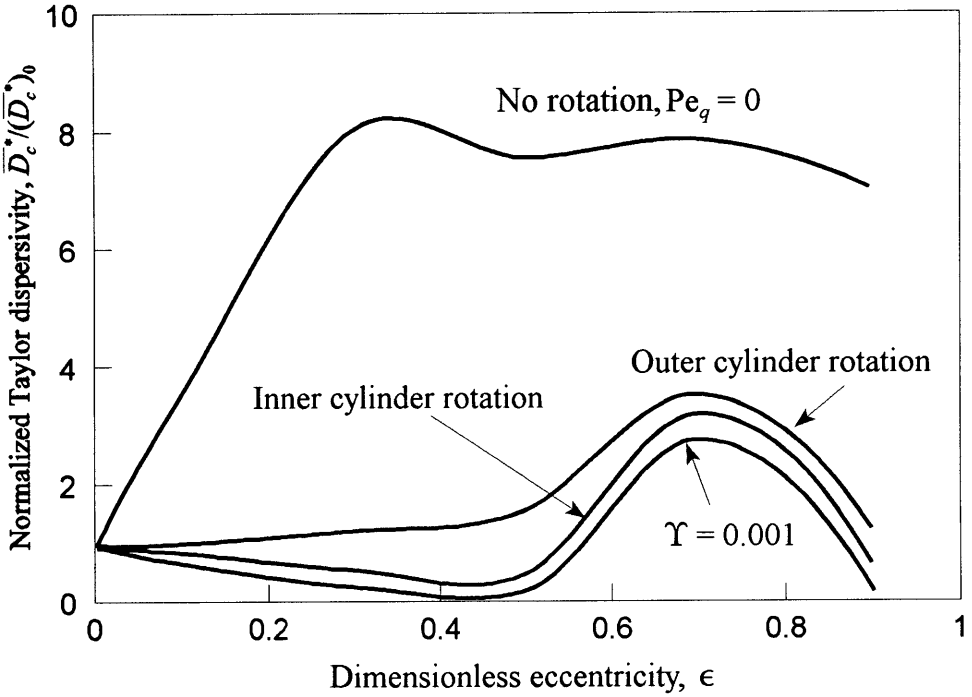

Figure 4-13: Dependence upon eccentricity of the ratio of the convective contribution $\overline{D_c^*}$ to the dispersivity to its value $(\overline{D_c^*})_0$ for concentric cylinders in the absence of reaction and transverse flow, with $R_i/R_o = 0.3$, $\mathrm{Pe}_q = 5000$ and $\Omega_i/\Omega_o = 6$.

4.6.3 Convective dispersivity

Figure 4-13 portrays the dimensionless convective contribution $\overline{D_c^*}/(\overline{D_c^*})_0$ to the dispersivity, in which $(\overline{D_c^*})_0$ represents the convective or Taylor dispersivity occurring for the case of concentric cylinders and in the absence of transverse flow. The diminution of solute concentration along the slower-moving streamlines resulting from reaction at the outer wall causes the dispersivity in the absence of transverse flow to be less than that observed by Sankarasubramanian & Gill (1971). In both the present work and that of the afore-mentioned authors the dispersivity increases markedly as the eccentricity is increased. This phenomenon is caused by the increasing gradients arising in the axial velocity profile with increasing eccentricity. The presence of steady transverse convection, as embodied in the pair of curves for the respective individual rotations of the inner and outer cylinders, acts to suppress most of this increase by allowing a solute particle to cross-sectionally sample the axial streamlines more rapidly. As evidenced by the $\Upsilon = 0.001$ data, the effect of laminar chaos is to further decrease the convective dispersion as a consequence of the enhanced transverse transport.

The Pe_q dependence of the convective dispersivity for $\epsilon = 0.5$ is shown in figure 4-14. At large Pe_q, when the cylinders are rotated alternately ($\Upsilon = 0.01$), the dispersivity achieves only about 5% of the value arising in the complete absence of rotation, and only one-half of the value attained when the inner cylinder is rotated continuously. For uniform rotation of the inner cylinder, as well as for alternate rotation of both cylinders, the Taylor dispersivity increases with Pe_q for small Péclet numbers, then subsequently decreases with further increases of Pe_q, as expected. This initial increase is caused by an enhancement in the probability of a tracer particle being found on one of the slower-moving streamlines, a result of the recirculation existing near the outer wall. For larger Pe_q this effect is ultimately overcome by the diminished time required for a solute particle to cross-sectionally sample all of the axial streamlines.

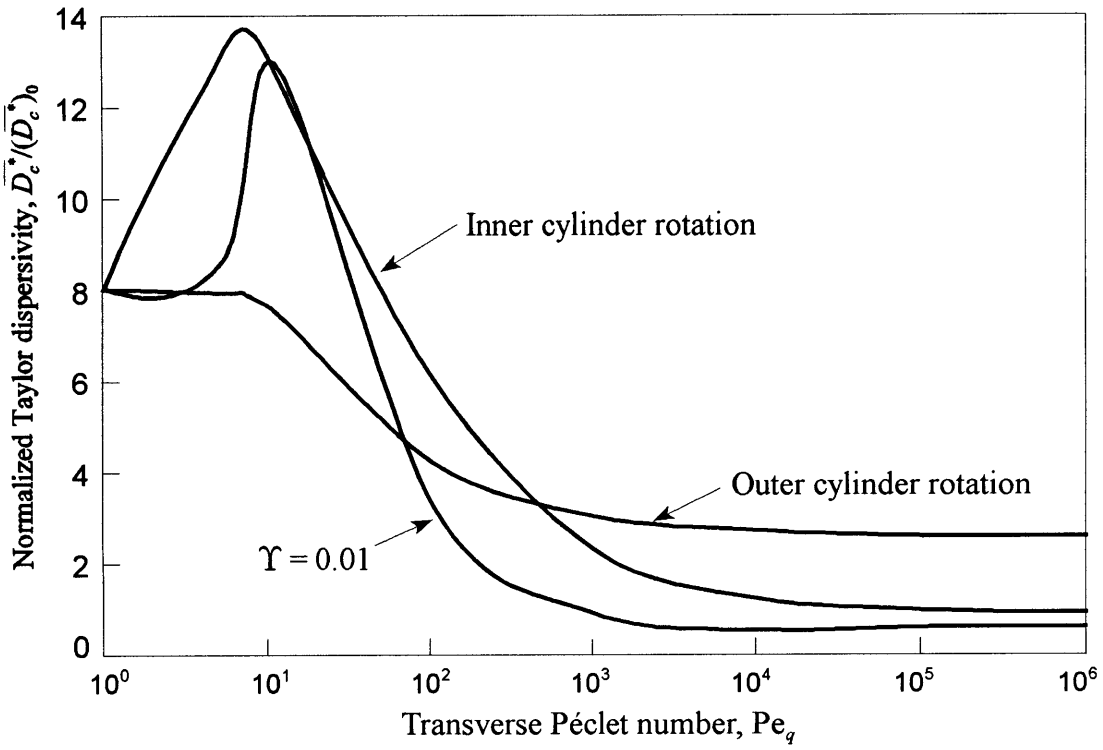

Figure 4-14: Dependence of the normalized convective, Taylor contribution to the dispersivity upon Pe_q, with $R_i/R_o = 0.3$, $\epsilon = 0.5$, and $\Omega_i/\Omega_o = 6$.

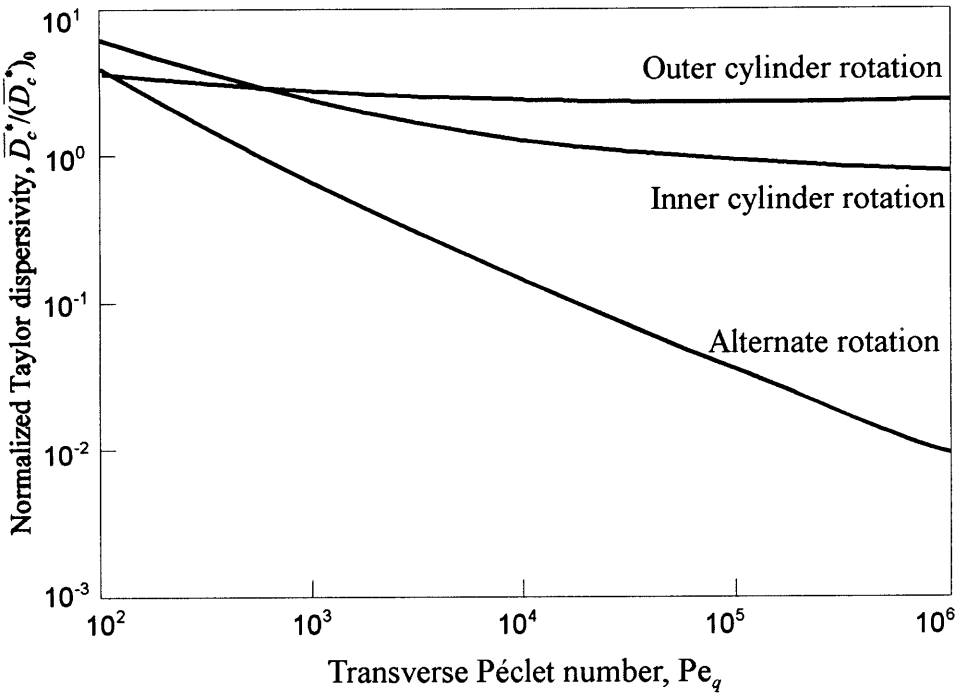

Figure 4-15: Dependence of the Taylor contribution to the dispersivity at the optimum alternation period upon Pe_q, with $R_i/R_o = 0.3$, $\epsilon = 0.5$, and $\Omega_i/\Omega_o = 6$.

The convective dispersivity achieved at the optimum alternation period is displayed as a function of Pe_q in figure 4-15. The alternation period that maximizes the reaction rate is the same as that which minimizes dispersion for large Pe_q. While the dispersivities for continuous rotation of either of the cylinders reach asymptotic values for large transverse Péclet numbers, that for alternate rotation at the optimum period decays as approximately $\mathrm{Pe}_q^{-0.65}$. Thus, the dispersivity under these circumstances is no longer inversely proportional to D, instead varying as $D\mathrm{Pe}_q^{-0.65}\mathrm{Pe}_Q^2 \propto D^{-0.35}$. This behaviour is consistent with the results of Mezić, Brady & Wiggins (1996), which show that the axial dispersivity does not vary inversely with the molecular diffusivity when an ergotic transversal flow is present. However, the Pe_q dependence in this case is different than the $\mathrm{Pe}\ln\mathrm{Pe}$ dependence found by Jones & Young (1994) in the 'twisted-pipe' flow.

4.7 Conclusions

In addition to affecting the three phenomenological macrotransport coefficients appearing in the macrotransport equation (4.4-10), the presence of chaotic advection also reduces the length of time required before the asymptotic description of the transport process embodied in (4.4-10) becomes applicable. In the absence of transverse convection, this description is valid only for times exceeding a characteristic cross-sectional diffusion time, $(R_o - R_i)^2/D$. For species with small diffusivities this restriction may be prohibitively long, allowing the solute particle to exit the duct (and hence be monitored) before the asymptotic theory described here becomes valid. By enhancing the lateral transport rate, the presence of laminar chaos significantly reduces the amount of time required to reach this asymptotic state. For example, with the arbitrarily chosen, spatially-uniform initial condition used in our calculations, and for the case where rotation is absent and $\epsilon = 0.5$, the reaction-rate constant achieved

a value lying within 1% of its ultimate, asymptotic value in a dimensionless time interval of $\tau = 0.28$ following its introduction. This compares with the very much smaller times of 1.2×10^{-2} and 1.5×10^{-3} required to achieve the same 99% asymptote for alternation at the optimum frequency with $\mathrm{Pe}_q = 10^4$ and 10^5, respectively. This finding is consistent with the analysis of Jones (1994), which showed that the time required for Taylor dispersion to be valid in the chaotic flow in a twisted pipe is $t \gg R/U\mathrm{lnPe}$ rather than $t \gg R^2/D$ as for nonchaotic flow.

From the results presented here it is evident that laminar chaotic advection not only significantly enhances the *extent* mixing of an inhomogeneous fluid, as has been previously demonstrated (Aref & Balachandar 1986, Chaiken *et al.* 1987, Swanson & Ottino 1990), but also increases the effective transverse transport *rate*. In particular, it is seen that the deposition or reaction rate may be enhanced at least severalfold over that achieved in the complete absence of transverse convection, or when one of the two cylinders is continuously and singly rotated. For $\mathrm{Pe}_q = 5000$ the maximum reaction rate attainable is approximately 2.5 times that obtained for the purely diffusive case, or 30% greater than that attainable by rotating the inner cylinder singly (figure 4-5). For very large $\mathrm{Pe}_q(10^6)$, the maximum deposition rate in the presence of laminar chaos (figure 4-10) is nearly five times that achieved solely by steady rotation of the inner cylinder alone (figure 4-7), the maximum rate achievable by regular, nonchaotic, secondary convective transport.

Lateral transport enhancement is also observed to affect both the mean axial solute velocity and convective dispersivity. Explicitly, the effect of chaotic transport is to cause the mean value of the axial solute velocity through the annulus to approach that of the solvent, despite the selective removal of solute from the slower-moving axial streamlines. At the same time, the existence of laminar chaos acts to dramatically decrease the Taylor dispersivity by as much as several orders of magnitude over that achievable by non-chaotic advection. It was also noted that any change of parameters

that serves to increase the deposition rate will, in most cases, decrease the dispersivity, although this is not always the case. The most notable exception occurs at small Pe_q, where the dispersivity increases with increasing Pe_q, simultaneous with the deposition rate. These differences in behaviour arise from the fact that whereas the deposition rate depends exclusively on cross-sectional transport, the axial dispersivity depends jointly on both the transverse and axial transport. Therefore, for one seeking a computational means of evaluating the transport effectiveness of a given flow field, the deposition rate is the most sensitive of the three possible phenomenological measures by virtue of its exclusive dependence on the transverse transport processes.

Poincaré maps, while providing a qualitative view of the extent of chaotic transport, as well as a visual image of which regions of the flow are affected by laminar chaos, furnish no directly usable engineering design information regarding the transverse transport rate (Swanson & Ottino 1990). In contrast, the present work provides a quantitative measure of the degree of transport enhancement arising from the presence of chaotic advection. In particular, Poincaré sections indicate that, in general, longer switching periods lead to a greater extent of mixing. Here, it was found that an optimum alternation frequency exists with respect to the transport rate. Moreover, our analysis incorporates the effect of molecular diffusion, demonstrating that even at very large transverse Péclet numbers, the presence of molecular diffusion can significantly affect the transport rate beyond that occasioned by convection (i.e., laminar chaos) alone, provided that sufficient time is allowed. On a broader theme, quantitative understanding of the interaction between molecular diffusion and laminar chaos may have important ramifications in elaborating the much debated (Glotefety, Taylor & Zoller 1983) role of molecular diffusion in turbulent chaos.

References

[1] AREF, H. & BALACHANDAR, S. 1986 Chaotic advection in a Stokes flow. *Phys. Fluids* **29**, 3515–3521.

[2] BALLAL, B. Y. & RIVLIN, R. S. 1976 Flow of a Newtonian fluid between eccentric rotating cylinders: inertial effects. *Archiv. Rat. Mech. Anal.* **62**, 237–294.

[3] BRYDEN, M.D. & BRENNER, H. 1996*a* Effect of laminar chaos on reaction and dispersion in eccentric annular flow. *J. Fluid Mech.* **325**, 219–237.

[4] CHAIKEN, J., CHU, C. K., TABOR, M., & TAN, Q. M. 1987 Lagrangian turbulence and spatial complexity in a Stokes flow. *Phys. Fluids* **30**, 687–694.

[5] GLOTEFETY, D. E., TAYLOR, A. E. & ZOLLER, W. H. 1983 Atmospheric dispersion of vapors: Are molecular properties unimportant? *Science*. **219**, 843–845.

[6] HAPPEL, J. & BRENNER, H. 1983 *Low Reynolds Number Hydrodynamics*. Kluwer.

[7] JONES, S. W. 1994 Interaction of chaotic advection and diffusion. *Chaos, Solitons, & Fractals* **4**, 929–940

[8] KAPER, T. J. & WIGGINS, S. 1993 An analytical study of transport in Stokes flows exhibiting large-scale chaos in the eccentric journal bearing. *J. Fluid Mech.* **253**, 211–243.

[9] KUSCH, H. A. & OTTINO, J. M. 1992 Experiments on mixing in continuous chaotic flows. *J. Fluid Mech.* **236** 319–348.

[10] MEZIĆ, I., BRADY, J. F. , & WIGGINS, S. 1996 Maximal effective diffusivity for time periodic incompressible fluid flows. To appear in *SIAM J. Appl. Maths.*

[11] PIERCY, N. A. V., HOOPER, M. S. & WINNEY, H. F. 1933 Viscous flow through pipes with cores. *Phil. Mag.* **15**, 647–676.

[12] SAN ANDRES, A. & SZERI, A. Z. 1984 Flow between eccentric rotating cylinders. *J. Appl. Mech.* **51**, 869–879.

[13] SANKARASUBRAMANIAN, R. & GILL, W. N. 1971 Taylor dispersion in laminar flow in an eccentric annulus. *Int. J. Heat Mass Trans.* **14**, 905–919.

[14] SHAPIRO, M. & BRENNER, H. 1986 A reactive Taylor dispersion model of aerosol collection by fibrous and granular filters. *Proceedings of the 1986 CRDEC Conference on Obscuration and Aerosol Reseach.* Chemical Research, Development and Engineering Center ,U.S.Army. Edgewood, Maryland.

[15] SHAPIRO, M., KETTNER, I. J., & BRENNER, H. 1991 Transport mechanics and collection of submicrometer particles in fibrous filters. *J. Aerosol Sci.* **22**, 707–722.

[16] SHAPIRO, M. & BRENNER, H. 1990 Taylor dispersion in the presence of time-periodic convection phenomena. Part 1. Local-space periodicity. *Phys. Fluids* A. **10**, 1731–1743.

[17] SNYDER, W. T. & GOLDSTEIN, G. A. 1965 An analysis of fully developed laminar flow in an eccentric annulus. *AIChE J.* **11**, 462–467.

[18] SWANSON, P. D. & OTTINO, J. M. 1990 A comparative computational and experimental study of chaotic mixing of viscous fluids. *J. Fluid Mech.* **213**, 227–249.

[19] TAYLOR, G. I. 1953 Dispersion of soluble matter in solvent flowing slowly through a tube. *Proc. R. Soc. Lond.* A **219**, 186–203.

Chapter 5

Chaotic streamlines and mass-transfer enhancement within a non-neutrally buoyant droplet undergoing simple shear

Abstract

The Stokes flow occurring within a non-neutrally buoyant spherical droplet suspended in an immiscible liquid which is undergoing simple shear is shown to be chaotic under many circumstances for which the droplet translates by buoyancy through the entraining fluid. This flow is easily produced, for example, when the droplet rises (or falls) through the annular space of a vertical concentric cylinder Couette viscometer or through a vertical Poiseuille flow. The parameters studied include: (i) droplet/bulk fluid viscosity ratio; (ii) shear strength/bubble rise velocity ratio; and (iii) the angle between the translational bubble velocity vector and the vorticity vector characterizing the undisturbed shear. Streamlines existing within a droplet that translates perpendicular to this vorticity vector are shown to be non-chaotic for all choices of physical parameters. Other relative orientations frequently contain chaotic trajectories. When solute initially dissolved within the droplet is extracted into the bulk fluid, the resulting overall mass-transfer coefficient (calculated via generalized Taylor dispersion theory) quantifying the extraction rate at asymptotically long times is shown to be significantly higher in the chaotic flow case.

5.1 Introduction

In addition to the enhancement of reaction or deposition rates and the reduction of axial convective dispersion discussed in the previous chapter, many other potential practical applications of laminar chaos for enhancing transport rates remain to be investigated. This chapter addresses one such application, the transport of a passive solute from a non-neutrally buoyant spherical droplet into an entraining bulk fluid which is undergoing simple shear. Chaotic Stokes flows within a spherical domain have been studied by Bajer & Moffatt (1990) as well as by Stone, Nadim & Strogatz (1991), the former considering a general quadratic flow occurring within a sphere and the latter the internal streamlines for a neutrally-buoyant spherical droplet dispersed in a fluid which is undergoing a general linear flow. Another three-dimensional confined flow exhibiting chaotic behavior is the time-dependent spherical Couette flow considered by Cartwright, Feingold & Piro (1996). The work of Stone *et al.* (1991) is the most relevant in the context of our work. They demonstrated that the particle paths within a drop immersed in a general linear Stokes flow may wander chaotically, with the extent of chaotic motion depending upon the orientation of the vorticity vector relative to the principal axes of strain of the undisturbed shear flow, as well as upon the relative magnitudes of the vorticity and shear rate. However, they did not consider the circumstances of a non-neutrally buoyant drop (which translates relative to the bulk fluid), which their preliminary results suggested exhibited behavior similar to that observed for their neutrally-buoyant case. In addition, they noted that the internal pathlines arising for the simple shear flow case are non-chaotic.

In the present chapter we focus on the superposition of the two above-mentioned flows, whereby a spherical drop translates through a simple shear flow. In combination, these elementary flows can display chaotic behavior within the droplet. The structure of the resulting Poincaré sections differs appreciably from those observed in the flows considered by Stone *et al.* (1991). Potential fundamental and practical

interest centers on the flows considered herein owing to the ease with which they can be realized experimentally, in addition to their immediate applicability to common chemical engineering processes such as liquid-liquid extraction. Poincaré sections for these flows are presented in §5.3, and the parameter ranges established for which chaotic flow occurs. Section 5.4 presents values obtained for the overall mass-transfer coefficient quantifying the transport of a passive solute from the droplet interior into the external fluid phase. Results are given for circumstances in which the flow internal to the drop is chaotic, as well as when it is non-chaotic. These mass-transfer data provide a quantitative global measure of the chaotically-enhanced improvement in extraction rate.

5.2 The flow field internal to the drop

The circumstance to be considered is that of a spherical droplet translating by buoyancy through a fluid undergoing a simple shear flow. Different angles α between the direction of the vorticity vector ω of the undisturbed shear flow and the direction of the gravity vector $\mathbf{g}$ will be investigated, with particular attention paid to the limiting cases in which ω is either parallel ($\alpha = 0$) or perpendicular ($\alpha = \pi/2$) to gravity. Each of these configurations is easily produced: the former results from allowing the bubble to rise or fall through the annular space between two vertical concentric cylinders, wherein a Couette flow is maintained by their relative rotation; the latter results when a bubble rises or falls within a Poiseuille flow occurring in a vertical tube. [For definiteness in the subsequent analysis, the relative translational motion of the droplet will always be described as if it were rising through the fluid (i.e. moving opposite to the direction of gravity).] Intermediate angle flows ($0 < \alpha < \pi/2$) are also easily realized by combining the circular Couette flow with an annular Poiseuille flow. As will be seen later, the two limiting angles yield flows which display strikingly

different behavior, with the $\alpha = 0$ case containing large regions in which the particle paths within the droplet are chaotic, whereas the $\alpha = \pi/2$ case contains only periodic pathlines. In circumstances where the externally-imposed flow is not strictly a *linear* shear flow it may nevertheless be regarded as such in proximity to the droplet, provided that the droplet radius a is small compared with both the characteristic linear dimension of the apparatus in which the external flow is generated and the distance of the droplet from the walls of this apparatus. The droplet will be assumed to remain spherical, a condition which requires *inter alia* that the respective Reynolds numbers based on translation and shear both be small compared to unity, and that the interface be inviscid [i.e. devoid of any special interfacial rheological properties (Edwards, Brenner & Wasan 1991) other than interfacial tension]. Accordingly, in the quasi-steady Stokes flow case the complete flow occurring within the droplet is simply the linear superposition of the respective flows resulting from the bubble's translation through the quiescent fluid and from the external shear flow for the neutrally-buoyant droplet case.

The internal flow created by the bubble's translation is an axisymmetric Stokes flow of the form (Hadamard 1911)

$$\mathbf{v}_T = \frac{1}{2a^2(1+\sigma)}\mathbf{U}\cdot[\mathbf{xx} - (2r^2 - a^2)\mathbf{I}], \tag{5.2-1}$$

in which $\sigma = \mu_i/\mu_o$ is the droplet/external-fluid viscosity ratio, $\mathbf{x}$ is the position vector measured from the center of the drop, $r^2 = \mathbf{x}\cdot\mathbf{x}$, and

$$\mathbf{U} = \frac{2a^2\Delta\rho g}{9\mu_o}\frac{1+\sigma}{\frac{2}{3}+\sigma}\hat{\mathbf{g}} \tag{5.2-2}$$

is the bubble velocity, with $\Delta\rho$ the algebraically-signed droplet/external-fluid density difference, $g = |\mathbf{g}|$ the acceleration of gravity, $\hat{\mathbf{g}} \equiv \mathbf{g}/g$ a unit vector parallel to gravity, and a the droplet radius. Typical streamlines resulting from this flow are plotted in

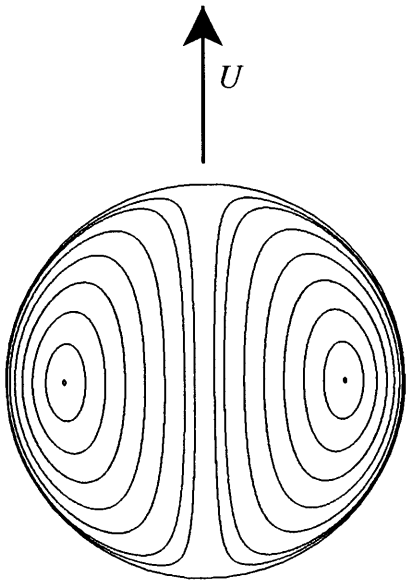

Figure 5-1: Streamlines internal to a spherical droplet rising by buoyancy through a quiescent fluid.

figure 5-1.

A general external shear flow of the form $\mathbf{v}^\infty = \mathbf{x} \cdot \mathbf{G}$, with $\mathbf{G} \equiv \nabla \mathbf{v}^\infty$ the undisturbed velocity gradient, induces a fully three-dimensional flow within the droplet. The internal flow field for a neutrally-buoyant droplet possessing an inviscid interface and suspended within such a shear flow is given by Taylor (1932) as

$$\mathbf{v}_G = \frac{1}{4a^2(1+\sigma)}[(5r^2 - 3a^2)(\mathbf{G} + \mathbf{G}^\dagger) \cdot \mathbf{x} - 2\mathbf{x}\mathbf{x} \cdot \mathbf{G} \cdot \mathbf{x}] + \frac{1}{2}\omega \times \mathbf{x}, \qquad (5.2\text{-}3)$$

with $\omega = \nabla \times \mathbf{v}^\infty$ the vorticity vector. For the simple shear flow $\mathbf{v}^\infty = \mathbf{i_2} G x_1$, we have that $\mathbf{G} = \mathbf{i_1}\mathbf{i_2} G$ and $\omega = \mathbf{i_3} G$, with (x_1, x_2, x_3) a system of right-handed rectangular Cartesian coordinates, $(\mathbf{i_1}, \mathbf{i_2}, \mathbf{i_3})$ the corresponding unit vectors, and G the shear rate. Typical internal streamlines generated by this flow are shown in figure 5-2. Note that as σ increases, the streamlines approach those for a solid-body rotation. It will be shown later that no chaotic flow exists for these large values of σ.

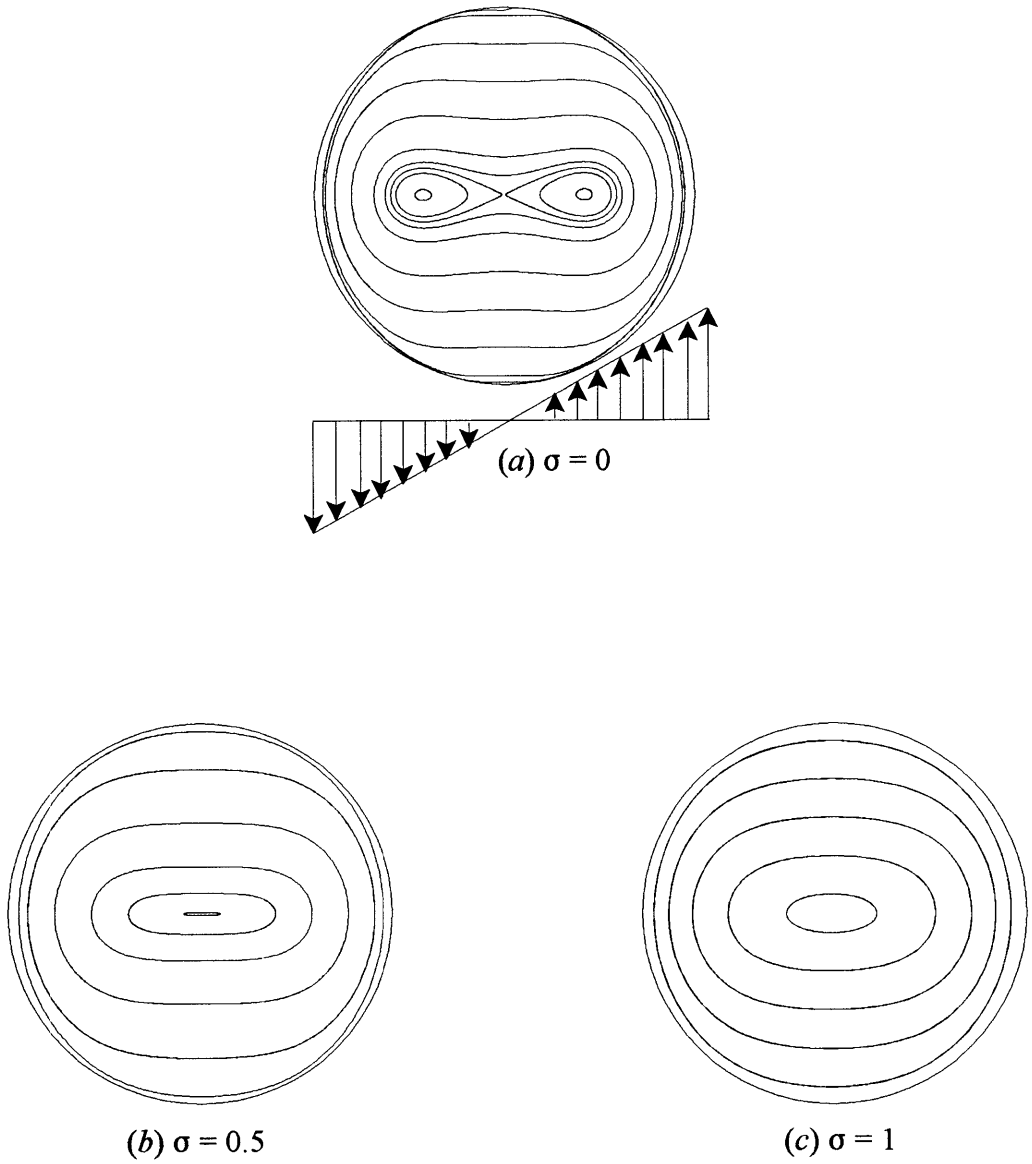

Figure 5-2: Streamlines internal to a neutrally-buoyant spherical droplet suspended in a fluid undergoing simple shear flow for various viscosity ratios. The streamlines shown are those lying in the meridian plane containing the simple shearing flow.

5.3 Chaotic trajectories within the drop: Poincaré sections

A qualitative description of the flow may be obtained through the use of Poincaré sections. In the present case we integrate the equation

$$\frac{d\mathbf{x}}{dt} = \mathbf{v}(\mathbf{x}) \tag{5.3-4}$$

governing the Lagrangian trajectories $\mathbf{x} \equiv \mathbf{x}(\mathbf{x}_0, t)$ of the fluid particles, with $\mathbf{v}$ the vector velocity field arising from the appropriate superposition of (5.2-1) and (5.2-3), and $\mathbf{x}$ the position vector at time t of the particular fluid particle whose position vector at time $t = 0$ was $\mathbf{x}_0$. Poincaré sections may then be obtained in an appropriately chosen plane, in this case the meridian plane whose unit normal is $\hat{\mathbf{g}}$. These plots are similar to those obtained by Stone *et al.* (1991) for more general shear flows.

Three non-dimensional fluid-mechanical parameters arise in the present study: (i) the ratio $\hat{G} \equiv aG/U$, representing the strength of the shear field relative to the bubble rise velocity $U = |\mathbf{U}|$; (ii) the internal/external viscosity ratio σ; and (iii) the angle $\alpha = \cos^{-1}(\mathbf{i}_3 \cdot \hat{\mathbf{g}})$ $(0 \leqslant \alpha \leqslant \pi/2)$ between the undisturbed vorticity vector and the direction of gravity. [The orientation of the x_1 coordinate is maintained such that throughout this chapter the angle $\cos^{-1}(\mathbf{i}_1 \cdot \hat{\mathbf{g}}) = \pi/2$.]

Displayed in figure 5-3 are the Poincaré sections for $\hat{G} = 1$, $\alpha = 0$ (corresponding to a bubble rising perpendicularly to the shear plane), and for varying viscosity ratios σ. As is evident, the extent of the chaotic region decreases with increasing σ. Indeed, as $\sigma \to \infty$ the flow becomes completely non-chaotic, with the flow internal to the droplet being simply a rigid-body rotation at angular velocity $1/2\omega$.

Figure 5-4 displays Poincaré sections for $\sigma = 0$, $\alpha = 0$, and for several values of $\hat{G}$. For small shear rates, such as $\hat{G} = 0.1$, the particle trajectories are quasiperiodic,

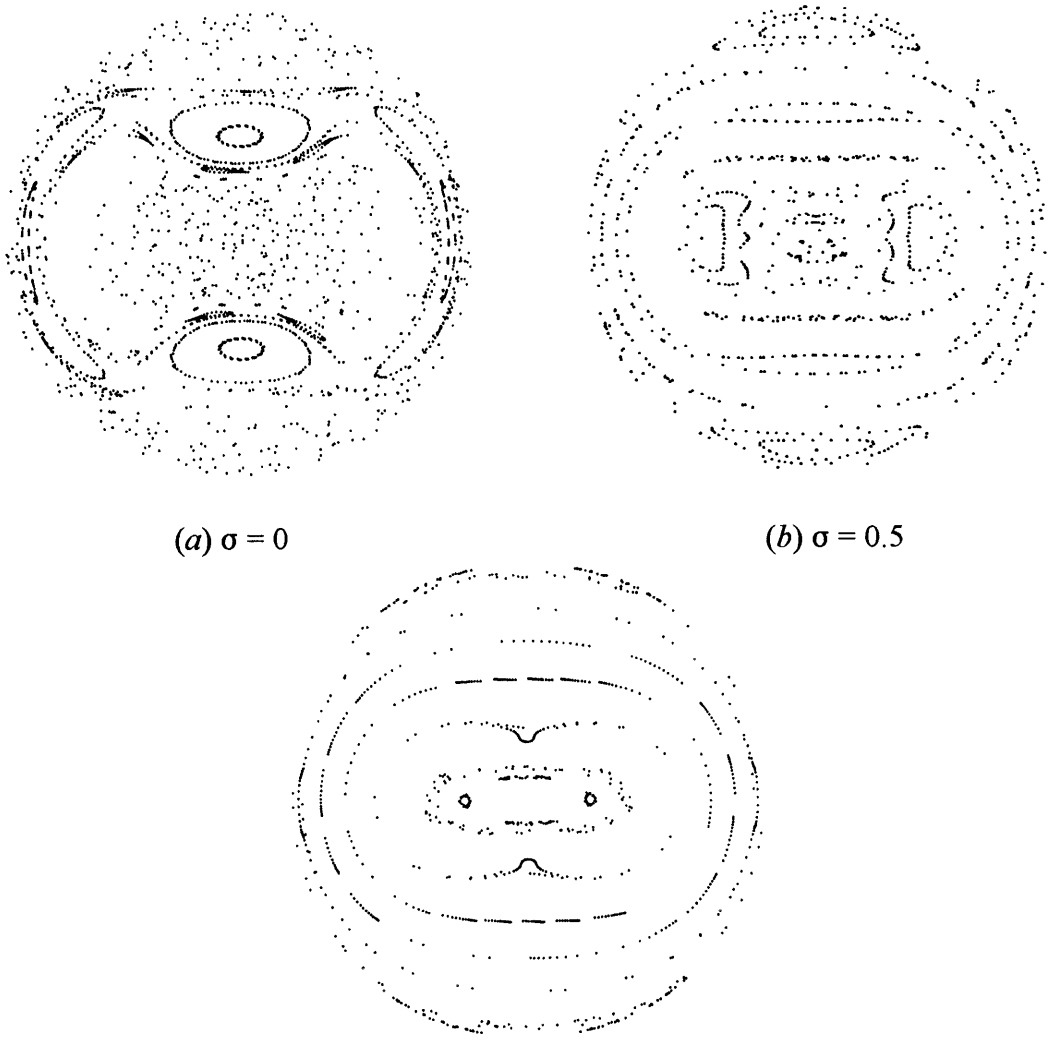

(*a*) σ = 0

(*b*) σ = 0.5

(*c*) σ = 1

Figure 5-3: Poincaré sections for $\hat{G} = 1$, $\alpha = 0$ and the indicated viscosity ratios.

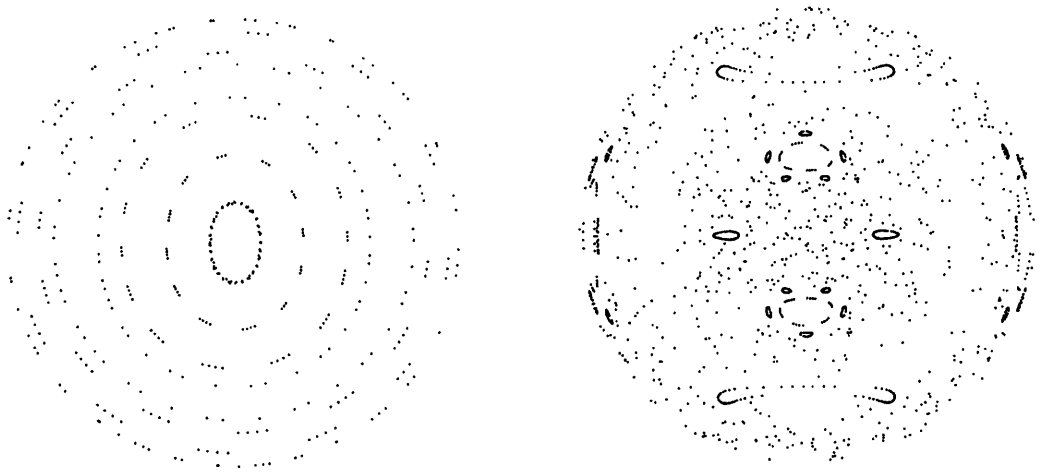

(*a*) $\hat{G} = 0.1$ (*b*) $\hat{G} = 0.5$

Figure 5-4: Poincaré sections for $\sigma = 0$, $\alpha = 0$, and the indicated shear strength ratios.

with particles traversing the surface of a torus (see figure 5-5). Larger values of $\hat{G}$ result in correspondingly larger regions of the flow containing chaotic trajectories.

Figure 5-6 depicts the Poincaré section resulting when $\hat{G} = 1$, $\sigma = 0$, and $\alpha = \pi/4$. This flow exhibits considerable chaotic behavior. In contrast, for $\alpha = \pi/2$ the resulting particle trajectories differ qualitatively from those at other angles. Indeed, since the respective internal flows generated by the translational and shear flows lie in the same plane, the resulting particle trajectories are purely periodic.

5.4 Effective mass-transfer coefficient

This section furnishes a calculation of the rate at which a passive solute, initially dissolved in the droplet and absent from the bulk fluid, is transferred into the latter. The resistance to interphase mass transfer will be assumed governed locally by an external mass-transfer coefficient k which is independent of surface position. [Our analytical and computational methods are equally applicable to circumstances in which the mass-transfer coefficient k, rather than being constant, varies in a prescribed

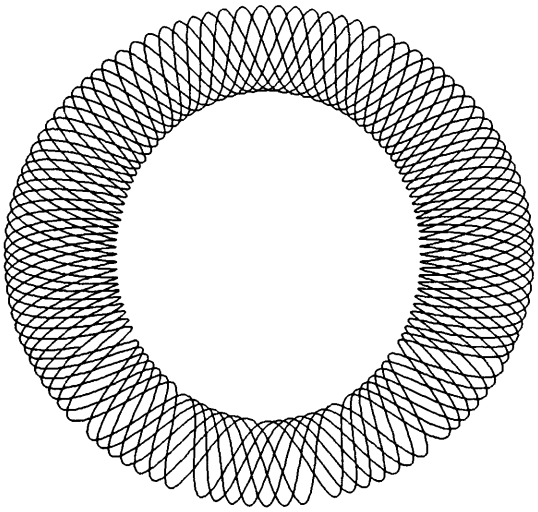

Figure 5-5: Typical trajectory of a particle with $\hat{G} = 0.1$, $\sigma = 0$, and $\alpha = 0$

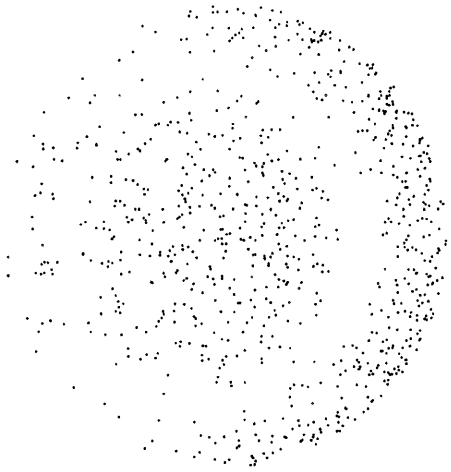

Figure 5-6: Poincaré section for $\sigma = 0$, $\alpha = \pi/4$, and $\hat{G} = 1$

manner over the surface of the droplet (e.g. Lochiel & Calderbank 1964, Baird & Hamielec 1962).] Our goal is to determine the overall rate of interphase mass transfer by investigating the internal convective and diffusive transport processes occurring within the droplet. During the process the external fluid will be assumed to act simply as an infinite reservoir for solute, and hence to undergo no changes itself in solute concentration.

The instantaneous solute concentration $c(\mathbf{x}, t)$ within the droplet obeys the standard convective-diffusive equation

$$\frac{\partial c}{\partial t} + \mathbf{v} \cdot \nabla c - D\nabla^2 c = 0, \tag{5.4-5}$$

subject to the respective initial and boundary conditions,

$$c = c_0 \quad \text{at} \quad t = 0, \tag{5.4-6}$$

$$D\frac{\partial c}{\partial r} = -kc \quad \text{at} \quad r = a, \tag{5.4-7}$$

where $c_0 \equiv c(\mathbf{x}, 0)$ is taken to be a constant. The results ultimately obtained for the overall mass-transfer coefficient K defined in (5.4-8) are independent of this arbitrary choice of initial solute distribution, the constancy of c_0 being chosen merely for convenience.

These equations were solved numerically using an alternating-direction finite-difference method, and the overall mass-transfer coefficient subsequently calculated as

$$K = -\lim_{t\to\infty} \frac{1}{\Delta t} \ln\left(\frac{\int_V c(\mathbf{x}, t + \Delta t)dV}{\int_V c(\mathbf{x}, t)dV}\right), \tag{5.4-8}$$

in which Δt is an arbitrarily short time interval and V denotes the droplet domain. This approach is equivalent to solving the generalized Taylor dispersion zeroth-order local moment eigenvalue problem (Brenner & Edwards 1993). [See Edwards, Shapiro

& Brenner (1993) for a proof of this equivalence.] This asymptotic mass-transfer coefficient provides a global measure of the effectiveness of the chaotic flow field in enhancing the solute transport processes occurring within the droplet. It has the advantage of being independent of initial conditions, and is comparable in nature to the effective reaction-rate coefficient (Bryden & Brenner 1996) for circumstances wherein the solute is depleted by a first-order irreversible chemical reaction (quantifies by a kinetic reaction-rate coefficient k) occurring at the interface. The global physical significance of K lies in the fact that it appears as the coefficient of the exponential decay term in the asymptotic relation

$$M(t) \sim M_f \mathrm{e}^{-Kt} \tag{5.4-9}$$

governing the mass $M(t) = \int_V c(\mathbf{x}, t) dV$ of solute remaining in the droplet at time t for times t satisfying the inequality $t >> a^2/D$, with M_f the fictitious mass of solute initially present (Shapiro & Brenner 1987); that is, $M_f \neq M(0)$, where $M(0) = \int_V c(\mathbf{x}, 0) dV \equiv c_0 V$ in present circumstances. Calculation of M_f is discussed in §5 (see table 5.1).

For a fixed Sherwood number Sh= ka/D, we parametrically explored the effects on K of varying the: (i) translational Péclet number (Pe = Ua/D); (ii) shear strength/bubble rise velocity ratio $\hat{G}$; (iii) relative orientation α of the shear and translational flows; and (iv) viscosity ratio σ. Typical Péclet numbers for liquid droplets of diameters 0.1 to 10 mm are of order 10^5 to 10^{10} for hydrocarbon-aqueous systems. Such extremely high Péclet numbers can cause numerical instabilities in the requisite calculations. However, it proved unnecessary to carry out calculations at very large Péclet numbers, since clearly defined trends became evident at much smaller values. Indeed, for many sets of parameters an asymptotic limit was already achieved at values of Pe ≈ 100. Asymptotic limits were also observed at large Sher-

wood numbers. All the calculations reported here employed a value of Sh = 100, just slightly below the asymptotic limit at which the interphase transport rate becomes independent of k. Thus, the results reported herein furnish an approximation to the case wherein the external mass-transfer coefficient becomes infinite; that is, when the boundary condition (5.4-7) is replaced by the condition $c = 0$ at $r = a$.

Figure 5-7 displays the effective mass-transfer coefficient K as a function of Pe for $\alpha = 0$, $\sigma = 0$, and for various values of $\hat{G}$. With the exception of the $\hat{G} = 0.1$ case, each of these flows possesses chaotic regions (see figures 5-3a and 5-4). Also shown are the mass-transfer coefficients obtained when only one of the two basic flows, shear or translation, is present. For small Péclet numbers the extraction rate approaches that occurring in the absence of flow, namely the smallest root of $\tan\lambda = \lambda/(1-\mathrm{Sh})$, with $\lambda = Ka^2/D|_{\mathrm{Pe}=0}$ (approximately 9.67 for the present value of Sh = 100). From these results, it is clear that those flows which are chaotic, cf. figures 5-3(a) and 5-4(b), result in the largest extraction rates, whereas the quasiperiodic case ($\hat{G} = 0.1$) is nearly indistinguishable from the case of pure translational motion. The extraction rate induced by the shear flow alone is scarcely larger than that for the purely diffusive case. The latter behavior is expected, since many of the streamlines for this case resemble those for solid-body rotation; and a purely rotary internal flow contributes nothing to the transport of solute towards the droplet surface. From a comparison of figures 5-3(a) and 5-4(b) it is not obvious which of the two flows, $\hat{G} = 0.5$ or $\hat{G} = 1$, is the more chaotic in nature, since each Poincaré section contains several regular islands. In contrast with such purely qualitative attempts to distinguish the more chaotically effective of these two flows, the quantitative rate results of figure 5-7 clearly distinguish between them.

The influence of the viscosity ratio σ on mass transfer is illustrated in figure 5-8. Again, it is seen that those flows which appear visually to be most chaotic result in the largest mass-transfer rates.

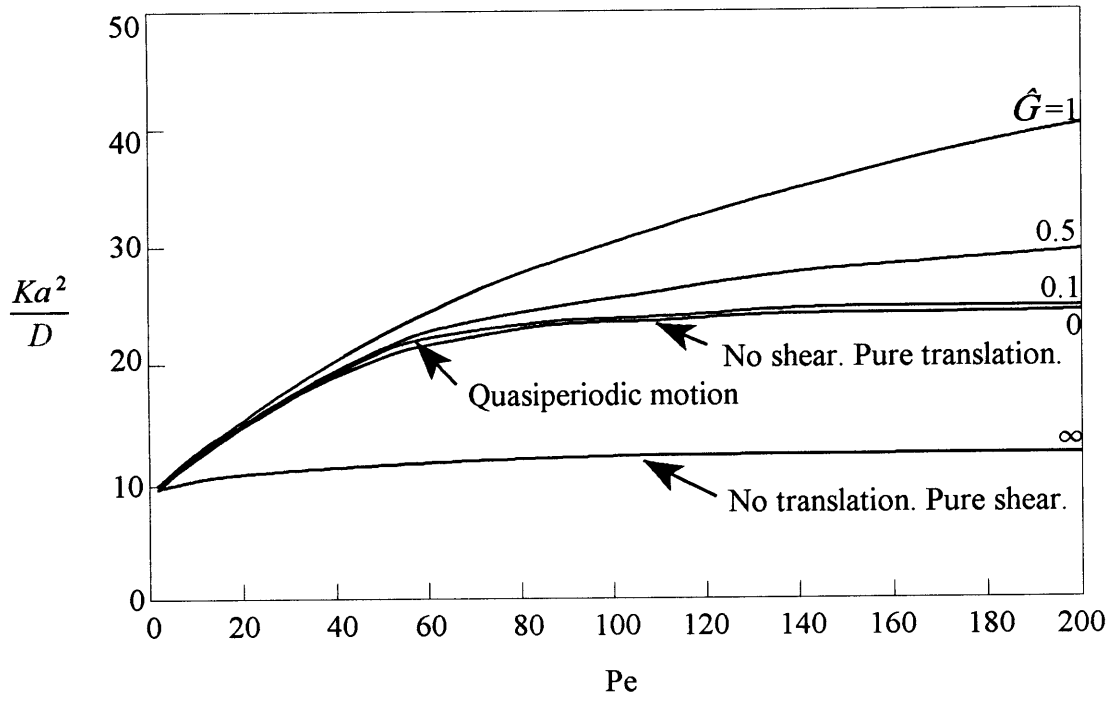

Figure 5-7: Effective mass-transfer coefficient as a function of Péclet number for $\alpha = 0$, $\sigma = 0$, Sh=100, and various values of $\hat{G}$. The value $\hat{G} = \infty$ corresponds to the case of no translation of the droplet. (In this case the value appearing on the abscissa is the shear Péclet number, $\mathrm{Pe}_G = a^2\hat{G}/D$. For a given Pe_G the strength of the shear field is identical to that present for $\mathrm{Pe} = \mathrm{Pe}_G$ and $\hat{G} = 1$.)

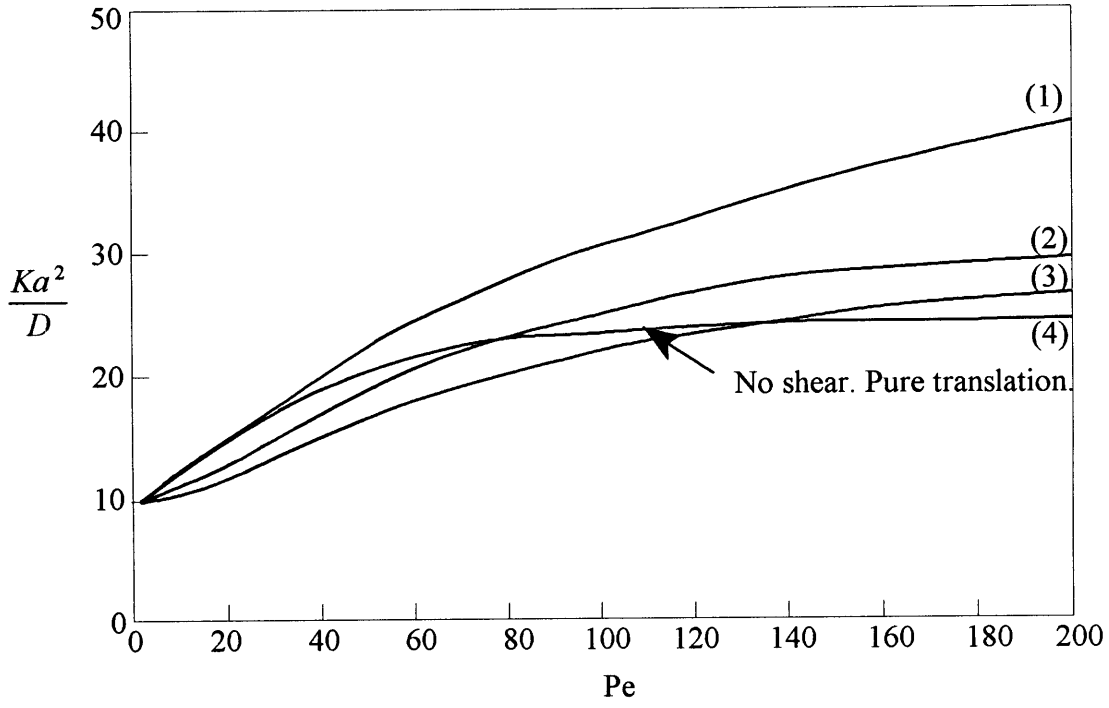

Figure 5-8: Effective mass-transfer coefficient as a function of Péclet number for $\alpha = 0$, Sh=100 and (1) $\hat{G} = 1$, $\sigma = 0$; (2) $\hat{G} = 1$, $\sigma = 0.5$; (3) $\hat{G} = 1$, $\sigma = 1$; (4) $\hat{G} = 0$, $\sigma = 0$.

Figure 5-9 furnishes the effective extraction rate as a function of Pe (with $\sigma = 0$ and $\hat{G} = 1$) for three possible relative orientations α of the directions of gravity and shear, namely : (i) $\alpha = 0$ (translational motion parallel to the vorticity vector); (ii) $\alpha = \pi/2$ (translational motion perpendicular to the vorticity vector); (iii) $\alpha = \pi/4$. As noted earlier, when $\alpha = \pi/2$ the trajectories are periodic, whereas in the remaining cases they are largely chaotic. It is clear that the chaotic flows again result in the greater extraction rates. Indeed, the effective mass-transfer coefficient in the $\alpha = \pi/2$ case is even less than that occurring in the absence of shear! This result is a consequence of the streamline pattern for this flow. Superposition of translation and shear lying in the same plane results in the disappearance of streamlines that circulate from the center of the droplet towards the exterior, despite their presence in the case of pure translation. Rather, the streamlines are now closer in configuration to concentric circles, thus contributing little to the extraction rate. Finally, the mass-transfer coefficient is seen to be greater for $\alpha = 0$ than for $\alpha = \pi/4$ despite the apparently larger extent of chaos visible in the latter case. Thus, the *extent* of the chaos does not always provide an accurate qualitative correlation of the global *rate* of transport.

5.5 Discussion

Although only bubbles with inviscid interfaces have been considered, the results obtained herein may nonetheless be applied to circumstances in which the interface is viscous (i.e. possesses its own intrinsic Newtonian interfacial rheological properties), provided that appropriate changes are made in the respective denominators of (5.2-1) and (5.2-3), as well as in the magnitude U of the translational velocity. This is a consequence of the fact that the configuration of the streamlines arising from the bubble's translational motion are unaffected by the existence of interfacial viscosity; only

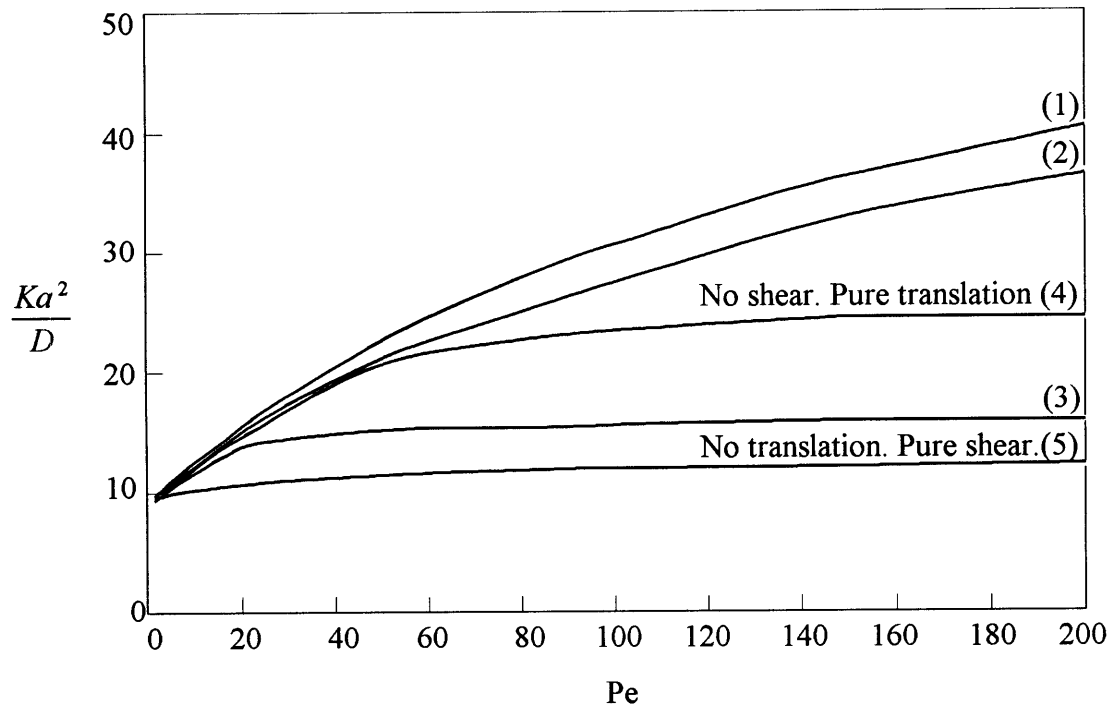

Figure 5-9: Effective mass-transfer coefficient as a function of Péclet number for $\sigma = 0$, Sh =100, and: (1) $\hat{G} = 1$, $\alpha = 0$; (2) $\hat{G} = 1$, $\alpha = \pi/4$; (3) $\hat{G} = 1$, $\alpha = \pi/2$; (4) $\hat{G} = 0$; (5) no translation ($\hat{G} \to \infty$).

σ	$\hat{G}$	α	Ka^2/D	$M_f/M(0)$
0	0	0	24.4	0.83
0	∞	0	12.0	0.60
0	0.1	0	23.5	0.83
0	0.5	0	29.4	0.84
0	1	0	40.6	1.14
0.5	1	0	30.5	0.95
1	1	0	26.5	0.93
0	1	$\pi/4$	36.7	1.22
0	1	$\pi/2$	15.8	0.54

Table 5.1: Effective mass-transfer coefficient Ka^2/D and fictitious/true initial solute mass ratio $M_f/M(0)$ for the uniform initial solute concentration case, with Pe=200, Sh=100, and the parametric trio sets cited herein.

the magnitude of U is influenced by the interfacial rheology (Edwards *et al.* 1991). Thus, the velocity field resulting from translational motion occurring in the presence of interfacial rheology is identical to that for an inviscid bubble, with the quantity $\sigma + \kappa^s/a\mu_o$ (in which κ^s is the surface dilatational viscosity) appearing in the place of the viscosity ratio σ in (5.2-1) and (5.2-2). Similarly, for small Reynolds and capillary numbers, interfacial rheology affects the droplet velocity field created by the external shear flow only through the denominator appearing on the right-hand side of (5.2-3) (Edwards *et al.* 1991), in which σ is then replaced by $\hat{\sigma} \stackrel{\text{def}}{=} \sigma + (5\mu_o a)^{-1}(4\mu^s + 6\kappa^s)$, with μ^s the surface shear viscosity. Furthermore, the value of $\hat{\sigma}$ varies over the range 0 to ∞ for both viscous and inviscid interfaces. Hence, by means of appropriate scaling, the results found here may also be applied to circumstances in which the interface is viscous.

In order to use (5.4-9) to predict the amount of solute remaining within the droplet at a given time t after the experiment commences, it is necessary to calculate the *fictitious* amount of solute M_f initially present in the droplet at $t = 0$ (Brenner & Edwards 1993). Use of a fictitious initial value in place of the true value corrects for those transport processes occurring prior to the time $t = O(a^2/D)$ at which the present global asymptotic description embodied in (5.4-9) becomes valid. Calculation

of M_f requires determining the solution $A(\mathbf{x})$ of the steady-state differential equation

$$\mathbf{v} \cdot \nabla A + D\nabla^2 A + KA = 0, \tag{5.5-10}$$

subject to the respective boundary and normalization conditions

$$D\frac{\partial A}{\partial r} = -kA \quad \text{at} \quad r = a, \tag{5.5-11}$$

$$\int_V P_0^\infty A dV = 1, \tag{5.5-12}$$

in which

$$P_0^\infty(\mathbf{x}) = \lim_{t\to\infty} \left\{ c(\mathbf{x},t) \Big/ \int_V c(\mathbf{x},t) dV \right\} \tag{5.5-13}$$

represents the long-time, 'non-reactive', zeroth-order, local moment (Brenner & Edwards 1993). For a specified true initial solute concentration $c(\mathbf{x},0)$, the fictitious mass M_f of solute initially present in the droplet is then found through the quadrature

$$M_f = \int_V c(\mathbf{x},0) A(\mathbf{x}) dV. \tag{5.5-14}$$

For Pe=200, table 5.1 displays the ratio of fictitious to true initial solute masses, $M_f/M(0)$, where $M(0) \equiv c_0 V$ is the true mass of solute initially present in the drop for the case described by (5.4-5) to (5.4-7). Equivalently, if we define a fictitious (uniform) initial solute concentration c_f as $c_f = M_f/V$, then $M_f/M(0) \equiv c_f/c_0$ represents the ratio of fictitious to true initial homogeneous solute concentration in the droplet.

The problem of extracting a solute from a translating droplet was addressed by Kronig & Brink (1949). They found an approximate solution for asymptotically large Péclet and Sherwood numbers. The asymptotic global extraction-rate coefficient $Ka^2/D = 24.4$ furnished by our calculations in the absence of shear (cf. table 5.1)

agrees quite well with the limiting value of 26.85 found by Kronig & Brink (1949) for the infinite Sherwood number case, the slight difference presumably being due to the difference in Sherwood numbers. However, our fictitious/true initial mass ratio of $M_f/M(0) = 0.83$ is larger than the value of 0.65 quoted by Kronig & Brink (1949). Our calculations showed that this latter quantity approaches its limiting asymptotic value at much larger values of both Pe and Sh than does K. Additional calculations performed with Sh=500 and Sh=800 (in place of Sh=100) and Pe=200 each provided identical values of 25.8 and 0.69 for the respective values of Ka^2/D and $M_f/M(0)$, whereas a calculation with Sh=500 and Pe=300 provided the respective values of 26.1 and 0.66, suggesting the possibility of excellent agreement between these two very different modes of calculation at Sh= ∞, Pe=∞.

5.6 Conclusions

We have demonstrated that chaotic low Reynolds number flows can arise within a spherical droplet by superposing translational and simple shear flows. Moreover, the presence of chaotic streamlines is shown to significantly increase the rate of extraction of a solute from the interior of the droplet into the bulk fluid, an observation of potential practical importance in the design of mass-transfer devices.

The class of flows studied herein possesses the distinct advantage of being easily realized with elementary equipment. Thus, unique opportunities exist for experimental studies of these chaotic flows. In this context, tracer studies similar to those undertaken for two-dimensional, time-dependent, chaotic flows (e.g. Swanson & Ottino 1990, Kusch & Ottino 1992, Dutta & Chevray 1995, Saatdjian *et al.* 1996), and three-dimensional, spatially periodic, chaotic flows (e.g. Kusch & Ottino 1992), as well as solute extraction experiments, would be expected to usefully supplement the present theoretical analysis. Such realizations would hopefully demonstrate the

practical applications of chaotic flows towards improving industrial mass-transfer processes.

The occurrence of chaos in such elementary circumstances as those studied here suggests that other simple, practically relevant, chaotic flows exist, and that they merely await discovery and/or theoretical elucidation before being put to productive use in industrial applications. Indeed, it appears that in many laminar flows, chaos may be the rule rather than the exception.

References

[1] BAIRD, M.H. I. & HAMIELIC, A.E. 1962 Forced convection transfer around spheres at intermediate Reynolds numbers. *Can. J. Chem. Engng*, **10** 119–121.

[2] BAJER, K. & MOFFATT, H.K. 1990 On a class of steady confined Stokes flows with chaotic streamlines. *J. Fluid Mech.* **212**, 337–363.

[3] BRENNER, H. & EDWARDS, D. A. 1993 *Macrotransport Processes.* Butterworth-Heinemann.

[4] CARTWRIGHT, J.H.E., FEINGOLD, M. & PIRO, O. 1996 Chaotic advection in three-dimensional unsteady incompressible laminar flow. *J. Fluid Mech.* **316**, 259 –284.

[5] DUTTA, P. & CHEVRAY, R. 1995 Enhancement of mixing by chaotic advection with diffusion. *Exp. Thermal Fluid Sci.* **11**, 1-12.

[6] EDWARDS, D.A., BRENNER, H. & WASAN, D.T. 1991 *Interfacial Transport Processes and Rheology*. Butterworth-Heinemann.

[7] EDWARDS, D.A., SHAPIRO, M. & BRENNER, H. 1993 Dispersion and reaction in two-dimensional model porous media. *Phys. Fluids A* **5**, 837–858.

[8] HADAMARD, J.S. 1911 Mouvement permenent lent d'une sphere liquide et visqueuse dans un liquide visqueux. *Comp. Rend. Acad. Sci.* **152**, 1735–1738.

[9] HAPPEL, J. & BRENNER, H. 1983 *Low Reynolds Number Hydrodynamics.* Kluwer.

[10] KRONIG, R. & BRINK, J.C. 1949–1951 On the theory of extraction from falling droplets. *Appl. Sci. Res.* **A2**, 142–154.

[11] KUSCH, H.A. & OTTINO, J.M. 1992 Experiments on mixing in continuous chaotic flows. *J. Fluid Mech.* **236**, 319–347.

[12] LOCHIEL , A.C. & CALDERBANK, P.H. 1964 Mass transfer in the continuous phase around axisymmetric bodies of revolution. *Chem. Engng Sci.* **19**, 472–484.

[13] SAATDJIAN, E., MIDOUX, N., GASTOU CHASSAING, M.I., LEPREVOST, J.C. & ANDRÉ, J.C. 1996 Chaotic mixing and heat transfer between confocal ellipses: experimental and numerical results. *Phys. Fluids* **8**, 677–691.

[14] SHAPIRO, M. & BRENNER, H. 1987. Chemically reactive generalized Taylor dispersion phenomena. *AIChE J.* **33**, 1155–1167.

[15] STONE, H.A., NADIM, A. & STROGATZ, S. 1991 Chaotic streamlines inside drops immersed in steady Stokes flows. *J. Fluid Mech.* **232**, 629–646.

[16] SWANSON, P.D. & OTTINO, J.M. 1990 A comparative computational and experimental study of chaotic mixing of viscous fluids. *J. Fluid Mech.* **213**, 227–249.

[17] TAYLOR, G.I. 1932 The viscosity of a fluid containing small drops of another fluid. *Proc. Roy. Soc. Lond.* A **138**, 41–48.

Appendix A

Program for calculating effective reaction rate, velocity, and convective dispersivity in chaotic flow between rotating eccentric cylinders

```
************************************************************
* This program calculates effective reaction rate (infinitely fast reaction),
* velocity, convective dispersivity. It uses the LU decomposition subroutine
* ARROW, written by Paul Thomas in Prof. R.A. Brown's research group.
************************************************************
* files:
* input = input file
* c.dat = records calculated coeffeicients
* vin.dat = stores x,y and components of velocity (tecplot format)
* p1.dat = stores concentration profile (P0) after rotation of outer cylinder
* p2.dat = stores concentration profile (P0) after rotation of inner cyl.
************************************************************
```

```
* variables:
* (variables ending in 1 refer to outer cylinder, 2 to inner)
* b1,b2=banded part of matrix
* row1,row2 = bottom rows of matrix
* corn1,corn2 = bottom right corner of matrix
* col1,col2 = right-hand columns of matrix
* storep = temporary storage of P0 field, arguments are (space,time)
* storepb = temporary storage of B field
* f = matrix of P0 and B fields (P0=1, B=2)
* ve1,ve2 = eta component of velocity
* vz1,vz2 = zeta " " "
* v = axial velocity
* PAsum = sum of P and A fields over all space & one time period
* Ubar = avg velocity
* Uold = avg vel. from previos calculation
* oldrate = rate from previous calculation
* h = metrical coefficient
* delt =time step
* deln = grid spacing in eta direction
* delz = grid spacing in zeta direction
*****************************************************************
* variables in input file
* numsit= number of different velocity schemes to calculate
* tau = variable to determine if pivoting is used (see arrow.f)
* pout = 1 to store P0 profiles, anything else otherwise
* num = number of geometries to calculate
* tol = relative error tolerance (accuracy needed before stopping calculations)
* in = 1 to display calculations to screen, anything else otherwise
* sizen = number of grid points in eta direction
* sizez =      "                    zeta      "
* delt = time step
* maxit = maximimum number of iterations
* Pe = transverse Peclet number
* max2n = time to rotate inner cylinder*2
* max1n = "      "      outer "*2
* rratio = inner/outer radius ratio
* eta1 = inner cylinder eta value
* eta2 = outer
* c = c (determined from bipolar coordinate geometry)
* eps = degree of eccentricity
*****************************************************************

      program chaos
      double precision b1(181,3601),col1(181,3601),row1(3601,181)
      double precision corn1(181,181),corn2(181,181)
      double precision storepb(3601,300)
      double precision b2(181,3601),col2(181,3601),row2(3601,181)
      double precision f(3601,2),eta1,eta2,c,ve1(3601),vz1(3601)
      double precision ve2(3601),vz2(3601)
      double precision v(3601),PAsum,storep(3601,300),Ubar,Uold
      double precision del,term,sum,deleta,h,eta,zeta,delt,a
      double precision sdel,s1,s2,cdel,c1,c2,oldrate
      double precision deln,delz,delb,dels,conv,Pe
      double precision h1,h2,h3,h4,h5,h6,h7,h8,f13,f14
```

```
double precision f1,f2,f3,f4,f5,f6,f7,f8,f9,f10,f11,f12
real tau1,tau2,detlog,x,y,tol,max2n,max1n,tau
integer n,lrhs,iarrow,nod,nrhs,jna,maxit,first,sec,num,pout
integer sizen,sizez,ja,lbd,iband,jn,isign,count,optime,oppos
parameter (pi=3.14159265359)

open(unit=2,file='input',status='old')
open(unit=3,file='c.dat',status='unknown')
open(unit=10,file='vin.dat',status='unknown')
open(unit=7,file='p1.dat',status='unknown')
open(unit=8,file='p2.dat',status='unknown')

read(2,*) numsit,tau,pout

do 6000 nnn=1,numsit
read(2,*) num,tol,in,sizen,sizez,delt,maxit,orat
read(2,*) Pe,max2n,max1n,rratio

write(3,*) 'Rratio: ',rratio
write (3,*) 'Pe: ',real(Pe)
write (3,*) 'Win/Wout: ', orat
write(3,*) 'tau in: ' ,real(max2n/2)
write(3,*) 'tau out: ',real(max1n/2)
write(3,*)

do 5000 nm=1,num

read (2,*) eta1,eta2,c
read (2,*) eps

lrhs=2
iarrow=sizen
nrhs=2
jna=3601
jn=3601
ja=181
tau1=tau
tau2=tau
lbd=181

deln=1.0/(sizen)
delz=1.0/sizez
nod=sizen*(sizez-1)
iband=2*sizen+1
deleta=eta1-eta2

max2=nint(max2n/deleta**2/delt)
max1=nint(max1n/deleta**2/delt)
************************************************************
******* VELOCITY PROFILE************************************
************************************************************
sdel=sinh(deleta)
s2=-sinh(eta2)
s1=-sinh(eta1)
```

```
      cdel=cosh(deleta)
      c1=cosh(eta1)
      c2=cosh(eta2)
      del=deleta**2-sdel**2
      delb=deleta*cdel-sdel
      dels=sdel*(2*s1*s2*sdel-deleta*(s1**2+s2**2))
      h1=deleta*s2-s1*sdel
      h2=-deleta*s1+s2*sdel
      h3=-eta2*s1*sdel+eta1*deleta*s2
      h4=eta1*s2*sdel-eta2*deleta*s1
      h5=eta2*c1*sdel-eta1*deleta*c2
      h6=-eta1*c2*sdel+eta2*deleta*c1
      h7= s1*c2*sdel-eta2/2.0*sinh(-2.0*eta1)
     $     +0.5*eta1*sinh(-2.0*eta2)+eta1*deleta
      h8=-c1*c2*sdel-eta1*c2**2+eta2*c1**2
      f1=1.0/del*(delb/dels*h1*h7+h3)
      f2=1.0/del*(delb/dels*h2*h7+h4)
      f3=1.0/del*(delb/dels*h1*h8+h5)
      f4=1.0/del*(delb/dels*h2*h8+h6)
      f5=h1/dels*cdel
      f6=h2/dels*cdel
      f7=-s1/dels*sdel**2
      f8=-s2/dels*sdel**2
      f9=0.5*sinh(eta1+eta2)*h1/dels
      f10=0.5*sinh(eta1+eta2)*h2/dels
      f11=0.5*cosh(eta1+eta2)*h1/dels
      f12=0.5*cosh(eta1+eta2)*h2/dels
      f13=0.5*(sdel-2.0*eta1*cdel)*h1/dels
      f14=0.5*(sdel-2.0*eta1*cdel)*h2/dels


      do 5 m=1,sizen*sizez
         call calch(sizen,m,deleta,deln,delz,c,h,eta1,eta,zeta)
         eta=-eta

         phi= ((f1+f5*eta)*cosh(eta)+(f3+f7*eta)*sinh(eta)+
     $        cos(zeta)*(f9*cosh(2*eta)+f11*sinh(2*eta)-f5*eta+f13))
         ve1(m)=sin(zeta)*(f9*cosh(2*eta)+f11*sinh(2*eta)-f5*eta+f13)
     $        +sin(zeta)/(cosh(eta)-cos(zeta))*phi
         term=(f1+f5*eta)*sinh(eta)+(f3+f7*eta)*cosh(eta)
         term=term+f5*cosh(eta)+f7*sinh(eta)
         term=(term+cos(zeta)*(f9*2*sinh(2*eta)+2*f11*cosh(2*eta)-f5))
         vz1(m)=term-sinh(eta)/(cosh(eta)-cos(zeta))*phi

         phi=((f2+f6*eta)*cosh(eta)+(f4+f8*eta)*sinh(eta)+
     $        cos(zeta)*(f10*cosh(2*eta)+f12*sinh(2*eta)-f6*eta+f14))
         ve2(m)=sin(zeta)*(f10*cosh(2*eta)+f12*sinh(2*eta)-f6*eta+f14)
     $        +sin(zeta)/(cosh(eta)-cos(zeta))*phi
         ve2(m)=-ve2(m)*orat*c/s1
         term=(f2+f6*eta)*sinh(eta)+(f4+f8*eta)*cosh(eta)
         term=term+f6*cosh(eta)+f8*sinh(eta)
         term=(term+cos(zeta)*(f10*2*sinh(2*eta)+2*f12*cosh(2*eta)-f6))
         vz2(m)=term-sinh(eta)/(cosh(eta)-cos(zeta))*phi
         vz2(m)=-vz2(m)*orat*c/s1
```

```
5       continue

        do 6 m=0,sizez-1
        ve1(m*sizen+1)=0.0
        ve2(m*sizen+1)=0.0
        vz1(m*sizen+1)=0.0
6       continue

        if (pout.eq.1) then
        write(10,*) 'ZONE I=',sizez+1,'J=',sizen
        do 11031 i=1,sizen
             do 11041 j=1,sizez
             m=(j-1)*sizen+i
             call calch(sizen,m,deleta,deln,delz,c,h,eta1,eta,zeta)
             denom=cosh(eta)-cos(zeta)
             x=c*sinh(eta)/denom
             y=c*sin(zeta)/denom
             dxdz=-sinh(eta)*sin(zeta)/h**2/c
             dxde=cosh(eta)/h-sinh(eta)**2/h**2/c
             vx=h*(vz2(m)*dxdz+ve2(m)*dxde)

             dydz=cos(zeta)/h-sin(zeta)**2/h**2/c
             dyde=sin(zeta)*sinh(eta)/h**2/c
             vy=h*(vz2(m)*dydz+ve2(m)*dyde)
             write(10,*) x,y,real(vx), real(vy)
11041        continue
             m=i
             call calch(sizen,m,deleta,deln,delz,c,h,eta1,eta,zeta)
             denom=cosh(eta)-cos(zeta)
             x=c*sinh(eta)/denom
             y=c*sin(zeta)/denom
             dxdz=-sinh(eta)*sin(zeta)/h**2/c
             dxde=cosh(eta)/h-sinh(eta)**2/h**2/c
             vx=h*(vz2(m)*dxdz+ve2(m)*dxde)

             dydz=cos(zeta)/h-sin(zeta)**2/h**2/c
             dyde=sin(zeta)*sinh(eta)/h**2/c
             vy=h*(vz2(m)*dydz+ve2(m)*dyde)
             write(10,*) x,y,real(vx), real(vy)
11031   continue
        end if
        **********axial velocity**************************************
        coth1=cosh(eta1)/sinh(eta1)
        coth2=cosh(eta2)/sinh(eta2)
        f1=(eta1*coth2-eta2*coth1)/2.0/deleta
        f2=(coth1-coth2)/2.0/deleta
        do 7 i=1,sizen*sizez
             call calch(sizen,i,deleta,deln,delz,c,h,eta1,eta,zeta)
             v(i)=f1+f2*eta-0.5*cosh(eta)/sinh(eta)
             do 8 n=1,20
                  oldv=v(i)
                  den=(exp(2.0*n*eta1)-exp(2.0*n*eta2))
                  An=(coth1-coth2)/den
                  Bn=(exp(2.0*n*eta1)*coth2-exp(2.0*n*eta2)*coth1)/den
```

```
                v(i)=v(i)+cos(n*zeta)*(An*exp(n*eta)+
     $                (Bn-cosh(eta)/sinh(eta))*exp(-n*eta))
                if(abs((v(i)-oldv)/v(i)).lt.1e-6) then
                  goto 7
                end if
8           continue
7       continue

        Vbar=0.0
        area=0.0
        Vmax=0.0
        do 1100 j=1,sizen*sizez
            if(v(j).gt.Vmax) vmax=v(j)
            call calch(sizen,j,deleta,deln,delz,c,h,eta1,eta,zeta)
            Vbar=Vbar+1/h**2*v(j)
            area=area+1/h**2
1100    continue
        Vbar=Vbar/area

        write(*,*) Vbar, Vmax/Vbar

        **********initial conditions*************************************
        do 10 m=1,sizen*sizez
            f(m,1) = 1.0
            f(m,2) = (V(i)-Vbar)*delt*deleta**2
10      continue
        ****************************************************************
        call makemat(ve1,vz1,Pe,delt,sizen,sizez,b1,deleta,deln,delz,
     $      c,col1,row1,corn1,eta1)
        call makemat(ve2,vz2,Pe,delt,sizen,sizez,b2,deleta,deln,delz,
     $      c,col2,row2,corn2,eta1)

        ************************************************************
        * begin computation
        ************************************************************
        do 1000 count=1,maxit
        oldrate=rate
        sum=0.0
        ***** calculate total P0 in annulus **********************
        do 100 j=1, sizen*sizez
            call calch(sizen,j,deleta,deln,delz,c,h,eta1,eta,zeta)
            sum=sum+1/h**2*f(j,1)
100     continue
        ************************************************************
        ****** normalize to 1 ************************************
        do 101 i=1,sizen*sizez
            f(i,1)=f(i,1)/sum
            f(i,2)=f(i,2)/sum
101     continue
        ************************************************************
        ********calulate rate of reaction ***********************
        time=delt*(max1+max2)*deleta**2/2.0
        rate=log(sum)/time
        Ubar=Ubar/time
```

```
      Dbar=Dbar/time

      ******* signal error if any points have negative P0*****
      if (k.gt.0) then
           write(*,*) 'k neg',k
           write(3,*) 'k neg'
           goto 5000
      end if
      ********************************************************

      if (in.gt.0) then
           write(*,*) 'Ubar ',real(Ubar/Vbar), 'Dbar ',Dbar/Vbar**2, ' rate ',rate,k
      end if

      k=0
      if(abs((rate-oldrate)/rate).lt.tol) then
           if(abs((Dbar-Dold)/Dbar).lt.tol) goto 15
      end if

      Dold=Dbar
      Uold=Ubar
      Ubar=0.0
      Dbar=0.0
      if(count.eq.1) then
           PAsum=1.0
           Uold=Vbar
      end if
      if(max1.eq.0) goto 1001

      ***********rotate outer cylinder************************
      do 1500 first=1,max1
      call arrow(f,b1,col1,row1,corn1,detlog,isign,tau1,jn,iband,lbd,
     $     ja,jna,nrhs,nod,iarrow,lrhs)
      if (tau1.ne.-1) call makemat(ve1,vz1,Pe,delt,sizen,sizez,b1,
     $     deleta,deln,delz,c,col1,row1,corn1,eta1)

      do 1501 i=1,sizen*sizez
           if(f(i,1).lt.0) then
              k=k+1
           end if
           storep(i,first)=f(i,1)
           storepb(i,first)=f(i,2)
           f(i,2)=f(i,2)+(V(i)-Uold)*f(i,1)*delt*deleta**2
1501  continue
1500  continue

      tempDbar=0.0
      tempUbar=0.0

      do 1511 j=1,max1
           optime=max1+1-j
           tempUbar=0.0
           tempDbar=0.0
           PAsum=0.0
```

```
            do 1510 i=1,sizez*sizen
               call calch(sizen,i,deleta,deln,delz,c,h,eta1,eta,zeta)
               if (zeta.eq.0) then
                  oppos=i
               else
                  r=zeta/pi*sizen*sizez
                  oppos=i+sizen*sizez-r
               end if
               a=storep(oppos,optime)
               tempDbar=tempDbar+1.0/h**2*storepb(i,j)*a*(V(i)-Uold)
               tempUbar=tempUbar+1.0/h**2*storep(i,j)*a*V(i)
               PAsum=PAsum+a*storep(i,j)/h**2
1510        continue
               Ubar=Ubar+tempUbar/PAsum*delt/2.0*deleta**2
               Dbar=Dbar+tempDbar/PAsum*delt/2.0*deleta**2
1511     continue

         if (pout.eq.1) then
            rewind(7)
            write(7,*) 'ZONE I=',sizez+1,'J=',sizen
            do 1103 i=1,sizen
            do 1104 j=1,sizez
               m=(j-1)*sizen+i
               call calch(sizen,m,deleta,deln,delz,c,h,eta1,eta,zeta)
               denom=cosh(eta)-cos(zeta)
               x=c*sinh(eta)/denom
               y=c*sin(zeta)/denom
               write(7,*) x,y,real(f(m,1))
1104        continue
            m=i
            call calch(sizen,m,deleta,deln,delz,c,h,eta1,eta,zeta)
            denom=cosh(eta)-cos(zeta)
            x=c*sinh(eta)/denom
            y=c*sin(zeta)/denom
            write(7,*) x,y,real(f(m,1))
1103        continue
         end if
1001     if (max2.eq.0) goto 1000
         *********rotate inner cylinder ********************************
         do 1550 sec=1,max2
         call arrow (f,b2,col2,row2,corn2,detlog,isign,tau2,jn,iband,lbd,
     $        ja,jna,nrhs,nod,iarrow,lrhs)
         if(tau2.ne.-1) call makemat(ve2,vz2,Pe,delt,sizen,sizez,b2,
     $        deleta,deln,delz,c,col2,row2,corn2,eta1)

         do 1551 i=1,sizen*sizez
            storep(i,sec)=f(i,1)
            storepb(i,sec)=f(i,2)
            f(i,2)=f(i,2)+(V(i)-Uold)*f(i,1)*delt*deleta**2
1551     continue
1550     continue

         do 1561 j=1,max2
            optime=max2+1-j
```

```
            tempDbar=0.0
            tempUbar=0.0
            PAsum=0.0
            do 1560 i=1,sizen*sizez
               call calch(sizen,i,deleta,deln,delz,c,h,eta1,eta,zeta)
               if (zeta.eq.0) then
                  oppos=i
               else
                  r=zeta/pi*sizen*sizez
                  oppos=i+sizen*sizez-r
               end if
               a=storep(oppos,optime)
               tempDbar=tempDbar+1.0/h**2*storepb(i,j)*a*(V(i)-Uold)
               tempUbar=tempUbar+1.0/h**2*storep(i,j)*a*V(i)
               PAsum=PAsum+a*storep(i,j)/h**2
1560        continue
            Ubar=Ubar+tempUbar/PAsum*delt/2.0*deleta**2
            Dbar=Dbar+tempDbar/PAsum*delt/2.0*deleta**2
1561     continue

******output P0 profile************************************
         if (pout.eq.1) then
            rewind(8)
            write(8,*) 'ZONE I=',sizez+1,'J=',sizen
            do 1105 i=1,sizen
               do 1106 j=1,sizez
               m=(j-1)*sizen+i
               call calch(sizen,m,deleta,deln,delz,c,h,eta1,eta,zeta)
               denom=cosh(eta)-cos(zeta)
               x=c*sinh(eta)/denom
               y=c*sin(zeta)/denom
               write(8,*) x,y,real(f(m,1))
1106           continue
               m=i
               call calch(sizen,m,deleta,deln,delz,c,h,eta1,eta,zeta)
               denom=cosh(eta)-cos(zeta)
               x=c*sinh(eta)/denom
               y=c*sin(zeta)/denom
               write(8,*) x,y,real(f(m,1))
1105        continue
         end if
*********************************************************
1000     continue
         write(*,*) sum
         write(3,*) eps,-rate,Ubar/Vbar,Dbar/Vbar**2
         write(3,*)
         write(*,*) rate,Ubar/Vbar,Dbar/Vbar**2
5000     continue
6000     continue
         end

******calculate metrical coefficients**************************
         subroutine calch(sn,n,deleta,deln,delz,c,h,eta1,eta,zeta)
         integer sn,n,term
```

```
      double precision p,deln,delz,h,c,eta1,deleta,zeta,eta
      parameter(pi=3.14159265)
      p=1.0*(n-0.5)/sn
      term= aint(p)
      eta=deln*(n-term*sn-1)
      zeta=delz*(term)
      h=1.0/c*(cosh(-eta*deleta+eta1)-cos(zeta*2.0*pi))
      eta=eta1-eta*deleta
      zeta=zeta*2.0*pi
      return
      end
*********form matrix************************************************
      subroutine makemat(ve,vz,Pe,delt,sizen,sizez,b,deleta,deln,delz,
     $     c,col,row,corn,eta1)
      integer sizez,sizen
      double precision deln,delz,h,c,deleta,zeta,eta,delt,Pe
      double precision b(181,3601),col(181,3601),row(3601,181)
      double precision corn(181,181)
      double precision eta1,ve(3601),vz(3601)
      parameter(pi=3.14159265)
      do 13 m=1,sizen*sizez-sizen
         do 16 j=1,2*sizen+1
            b(j,m)=0.0
16       continue
         do 17 j=1,sizen
            col(j,m)=0.0
            row(m,j)=0.0
17       continue
13    continue
      do 30 m=1,sizen
         do 31 j=1,sizen
            corn(m,j)=0.0
31       continue
30    continue
      do 20 m=1,sizen*sizez-sizen
         call calch(sizen,m,deleta,deln,delz,c,h,eta1,eta,zeta)
         term=1.0/4.0/(pi*delz)**2*deleta**2
         b(sizen+1,m)=delt*h**2*(1.0/(deln)**2+term)+1.0
         b(sizen,m) =-0.5*h**2*delt*(1.0/deln)**2
         conv=delt*h/4.0*ve(m)*deleta/deln
         b(sizen,m)=b(sizen,m)-Pe*conv
         b(sizen+2,m) =-0.5*h**2*delt*(1.0/deln)**2
         b(sizen+2,m)=b(sizen+2,m)+Pe*conv
20    continue

      do 40 m=1,sizen
         b(1,m)=0.0
         call calch(sizen,m,deleta,deln,delz,c,h,eta1,eta,zeta)
         b(2*sizen+1,m)=-h**2/8.0
         b(2*sizen+1,m)= b(2*sizen+1,m)*(deleta/pi)**2
         b(2*sizen+1,m)=b(2*sizen+1,m)*delt/delz**2
         conv=delt/8.0/pi*h*deleta**2*vz(m)/delz
         b(2*sizen+1,m)=b(2*sizen+1,m)+Pe*conv
         col(m,m) = -h**2/8.0*(deleta/pi)**2*delt/delz**2
```

```
            col(m,m)=col(m,m)-Pe*conv
40      continue

        do 50 m=sizen+1,(sizez-2)*sizen
            call calch(sizen,m,deleta,deln,delz,c,h,eta1,eta,zeta)
            conv=delt/8.0/pi*h*deleta**2*vz(m)/delz
            b(1,m)=-h**2/8.0*(deleta/pi)**2*delt/delz**2-Pe*conv
            b(2*sizen+1,m)=-h**2/8.0*(deleta/pi)**2*delt/delz**2+Pe*conv
50      continue

        do 55 i=1,sizen
            m=(sizez-2)*sizen+i
            call calch(sizen,m,deleta,deln,delz,c,h,eta1,eta,zeta)
            conv=delt/8.0/pi*h*deleta**2*vz(m)/delz
            b(1,m)= -h**2/8.0*(deleta/pi)**2*delt/delz**2-Pe*conv
            col(i,m)= -h**2/8.0*(deleta/pi)**2*delt/delz**2+Pe*conv
55      continue

        do 60 i=1,sizen
            m=i+(sizez-1)*sizen
            call calch(sizen,m,deleta,deln,delz,c,h,eta1,eta,zeta)
            conv=delt/8.0/pi*h*deleta**2*vz(m)/delz
            row(i,i) =-h**2/8.0*(deleta/pi)**2*delt/delz**2+Pe*conv
            row(m-sizen,i)=-h**2/8.0*(deleta/pi)**2*delt/delz**2
            row(m-sizen,i)=row(m-sizen,i)-Pe*conv
            corn(i,i)= delt*h**2*((1.0/deln)**2
     $              +1.0/4.0*(deleta/delz/pi)**2)+1.0
            conv=delt*h*deleta/deln/4.0*ve(m)
            corn(i+1,i)= -0.5*h**2*delt*(1.0/deln)**2+Pe*conv
            corn(i-1,i)= -0.5*h**2*delt*(1.0/deln)**2-Pe*conv
60      continue

        do 70 m=0,sizez
            b(sizen,m*sizen+1) = 0.0
            b(sizen+2,m*sizen) = 0.0
            b(sizen+2,m*sizen+1)=2.0*b(sizen+2,m*sizen+1)
70      continue
        corn(2,1)=2.0*corn(2,1)
        end
```

Appendix B

Program to calculate extraction rate from a droplet

```
************************************************************************
* This program calculates the extraction rate from a droplet undergoing translation
* and simple shear. It uses the LU decomposition subroutine ARROW,
* written by Paul Thomas in Prof. R.A. Brown's research group.
************************************************************************
      program xtract
      integer sizeth,sizep,sizer,max,time,a,aa,ocoord,num
      double precision vr,vt,vp,delt,delth,delp,dely,shear,F,Pe,tol
      double precision P(70000),P1(70000),P2(70000),rate,sum,oldrate
      double precision r,t,dpdy,dp2dy,dpdt,dp2dt,dpdp,dp2dp,rhs(70000)
      double precision b(1600,6,90),d1(1600,90,1),e2(1,1)
      double precision c1(1600,1,90),e1(1600,1,1),bth(80,6,80)
      double precision ex,term,c2(1,80),d2(80,1),b2(2,6,80)
      double precision c(1,80),d(80,1),e(1,1),b1(6,80)
      double precision temp(70000),a1,alpha,beta,z,delz,ln,delr,bratio
      double precision cu1(70000),cu2(70000),cu3(70000),mtc,term1
      double precision oldsum1,oldsum2,oldsum3,oldsum4,oldsum5
      double precision c3(44,1,80),d3(44,80,1),e3(44,1,1)
      double precision angle2,angle1
      character*10 filename
      parameter(pi=3.14159265359)
      open(unit=2,file='expin1',status='old')
      read(2,*) num
      do 6000 count=1, num
      rate=1.0
      oldrate=1.0
      oldsum1=1.0
      oldsum2=2.0
      oldsum3=3.0
      oldsum4=4.0
      oldsum5=5.0
      read(2,*) filename,out,old
      read(2,*) delt,sizer,sizeth,sizep,shear,F,Pe,max,tol,tau
      read(2,*) a1,alpha,beta,mtc
      read(2,*) angle1,angle2
```

```
      angle1=angle1*Pi
      angle2=angle2*Pi
      delz=1.0/(real(sizeth)+1.0)
      delp=2.0*pi/real(sizep)
      ymax=log(1.0/(a1-1.0))
      ymin=log(1.0/a1)
      dely=(ymax-ymin)/real(sizer)
      ocoord=sizer*sizeth*sizep+2*sizer+1
      bratio=(beta+1)/(beta-1)
      ln=log(bratio)
      z=delz
      ex=(z-alpha)/(1.0-alpha)
      t=pi*((2.0*alpha+beta)*bratio**ex+2.0*alpha-beta)/
     $    2.0*alpha+1.0)/(1.0+bratio**ex)
      delth=t
      jn=80
      iband=3
      lbd=6
      ja=1
      jna=80
      nrhs=1
      lrhs=1
111   do 10 i=1,sizer
         y=i*dely+ymin
         r=a1-exp(-y)
         rold=r
         a=i+sizeth*sizep*sizer
         P(a)=1.0
         cu1(a)=0.0
         cu2(a)=0.0
         cu3(a)=0.0
         a=i+sizer+sizeth*sizep*sizer
         P(a)=1.0
         cu1(a)=0.0
         cu2(a)=0.0
         cu3(a)=0.0
         do11 j=0,sizeth-1
            do12 k=0,sizep-1
               a=i+sizer*j+sizeth*sizer*k
               P(a)=1.0
               cu1(a)=0.0
               cu2(a)=0.0
               cu3(a)=0.0
12          continue
11       continue
10    continue
      P(ocoord)=1.0
      cu1(ocoord)=0.0
      cu2(ocoord)=0.0
      cu3(ocoord)=0.0
      if (old.eq.1) then
         open(unit=4, file='savestate', status='old')
         read(4,*) P(ocoord),cu1(ocoord),cu2(ocoord),cu3(ocoord)
         do 2101 i=1,sizer
```

```
            a=i+sizeth*sizer*sizep
            read(4,*) P(a),cu1(a),cu2(a),cu3(a)
            a=a+sizer
            read(4,*) P(a),cu1(a),cu2(a),cu3(a)
            do 1102 j=1, sizeth
              do 1103 k=1,sizep
              a=i+(j-1)*sizer+(k-1)*sizer*sizeth
              read(4,*) P(a),cu1(a),cu2(a),cu3(a)
1103          continue
1102        continue
2101      continue
          close(4)
        end if
        do 18 j=1,sizeth
          z=j*delz
          ex= (z-alpha)/(1.0-alpha)
          t=pi*((2.0*alpha+beta)*bratio**ex+2.0*alpha-beta)/(2.0*alpha+1.0)
     $      /(1.0+bratio**ex)
          dzdt=2.0*beta*(2.0*alpha+1.0)*(1.0-alpha)/pi/ln/
     $      (beta*beta-((2.0*alpha+1.0)*t/Pi-2.0*alpha)**2)
          dz2dt=2.0*beta*(2.0*alpha+1.0)**2*(1.0-alpha)/pi**2/ln*
     $      2.0*((2.0*alpha+1.0)*t/Pi-2.0*alpha)
          term=(beta*beta-((2.0*alpha+1.0)*t/Pi-2.0*alpha)**2)**2
          dz2dt=dz2dt/term
          told=t
18      continue
        delr=a1-exp(-ymin-dely)
13      do 5000 time=1,max
        if (time.eq.1) then
        do 90 i=1,sizer
          c2(1,i)=0.0
          d2(i,1)=0.0
          c2(1,sizer+i)=0.0
          d2(sizer+i,1)=0.0
90      continue
*************step in r************************************************
*************************origin*************************************
        d2(1,1)=delt/2.0*(-1.0/delr**2)
        e2(1,1)=1.0+delt/2.0*(2.0/delr**2)
        d2(sizer+1,1)=delt/2.0*(-1.0/delr**2)
        end if
        a=(sizeth-1)*sizer/2+1
        aa=a+sizep/2*sizer*sizeth
        dp2dt=(P(a)-2.0*P(ocoord)+P(aa))/delr/delr
        a=sizer*sizeth*sizep/4+(sizeth-1)*sizer/2+1
        aa=a+sizer*sizeth*sizep/2
        dp2dp=(P(a)-2.0*P(ocoord)+P(aa))/delr/delr
        a=sizer*sizep*sizeth+1
        dp2dy=(P(a)-2.0*P(ocoord)+P(a+sizer))/delr/delr
        rhs(2*sizer+1)=P(ocoord)+delt/2.0*(2.0*dp2dt+2.0*dp2dp+dp2dy)
        rhs(2*sizer+1)=rhs(2*sizer+1)+23.0/12.0*cu1(ocoord)
       $    -4.0/3.0*cu2(ocoord)+5.0/12.0*cu3(ocoord)
*********************************z-axis*************************************
        do 100 i=1,sizer
```

```
      y=i*dely+ymin
      r=a1-exp(-y)
      term=exp(2.0*y)
      term1=exp(y)
      if (time.eq.1) then
        b2(1,1,i)=-delt/2.0*term/dely**2
        b2(1,1,i)=b2(1,1,i)+delt/2.0*(term1/r/dely+term/2.0/dely)
        b2(1,2,i)=1.0+delt/2.0*2.0/dely**2*term
        b2(1,3,i)=-delt/2.0*term/dely**2
        b2(1,3,i)=b2(1,3,i)-delt/2.0*(term1/r/dely+term/2.0/dely)
        if(i.eq.1) then
          c2(1,1)=b2(1,1,i)
          c2(1,sizer+1)=b2(1,3,i)+delt*(term1/r/dely+term/2.0/dely)
        end if
        b2(1,1,i+sizer)=b2(1,1,i)
        b2(1,2,i+sizer)=b2(1,2,i)
        b2(1,3,i+sizer)=b2(1,3,i)
      end if
      a=sizeth*sizer*sizep+i
      if (i.eq.1) then
        dp2dy=(P(a+1)-2.0*P(a)+P(ocoord))/dely/dely
        dpdy=(P(a+1)-P(ocoord))/dely/2.0
      else if (i.eq.sizer) then
        dp2dy=(-mtc*2.0*dely*P(a)/term1+P(a-1)-2.0*P(a)+P(a-1))/dely**2
        dpdy=-mtc*P(a)/term1
      else
        dp2dy=(P(a+1)-2.0*P(a)+P(a-1))/dely/dely
        dpdy=(P(a+1)-P(a-1))/2.0/dely
      end if
      aa=3*sizer*sizeth*sizep/4+i
      dp2dp=(P(sizer*sizeth*sizep/4+i)-2.0*P(a)+P(aa))/delth**2
      dp2dt=(P(i)-2*P(a)+P(sizeth*sizer*sizep/2+i))/delth**2
      rhs(i)=P(a)+delt/r**2*(dp2dt+dp2dp)+delt/2.0
     $     *(term*dp2dy+(term+term1*2.0/r)*dpdy)
      rhs(i)=rhs(i)+23.0/12.0*cu1(a)-4.0/3.0*cu2(a)+5.0/12.0*cu3(a)
      a=sizeth*sizer*sizep+sizer+i
      tcoord=i+sizer*(sizeth-1)
      pcoord=i+sizer*(sizeth-1)+sizer*sizeth*sizep/4
      if (i.eq.1) then
        dp2dy=(P(a+1)-2.0*P(a)+P(ocoord))/dely/dely
        dpdy=(P(a+1)-P(ocoord))/dely/2.0
      else if (i.eq.sizer) then
        dp2dy=(-mtc*2.0*dely*P(a)/term1+P(a-1)-2.0*P(a)+P(a-1))/dely**2
        dpdy=-mtc*P(a)/term1
      else
        dp2dy=(P(a+1)-2.0*P(a)+P(a-1))/dely/dely
        dpdy=(P(a+1)-P(a-1))/2.0/dely
      end if
      dp2dp=(P(pcoord)-2.0*P(a)+P(pcoord+sizer*sizeth*sizep/2))
      dp2dt=(P(tcoord)-2.0*P(a)+P(tcoord+sizer*sizeth*sizep/2))
      rhs(sizer+i)=P(a)+delt/(r*delth)**2*(dp2dp+dp2dt)
     $     +delt/2.0*(term*dp2dy+(term+2.0*term1/r)*dpdy)
      rhs(sizer+i)=rhs(sizer+i)+23.0/12.0*cu1(a)
     $     -4.0/3.0*cu2(a)+5.0/12.0*cu3(a)
```

```
100     continue
        if(time.eq.1) then
           term=exp(2.0*ymax)
           term1=exp(ymax)
           b2(1,1,1)=0.0
           b2(1,3,sizer)=0.0
           b2(1,2,sizer)=b2(1,2,sizer)+mtc*2.0*dely/term1*delt/2.0*
      $       (term1/r/dely+term/2.0/dely+term/dely**2)
           b2(1,1,sizer)=b2(1,1,sizer)
      $       -delt/2.0*(term1/r/dely+term/2.0/dely+term/dely**2)
           b2(1,1,sizer+1)=0.0
           b2(1,3,2*sizer)=0.0
           b2(1,2,2*sizer)=b2(1,2,sizer)
           b2(1,1,2*sizer)=b2(1,1,sizer)
        end if
        iarrow=1
        nod=2*sizer
        do 101 i=1,nod
           c(1,i)=c2(1,i)
           d(i,1)=d2(i,1)
           do 102 j=1,3
              b1(j,i)=b2(1,j,i)
102        continue
101     continue
        e(1,1)=e2(1,1)

        call arrow(rhs,b1,c,d,e,detlog,isign,tau,jn,iband,lbd,ja,
      $    jna,nrhs,nod,iarrow,lrhs)

        if (time.eq.1) then
           do 1001 i=1,nod
              c2(1,i)=c(1,i)
              d2(i,1)=d(i,1)
              do 1002 j=1,3
                 b2(1,j,i)=b1(j,i)
1002          continue
1001       continue
           e2(1,1)=e(1,1)
        end if
        do 105 i=1,sizer
           P1(sizer*sizeth*sizep+i)=rhs(i)
           P1(sizer*sizeth*sizep+sizer+i)=rhs(sizer+i)
105     continue
        P1(ocoord)=rhs(2*sizer+1)
********************** center points ***************************************
        do 110 k=1,sizep
           do 120 j=1,sizeth
              z=delz*j
              ex= (z-alpha)/(1.0-alpha)
              t=pi*((2.0*alpha+beta)*bratio**ex+2.0*alpha-beta)/
      $          (2*alpha+1.0) /(1.0+bratio**ex)
              cott=cos(t)/sin(t)
              term=(2.0*alpha+1.0)*t/Pi-2.0*alpha
              dzdt=2.0*beta*(2.0*alpha+1.0)*(1.0-alpha)/pi/ln/
```

```
$       (beta*beta-term*term)
        term=2.0*alpha+1.0
        dz2dt=2.0*beta*term*term*(1.0-alpha)/pi/pi/ln*
$       2.0*((2.0*alpha+1.0)*t/Pi-2.0*alpha)
        term=term*t/pi-2.0*alpha
        term=(beta*beta-term*term)
        term=term*term
        dz2dt=dz2dt/term
        do 130 i=1,sizer
        y=i*dely+ymin
        r=a1-exp(-y)
        term=exp(2.0*y)
        term1=exp(y)
        if((time.eq.1).and.(j.eq.1).and.(k.eq.1)) then
          b2(2,1,i)=((2.0*term1/r+term)/2.0/dely-term/dely/dely)*delt/2.0
          b2(2,2,i)=1.0+delt/2.0*2.0/dely/dely*term
          b2(2,3,i)=(-(2.0*term1/r+term)/dely/2.0-term/dely/dely)*delt/2.0
        end if
        call dpt(i,j,k,delz,sizer,sizeth,sizep,P,dpdt)
        call dp2t(i,j,k,delz,sizer,sizeth,sizep,P,dp2dt)
        call dpp(i,j,k,delp,sizer,sizeth,sizep,P,dpdp)
        call dp2p(i,j,k,delp,sizer,sizeth,sizep,P,dp2dp)
        call dpr(i,j,k,dely,sizer,sizeth,sizep,P,dpdy,mtc,term1)
        call dp2r(i,j,k,dely,sizer,sizeth,sizep,P,dp2dy,mtc,term1)
        a=i+(j-1)*sizer+(k-1)*sizer*sizeth
        rhs(i)=P(a)+delt*(dp2dt/r/r*dzdt*dzdt+(dz2dt+cott*dzdt)/r/r*dpdt
$       +dp2dp/r/r/sin(t)/sin(t)) +delt/2.0*(term*dp2dy+(term1*2.0/r+term)*dpdy)
        rhs(i)=rhs(i)+23.0/12.0*cu1(a)-4.0/3.0*cu2(a)+5.0/12.0*cu3(a)
        if (i.eq.1) then
          P0=P1(ocoord)
          rhs(1)=rhs(1)+P0*delt/2.0*(term/dely/dely-term1/dely/r
$           -term/dely/2.0)
        end if
130     continue

        if((time.eq.1).and.((j.eq.1).and.(k.eq.1))) then
          term=exp(2.0*ymax)
          term1=exp(ymax)
          b2(2,1,1)=0.0
          b2(2,3,sizer)=0.0
          b2(2,2,sizer)=b2(2,2,sizer)+mtc*2.0*dely/term1*delt/2.0*
$           (term1/r/dely+term/2.0/dely+term/dely**2)
          b2(2,1,sizer)=b2(2,1,sizer)-delt/2.0*(term1/r/dely+term/2.0/dely+term/dely**2)
        end if
        nod=sizer
        iarrow=0
        do 201 i=1,nod
          do 202 jj=1,3
            b1(jj,i)=b2(2,jj,i)
202       continue
201     continue

        call arrow(rhs,b1,c,d,e,detlog,isign,tau,jn,iband,lbd,ja,
$       jna,nrhs,nod,iarrow,lrhs)
```

```
            if((time.eq.1).and.(k.eq.1).and.(j.eq.1)) then
              do 2001 i=1,nod
                do 2002 jj=1,3
                  b2(2,jj,i)=b1(jj,i)
2002            continue
2001          continue
              tau=-1.0
            end if
            do 140 i=1,sizer
              a=i+(j-1)*sizer+(k-1)*sizer*sizeth
              P1(a)=rhs(i)
140         continue
120       continue
110     continue
        if(time.eq.1) tau=0.0
************************step in theta*****************************************
        do 210 k=1,sizep
        if (k.eq.sizep/2+1) goto 210
        if(time.eq.1) then
          if ((k.eq.1).or.(k.eq.2)) then
            tau=0.0
          else
            tau=-1.0
          end if
        end if
        do 220 i=1,sizer
          y=i*dely+ymin
          r=a1-exp(-y)
******************** z axis*********************************************
          if (k.eq.1) then
            ii=i
            if(time.eq.1) then
              do 5131 j=1,sizeth
                c3(ii,1,j+1)=0.0
                d3(ii,j+1,1)=0.0
                c3(ii,1,j+sizeth+1)=0.0
                d3(ii,j+sizeth+1,1)=0.0
5131          continue
              bth(ii,1,1)=0.0
              bth(ii,2,1)=1.0+delt/(r*delth)**2
              bth(ii,3,1)=-delt/2.0/(r*delth)**2
              bth(ii,1,sizeth+2)=-delt/2.0/(r*delth)**2
              bth(ii,2,sizeth+2)=1.0+delt/(r*delth)**2
              bth(ii,3,sizeth+2)=-delt/2.0/(r*delth)**2
              c3(ii,1,1)=-delt/2.0/(r*delth)**2
            end if
            a=sizer*sizeth*sizep+i
            aa=i
            dp2dt=(P(aa)-2.0*P(a)+P(aa+sizer*sizeth*sizep/2))/delth**2
            rhs(1)=P1(a)-delt/2.0*(dp2dt/r**2)
            a=sizer*sizeth*sizep+sizer+i
            aa=(sizeth-1)*sizer+i
            dp2dt=(P(aa)-2.0*P(a)+P(aa+sizer*sizeth*sizep/2))/delth**2
            rhs(sizeth+2)=P1(a)-delt/2.0*(dp2dt/r**2)
```

```
          end if
**************************center points ***********************************
          do 230 j=1,sizeth
            if (k.eq.1) then
              aa=j+1
            else
              aa=j
              ii=sizer+i
            end if
            z=delz*j
            ex= (z-alpha)/(1.0-alpha)
            t=pi*((2.0*alpha+beta)*bratio**ex+2.0*alpha-beta)/
     $        (2*alpha+1.0)/(1.0+bratio**ex)
            term=(2.0*alpha+1.0)*t/Pi-2.0*alpha
            dzdt=2.0*beta*(2.0*alpha+1.0)*(1.0-alpha)/pi/ln/
     $        (beta*beta-term*term)
            term=2.0*alpha+1.0
            dz2dt=2.0*beta*term*term*(1.0-alpha)/pi/pi/ln*
     $        2.0*(term*t/Pi-2.0*alpha)
            term=term*t/pi-2.0*alpha
            term=(beta*beta-term*term)
            term=term*term
            dz2dt=dz2dt/term
            cott=cos(t)/sin(t)
            a=i+(j-1)*sizer+(k-1)*sizer*sizeth
            call dpt(i,j,k,delz,sizer,sizeth,sizep,P,dpdt)
            call dp2t(i,j,k,delz,sizer,sizeth,sizep,P,dp2dt)
            rhs(aa)=P1(a)-delt/2.0*(dzdt**2*dp2dt/r**2+
     $        (dz2dt+dzdt*cott)/r**2*dpdt)

            if((time.eq.1).and.((k.eq.1).or.(k.eq.2))) then
              bth(ii,1,aa)=-(dzdt/r/delz)**2+(dz2dt+cott*dzdt)/delz/2.0/r**2
              bth(ii,1,aa)=bth(ii,1,aa)*delt/2.0
              bth(ii,2,aa)=1.0+2.0/2.0*delt*(dzdt/r/delz)**2
              bth(ii,3,aa)=-(dzdt/r/delz)**2-(dz2dt+cott*dzdt)/delz/2.0/r**2
              bth(ii,3,aa)=bth(ii,3,aa)*delt/2.0
            end if

            if (k.eq.1) then
              tt=Pi-t
              term=(2.0*alpha+1.0)*tt/Pi-2.0*alpha
              dzdt=2.0*beta*(2.0*alpha+1.0)*(1.0-alpha)/pi/ln/
     $          (beta*beta-term*term)
              term=2.0*alpha+1.0
              dz2dt=2.0*beta*term*term*(1.0-alpha)/pi/pi/ln*
     $          2.0*(term*tt/Pi-2.0*alpha)
              term=term*tt/pi-2.0*alpha
              term=(beta*beta-term*term)
              term=term*term
              dz2dt=dz2dt/term
              cott=cos(tt)/sin(tt)
              kk=k+sizep/2
              jj=sizeth-j+1
              a=i+(jj-1)*sizer+(kk-1)*sizer*sizeth
```

```
            call dpt(i,jj,kk,delz,sizer,sizeth,sizep,P,dpdt)
            call dp2t(i,jj,kk,delz,sizer,sizeth,sizep,P,dp2dt)
            rhs(aa+sizeth+1)=P1(a)-delt/2.0*(dzdt**2*dp2dt/r**2+
     $        (dz2dt+dzdt*cott)/r**2*dpdt)

            if (time.eq.1) then
              bth(ii,1,sizeth+2+j)=(-(dzdt/r/delz)**2-
     $            (dz2dt+cott*dzdt)/delz/2.0/r**2)*delt/2.0
              bth(ii,2,sizeth+2+j)=1.0+2.0/2.0*delt*(dzdt/r/delz)**2
              bth(ii,3,sizeth+2+j)=(-(dzdt/r/delz)**2+
     $            (dz2dt+cott*dzdt)/delz/2.0/r**2)*delt/2.0

              if(j.eq.sizeth-1) then
               c3(ii,1,2*sizeth+1)=bth(ii,3,2*sizeth+1)
               bth(ii,3,2*sizeth+1)=0.0
              end if

              if(j.eq.sizeth) then
               d3(ii,1,1)=bth(ii,3,2*sizeth+2)
               bth(ii,3,2*sizeth+2)=0.0
               d3(ii,2*sizeth+1,1)=bth(ii,1,2*sizeth+2)
               bth(ii,1,2*sizeth+2)=0.0
               e3(ii,1,1)=bth(ii,2,2*sizeth+2)
               bth(ii,2,2*sizeth+2)=0.0
              end if
            end if
          end if

          if ((time.eq.1).and.(k.eq.2)) then
            bth(ii,1,1)=0.0
            bth(ii,3,sizeth)=0.0
          end if

          if(k.ne.1) then
            if (j.eq.1) then
              rhs(j)=rhs(j)+delt/2.0*P2(sizer*sizeth*sizep+i)*
     $          (dzdt/r/delz*dzdt/r/delz-(dz2dt+dzdt*cott)/delz/r/r/2.0)
            else if (j.eq.sizeth) then
              rhs(j)=rhs(j)+delt/2.0*P2(sizer*sizeth*sizep+sizer+i)*
     $          (dzdt/r/delz*dzdt/r/delz+(dz2dt+dzdt*cott)/delz/r/r/2.0)
            end if
          end if
230       continue

          if (k.eq.1) then
            nod=2*sizeth+1
            iarrow=1
          else
            nod=sizeth
            iarrow=0
          end if

          do 301 inew=1,nod
            do 302 j=1,3
```

```
                  b1(j,inew)=bth(ii,j,inew)
302               continue
                  if (k.eq.1) then
                     c(1,inew)=c3(ii,1,inew)
                     d(inew,1)=d3(ii,inew,1)
                  end if
301            continue
               if (k.eq.1) e(1,1)=e3(ii,1,1)

               call arrow(rhs,b1,c,d,e,detlog,isign,tau,jn,iband,lbd,ja,
     $            jna,nrhs,nod,iarrow,lrhs)

               if((time.eq.1).and.((k.eq.1).or.(k.eq.2))) then
                  do 3001 inew=1,nod
                     do 3002 j=1,3
                        bth(ii,j,inew)=b1(j,inew)
3002                 continue
                     if(k.eq.1) then
                        c3(ii,1,inew)=c(1,inew)
                        d3(ii,inew,1)=d(inew,1)
                     end if
3001              continue
                  if (k.eq.1) e3(ii,1,1)=e(1,1)
               end if

               if (k.ne.1) then
                  do 240 j=1,sizeth
                     a=i+(j-1)*sizer+(k-1)*sizer*sizeth
                     P2(a)=rhs(j)
240               continue
               else
                  do 245 j=1,sizeth
                     a=i+(j-1)*sizer
                     P2(a)=rhs(j+1)
                     P2(a+sizer*sizeth*sizep/2)=rhs(3+2*sizeth-j)
245               continue
                  P2(sizer*sizeth*sizep+i)=rhs(1)
                  P2(sizer*sizeth*sizep+sizer+i)=rhs(sizeth+2)
               end if
220         continue
210         continue
*************************solve for origin************************************
            optheta=(sizeth-1)/2*sizer+1
            optheta2=optheta+sizer*sizeth*sizep/2
            P2(ocoord)=P1(ocoord)-delt/2.0*(P(optheta)-2.0*P(ocoord)
           $    +P(optheta2))/delr/delr+delt/2.0*(P2(optheta)+P2(optheta2))/delr/delr
            P2(ocoord)=P2(ocoord)/(1.0+2.0*delt/2.0/delr/delr)
            if(time.eq.1) then
               tau=0.0
            end if
*************************step in phi*****************************************
            do 300 i=1,sizer
               y=i*dely+ymin
               r=a1-exp(-y)
```

```
      do 310 j=1,sizeth
        z=delz*j
        ex=(z-alpha)/(1.0-alpha)
        t=pi*((2.0*alpha+beta)*bratio**ex+2.0*alpha-beta)/(2*alpha+1.0)
     $    /(1.0+bratio**ex)
        ii=i+sizer*(j-1)
        do 320 k=1,sizep-1
          if(time.eq.1) then
            c1(ii,1,k)=0.0
            d1(ii,k,1)=0.0
            b(ii,1,k)=-delt/(r*delp*sin(t))**2/2.0
            b(ii,2,k)=1.0+delt/2.0*2.0/(r*delp*sin(t))**2
            b(ii,3,k)=-delt/(r*delp*sin(t))**2/2.0
          end if
          call dpp(i,j,k,delp,sizer,sizeth,sizep,P,dpdp)
          call dp2p(i,j,k,delp,sizer,sizeth,sizep,P,dp2dp)
          a=i+(j-1)*sizer+(k-1)*sizeth*sizer
          rhs(k)=P2(a)-delt/2.0*(dp2dp/r**2/sin(t)**2)
320       continue
        if (time.eq.1) then
          b(ii,1,1)=0.0
          b(ii,3,sizep-1)=0.0
        end if
        k=sizep
        if (time.eq.1) then
          e1(ii,1,1)=b(ii,2,1)
          d1(ii,1,1)=-delt/(r*delp*sin(t))**2/2.0
          d1(ii,k-1,1)=-delt/(r*delp*sin(t))**2/2.0
          c1(ii,1,1)=-delt/(r*delp*sin(t))**2/2.0
          c1(ii,1,sizep-1)=-delt/(r*delp*sin(t))**2/2.0
        end if
        call dpp(i,j,k,delp,sizer,sizeth,sizep,P,dpdp)
        call dp2p(i,j,k,delp,sizer,sizeth,sizep,P,dp2dp)
        a=i+(j-1)*sizer+(k-1)*sizeth*sizer
        rhs(k)=P2(a)-delt/2.0*dp2dp/r**2/sin(t)**2
        iarrow=1
        nod=sizep-1
        do 401 inew=1,nod
          c(1,inew)=c1(ii,1,inew)
          d(inew,1)=d1(ii,inew,1)
          do 402 kk=1,3
            b1(kk,inew)=b(ii,kk,inew)
402       continue
401     continue
        e(1,1)=e1(ii,1,1)

        call arrow(rhs,b1,c,d,e,detlog,isign,tau,jn,iband,lbd,ja,
     $    jna,nrhs,nod,iarrow,lrhs)

        if(time.eq.1) then
          do 4001 inew=1,nod
            c1(ii,1,inew)=c(1,inew)
            d1(ii,inew,1)=d(inew,1)
            do 4002 kk=1,3
```

```
                  b(ii,kk,inew)=b1(kk,inew)
4002              continue
4001            continue
                e1(ii,1,1)=e(1,1)
              end if
              do 330 k=1,sizep
                a=i+(j-1)*sizer+(k-1)*sizer*sizeth
                temp(a)=rhs(k)
330           continue
310         continue
300       continue
*********************** solve for z-axis ************************************
          do 350 i=1,sizer
            a=i+sizer*sizeth*sizep
            y=i*dely+ymin
            r=a1-exp(-y)
            dp2dp=(P(sizep*sizer*sizeth/4+i)-2.0*P(a)
     $        +P(sizep*sizer*sizeth*3/4+i))/delth/delth
            temp(a)=P2(a)-delt/2.0*(dp2dp/r/r)+delt/2.0*
     $        (temp(sizep*sizer*sizeth/4+i)+temp(sizep*sizer*sizeth*3/4+i))
     $        /delth/delth/r/r
            temp(a)=temp(a)/(1.0+delt/2.0*2.0/delth/delth/r/r)
            a=i+sizer+sizer*sizeth*sizep
            aa=sizep*sizer*sizeth/4+sizer*(sizeth-1)+i
            dp2dp=(P(aa)-2.0*P(a)+P(aa+sizer*sizeth*sizep/2))
            dp2dp=dp2dp/delth/delth
            temp(a)=P2(a)-delt/2.0*(dp2dp/r**2)+delt/2.0*
     $        (temp(aa)+temp(aa+sizeth*sizep*sizer/2))/delth/delth/r/r
            temp(a)=temp(a)/(1.0+delt/2.0*2.0/delth/delth/r/r)
350       continue
************ solve r=0 ***************************************************
          aa=sizer*sizeth*sizep/4+(sizeth-1)/2*sizer+1
          P(ocoord)=P2(ocoord)-delt/2.0/delr/delr*
     $    (P(aa)-2.0*P(ocoord)+P(aa+sizer*sizep*sizeth/2))
     $    +delt/2.0*(temp(aa)+temp(aa+sizeth*sizer*sizep/2))/delr/delr
          P(ocoord)=P(ocoord)/(1.0+2.0*delt/2.0/delr/delr)
          do 1101 i=1,sizer
            a=i+sizer*sizeth*sizep
            P(a)=temp(a)
            P(a+sizer)=temp(a+sizer)
            do 1201 j=1,sizeth
              do 1301 k=1,sizep
                a=i+sizer*(j-1)+sizeth*sizer*(k-1)
                P(a)=temp(a)
1301          continue
1201        continue
1101      continue
********* update convection**************************************************
          do 600 i=1,sizer
            do 610 j=1,sizeth
              do 620 k=1,sizep
                a=i+sizer*(j-1)+sizeth*sizer*(k-1)
                cu3(a)=cu2(a)
                cu2(a)=cu1(a)
```

```
620          continue
610        continue
           a=i+sizer*sizep*sizeth
           cu3(a)=cu2(a)
           cu2(a)=cu1(a)
           a=a+sizer
           cu3(a)=cu2(a)
           cu2(a)=cu1(a)
600     continue
        a=ocoord
        cu3(a)=cu2(a)
        cu2(a)=cu1(a)
        do 700 i=1,sizer
           y=i*dely+ymin
           r=a1-exp(-y)
           term1=exp(y)
           do 710 j=1,sizeth
              z=delz*j
              ex=(z-alpha)/(1.0-alpha)
              t=pi*((2.0*alpha+beta)*bratio**ex+2.0*alpha-beta)/
     $           (2*alpha+1.0)/(1.0+bratio**ex)
              term=(2.0*alpha+1.0)*t/Pi-2.0*alpha
              dzdt=2.0*beta*(2.0*alpha+1.0)*(1.0-alpha)/pi/ln/
     $           (beta*beta-term*term)

              do 720 k=1,sizep
                 a=i+sizer*(j-1)+sizeth*sizer*(k-1)
                 call v(k,vr,vt,vp,t,delp,r,shear,F,Pe,angle1,angle2)
                 call dpt(i,j,k,delz,sizer,sizeth,sizep,P,dpdt)
                 call dpp(i,j,k,delp,sizer,sizeth,sizep,P,dpdp)
                 call dpr(i,j,k,dely,sizer,sizeth,sizep,P,dpdy,mtc,term1)
                 cu1(a)=-delt*(term1*vr*dpdy+dzdt*vt/r*dpdt+vp*dpdp)
720           continue
710        continue

           vr=Pe*(1.0-r*r)
           a=sizer*sizep*sizeth+i
           if (i.eq.1) then
              dp2dy=(P(a+1)-2.0*P(a)+P(ocoord))/dely/dely
              dpdy=(P(a+1)-P(ocoord))/dely/2.0
           else if (i.eq.sizer) then
              dp2dy=(-mtc*2.0*dely*P(a)/term1+P(a-1)-2.0*P(a)+P(a-1))/ dely/dely
              dpdy=(-mtc)*P(a)/term1
           else
              dp2dy=(P(a+1)-2.0*P(a)+P(a-1))/dely/dely
              dpdy=(P(a+1)-P(a-1))/2.0/dely
           end if
           cu1(a)=-delt*term1*vr*dpdy
           vx1=shearrate*r*sin(angle1)*(F*(5.0/3.0*r**2)-1.0)
           vx=Pe*vx1*cos(angle2)
           vy=Pe*vx1*sin(angle2)
           dpdt=(P(i)-P(i+sizer*sizeth*sizep/2))/delth/2.0
           cu1(a)=cu1(a)-delt*dpdt*vx
           dpdt=(P(i+sizer*sizeth*sizep/4)-P(i+sizer*sizeth*sizep*3/4))/2.0/delth
```

```
            cu1(a)=cu1(a)-delt*dpdt*vy
            a=a+sizer
            if (i.eq.1) then
               dp2dy=(P(a+1)-2.0*P(a)+P(ocoord))/dely/dely
               dpdy=(P(a+1)-P(ocoord))/dely/2.0
            else if (i.eq.sizer) then
               dp2dy=(-mtc*2.0*dely*P(a)/term1+P(a-1)-2.0*P(a)+P(a-1))/dely/dely
               dpdy=-mtc*P(a)/term1
            else
               dp2dy=(P(a+1)-2.0*P(a)+P(a-1))/dely/dely
               dpdy=(P(a+1)-P(a-1))/2.0/dely
            end if
            cu1(a)=-delt*term1*vr*dpdy
            dpdt=(P(i+(sizeth-1)*sizer)
     $         -P(i+(sizeth-1)*sizer+sizeth*sizer*sizep/2))/2.0/delth
            cu1(a)=cu1(a)-delt*dpdt*vx
            dpdt=(P(i+sizer*sizeth*sizep/4+sizer*(sizeth-1))
     $         -P(i+sizer*sizeth*sizep*3/4+sizer*sizeth-1))/2.0/delth
            cu1(a)=cu1(a)-delt*vy*dpdt
700      continue
         up=1+sizer*sizeth*sizep
         down=1+sizer+sizer*sizeth*sizep
         cu1(ocoord)=-delt*Pe*(P(up)-P(down))/delr/2.0
****************** calculate rate ***********************************************
         ncount=0.0
         sum=0.0
         do 400 i=1,sizer
            y=i*dely+ymin
            r=a1-exp(-y)
            do 410 j=0,sizeth-1
               z=delz*(j+1)
               ex= (z-alpha)/(1.0-alpha)
               t=pi*((2.0*alpha+beta)*bratio**ex+2.0*alpha-beta)/
     $         (2*alpha+1.0)/(1.0+bratio**ex)
               term=(2.0*alpha+1.0)*t/Pi-2.0*alpha
               dzdt=2.0*beta*(2.0*alpha+1.0)*(1.0-alpha)/pi/ln/
     $         (beta*beta-term*term)
               do 420 k=0,sizep-1
                  a=i+sizer*j+k*sizer*sizeth
                  term=P(a)*r*r*sin(t)
                  sum=sum+term*delz/dzdt*delp*dely*exp(-y)
                  if (P(a).lt.0)then
                     ncount=ncount+1
                  end if
                  if (ncount.gt.0) goto 5100
420            continue
410         continue
            if(P(i+sizer*sizeth*sizep).lt.0) then
               ncount=ncount+1
               goto 5100
            end if
            if(P(i+sizer*sizeth*sizep+sizer).lt.0) then
               ncount=ncount+1
               goto 5100
```

```
            end if
            term=exp(-y)*pi
            sum=sum+P(i+sizeth*sizer*sizep)*r*r*delth*delth*dely*term
            sum=sum+P(i+sizer+sizeth*sizer*sizep)*r*r*delth*delth*dely*term
400         continue
            if(P(occord).lt.0) then
               k=300
               goto 5100
            end if
            sum=sum+P(ocoord)*delr**3*4.0/3.0*Pi
            rate=-log(sum/oldsum5)/delt/5
            oldsum5=oldsum4
            oldsum4=oldsum3
            oldsum3=oldsum2
            oldsum2=oldsum1
            oldsum1=sum
            if(out.eq.1) then
               write(*,*) rate,sum,(rate-oldrate)/rate,time
               write(*,*)
            end if
            if(abs((rate-oldrate)/rate).lt.tol) goto 5100
            if((sum-oldsum5)/sum.gt.1.0) goto 5100
            if ((time/200.0).eq.aint(time/200.0)) then
               open(unit=4, file='savestate', status='unknown')
               write(4,*) P(ocoord),cu1(ocoord),cu2(ocoord),cu3(ocoord)
               do 501 i=1,sizer
                  a=i+sizeth*sizer*sizep
                  write(4,*) P(a),cu1(a),cu2(a),cu3(a)
                  a=a+sizer
                  write(4,*) P(a),cu1(a),cu2(a),cu3(a)
                  do 502 j=1, sizeth
                     do 503 k=1,sizep
                        a=i+(j-1)*sizer+(k-1)*sizer*sizeth
                        write(4,*) P(a),cu1(a),cu2(a),cu3(a)
503                  continue
502               continue
501            continue
               close(4)
            end if
4950        oldrate=rate
            tau=-1.0
5000        continue
5100        tau=-1.0
            open(unit=3,file=filename,status='unknown')
            if(ncount.gt.0) write(3,*) i,j,k,P(a)
            write(3,*) sizer,sizeth,sizep,delt,tol,a1,beta
            write(3,*) 'k:',mtc
            write(3,*) 'Pe: ',Pe
            write(3,*) 'F: ',F
            write(3,*) 'shear: ',shear
            write(3,*) 'net shear: ', shear*Pe
            write(3,*) 'alpha:',angle1
            write(3,*) 'beta:', angle2
            write(3,*) rate, oldrate,ncount,time
```

```
      write(3,*)
      close(3)
6000  continue
7000  end
*************************************************************************
      subroutine v(k,vr,vt,vp,t,delp,r,shear,F,Pe,A,B)
      integer k
      double precision p,r,t,x,y,z,x1,y1,z1,vx,vy,vz,vx1,vy1,vz1
      double precision vr,vt,vp,delp,shear,F,Pe,A,B,sigma
      sigma=2.0/3.0/F-1.0
      p=(k-1)*delp
      x=r*sin(t)*cos(p)
      y=r*sin(t)*sin(p)
      z=r*cos(t)
      x1=cos(B)*x+sin(B)*y
      y1=sin(B)*cos(A)*x+cos(A)*cos(B)*y+sin(A)*z
      z1=sin(A)*sin(B)*x-sin(A)*cos(B)*y+cos(A)*z
      vx1=shear*(F*y1*(5.0/3.0*r*r-1.0)-4.0/3.0*F*x1*x1*y1-y1)
      vy1=shear*(F*x1*(5.0/3.0*r*r-1.0)-4.0/3.0*F*x1*y1*y1+x1)
      vz1=-4.0/3.0*F*shear*z1*x1*y1
      vx=cos(B)*vx1-sin(B)*cos(A)*vy1+sin(A)*sin(B)*vz1
      vy=sin(B)*vx1+cos(A)*cos(B)*vy1-sin(A)*cos(B)*vz1
      vz=sin(A)*vy1+cos(A)*vz1
      vr=vx*sin(t)*cos(p)+vy*sin(t)*sin(p)+vz*cos(t)
      vt=vx*cos(t)*cos(p)+vy*cos(t)*sin(p)-vz*sin(t)
      vp=-vx*sin(p)+vy*cos(p)
      vr=Pe*(-cos(t)*(r*r-1.0)/(1.0+sigma)+vr)
      vt=Pe*(-sin(t)*(1.0-2.0*r*r)/(1.0+sigma)+vt)
      vp=Pe*vp/r/sin(t)
      return
      end
*************************************************************************
      subroutine dpr(i,j,k,dely,sizer,sizeth,sizep,P,dpdy,mtc,term1)
      integer i,j,k,sizer,sizeth,sizep,a,aa
      double precision dely,dpdy,P(70000),mtc,term1
      a=sizer*sizeth*(k-1)+sizer*(j-1)+i
      if (i.eq.1) then
         aa=sizer*sizeth*sizep+2*sizer+1
         dpdy=(P(a+1)-P(aa))/2.0/dely
      else if (i.eq.sizer) then
         dpdy=-mtc*P(a)/term1
      else
         dpdy=(P(a+1)-P(a-1))/2.0/dely
      end if
      return
      end
*************************************************************************
      subroutine dp2r(i,j,k,dely,sizer,sizeth,sizep,P,dp2dy,mtc,term1)
      integer i,j,k,sizer,sizeth,sizep,a,aa
      double precision dely,dp2dy,P(70000),mtc,term1
      a=sizer*sizeth*(k-1)+sizer*(j-1)+i
      if (i.eq.1) then
         aa=sizer*sizeth*sizep+2*sizer+1
         dp2dy=(P(a+1)-2.0*P(a)+P(aa))/dely/dely
```

```
      else if (i.eq.sizer) then
         dp2dy=(-mtc*2.0*dely*P(a)/term1+P(a-1)-2.0*P(a)+P(a-1))/dely/dely
      else
         dp2dy=(P(a+1)-2.0*P(a)+P(a-1))/dely/dely
      end if
      return
      end
*************************************************************************
      subroutine dpt(i,j,k,delth,sizer,sizeth,sizep,P,dpdt)
      integer i,j,k,sizer,sizeth,sizep
      double precision delth,dpdt,P(70000)
      a=sizer*sizeth*(k-1)+sizer*(j-1)+i
      if (j.eq.1) then
         dpdt=(P(a+sizer)-P(sizer*sizeth*sizep+i))/2.0/delth
      else if (j.eq.sizeth) then
         dpdt=(P(sizer*sizeth*sizep+sizer+i)-P(a-sizer))/2.0/delth
      else
         dpdt=(P(a+sizer)-P(a-sizer))/2.0/delth
      end if
      return
      end
*************************************************************************
      subroutine dp2t(i,j,k,delth,sizer,sizeth,sizep,P,dp2dt)
      integer i,j,k,sizer,sizeth,sizep
      double precision delth,dp2dt,P(70000),Ppi
      a=sizer*sizeth*(k-1)+sizer*(j-1)+i
      if (j.eq.1) then
         dp2dt=(P(a+sizer)-2.0*P(a)+P(sizer*sizeth*sizep+i))/delth/delth
      else if (j.eq.sizeth) then
         Ppi=(P(sizer*sizeth*sizep+sizer+i))
         dp2dt=(Ppi-2.0*P(a)+P(a-sizer))/delth/delth
      else
         dp2dt=(P(a+sizer)-2.0*P(a)+P(a-sizer))/delth/delth
      end if
      return
      end
*************************************************************************
      subroutine dpp(i,j,k,delp,sizer,sizeth,sizep,P,dpdp)
      integer i,j,k,sizer,sizeth,sizep
      double precision delp,dpdp,P(70000),opterm
      a=sizer*sizeth*(k-1)+sizer*(j-1)+i
      if (k.eq.1) then
         opterm=(P(a+sizer*sizeth*(sizep-1)))
         dpdp=((P(a+sizer*sizeth))-opterm)/delp/2.0
      else if (k.eq.sizep) then
         opterm=(P(a-sizer*sizeth*(sizep-1)))
         dpdp=(opterm-(P(a-sizer*sizeth)))/delp/2.0
      else
         dpdp=((P(a+sizer*sizeth))-(P(a-sizer*sizeth)))/2.0/delp
      endif
      return
      end
*************************************************************************
      subroutine dp2p(i,j,k,delp,sizer,sizeth,sizep,P,dp2dp)
```

```
      integer i,j,k,sizer,sizeth,sizep
      double precision delp,dp2dp,P(70000),opterm
      a=sizer*sizeth*(k-1)+sizer*(j-1)+i
      if (k.eq.1) then
         opterm=P(a+sizer*sizeth*(sizep-1))
         dp2dp=(P(a+sizer*sizeth)-2.0*P(a)+opterm)/delp/delp
      else if (k.eq.sizep) then
         opterm=P(a-sizer*sizeth*(sizep-1))
         dp2dp=(opterm-2.0*P(a)+P(a-sizer*sizeth))/delp/delp
      else
         dp2dp=(P(a+sizer*sizeth)-2.0*P(a)+P(a-sizer*sizeth))/delp/delp
      end if
      return
      end
*************************************************************************
```